The Thesis commitee for Steven Thomas Embleton

Certifies that this is the approved version of the following thesis:

Methodology for the Design of Hydrophone Acoustic Baffles and Supporting Materials

Preston S. Wilson, Supervisor

Michael R. Haberman

Methodology for the Design of Hydrophone Acoustic Baffles and Supporting Materials

by

Steven Thomas Embleton, B.S.

THESIS

Presented to the Faculty of the Graduate School of

The University of Texas at Austin

in Partial Fulfillment

of the Requirements

for the Degree of

Master of Science in Engineering

THE UNIVERSITY OF TEXAS AT AUSTIN

August 2011

This thesis is dedicated to my wife Amanda,

whose love and support made this work possible.

Acknowledgments

I would like to thank the numerous people whose help was invaluable in writing this thesis.

This thesis would not have been possible without the tireless efforts of Michael Haberman. During the many stages of this process his encouragement, revisions and great ideas kept me focused through the years. I am grateful for Preston Wilson whose advice and revisions greatly helped to shape and refine this work. I would also like to thank my colleagues at the Applied Research Laboratories at the University of Texas at Austin including Douglas Heyden for his support, Daniel Knapek for building the test fixtures, Clinton Johnson for designing and testing the example systems, and everyone else who contributed. Finally, I am eternally grateful to Lisa and Tom Embleton whose support and provision of countless opportunities helped me achieve my goals.

Methodology for the Design of Hydrophone Acoustic Baffles and Supporting Materials

Steven Thomas Embleton, M.S.E
The University of Texas at Austin, 2011

Supervisor: Preston S. Wilson

One key element of underwater transducer design is the acoustic baffle. Acoustic baffles isolate a structure, such as a submarine hull, from noise and vibration produced by the active elements of the transducer and vice versa. Baffle materials must meet many conflicting requirements such as the need to be lightweight while providing high acoustic isolation. Currently Syntactic Acoustic Damping Material (SADM) is widely used as the primary acoustic baffle material. However, SADM baffles have many undesirable characteristics such as high density, poor machinability, high lead content and depth dependent acoustical behavior.

The study of baffle materials is an under-represented area of sonar design. Most sonar transducer research focuses on the electrically active materials and their response to a variety of conditions. Relatively fewer studies have been devoted to understanding the effects of the supporting and baffle materials. This work considers the effects of the entire hydrophone system on the response while developing a method for aiding in proper system material selection.

This was accomplished by first developing a model for a transducer's response in a variety of conditions. The response was validated with numberical finite-element

models and experiments. Next, a generic model was developed that allows any number of layers with any material to be analyzed. This generic model is applied in concert with a material optimization method to aid in the selection of materials that will improve the transducer's response. The tools are finally applied to a simple real world problem to illustrate its strengths and weaknesses.

Table of Contents

List of Tables

List of Figures

Chapter 1

Introduction

1.1 Sonar History

The first recorded use of Sonar or SOund NAvigation and Ranging was in 1490 when Leonardo da Vinci claimed he could hear ships at great distances through a tube placed underwater. Underwater sound has since been used for a variety of purposes whose use constitutes the science of sonar. The systems that employ sound underwater are sonar systems. The first practical application of sonar systems was the submarine bell installed at lighthouses. By comparing the time between reception of a foghorn in air and a submarine bell underwater, ships at sea could calculate the distance to shore [4].

Interest was not significantly peaked however, until the days of World War I [4, 5]. The modern era of underwater sound as a quantitative subject began with the need to detect German U-boats. This led to the use of passive underwater sound detection and the beginning of research into piezoelectrics as active sources. Paul Langevin was a prominent French physicist who pioneered the use of piezoelectric ceramics as transducers [5]. During World War I Langevin began work on using these transducers to detect submarines by their reflected response. His work, however, was not finished until the war had ended. Since then, continued exploration and exploitation of the seas has led to an increase in research and use of sonar.

Today, acoustic waves remain the only practical means of carrying information

underwater, as other forms of radiation attenuate rapidly in water. Acoustic waves are used to detect and locate targets, measure characteristics of marine environments, measure the location and velocity of moving targets and to transmit communication signals. Civilian applications prevalent today are acoustic sounders, depth finders and fish finders, side-scan sonars that obtain detailed images, underwater mapping for the oil and off shore industries, acoustic communications, positioning and acoustic doppler systems [5].

There are two types of acoustic systems: active and passive. Active systems generate sound using a projector. This sound travels through the underwater environment and reflects off of boundaries and targets, creating echos that are recorded by a hydrophone. Passive systems do not project any sound, but use only a hydrophone to listen to the sound radiated by targets [4]. A simple passive sonar generally consists of at least the discrete components illustrated in Figure 1.1. The transducer array with which this work is mainly concerned houses a spatially distributed array of hydrophones. The benefits of an array of hydrophones is an improved signal-to-noise ratio, important for the detection of underwater targets [4]. Once the hydrophone has received a signal it is passed to the signal conditioner which amplifies and filters the signal. The receive beamformer then accepts the conditioned signal and combines them into many parallel channels to form a beam set which may finally be displayed [6].

1.2 Hydrophone Design

The hydrophone is device that converts an underwater acoustical pressure signal into an electrical voltage signal, similar to a microphone used in the air. Most modern hydrophones are based on piezoelectric transducers which generate a volt-

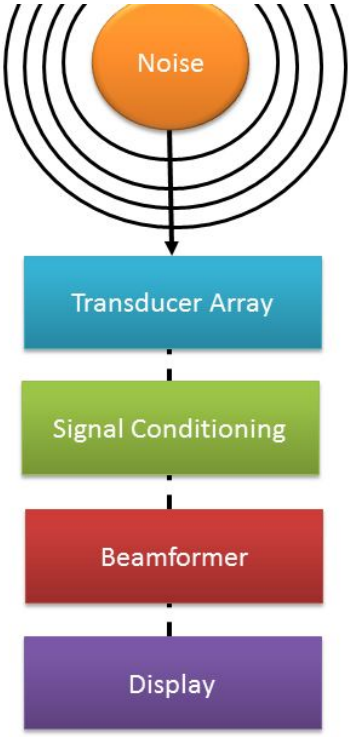

Figure 1.1: General passive sonar discrete components.

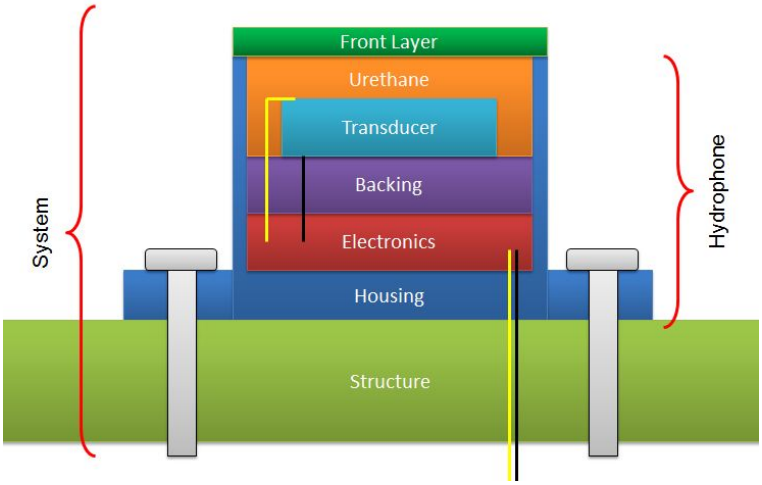

Figure 1.2: Illustration of a simple hydrophone design.

age proportional to the acoustic pressure [7]. When a sonar system is designed to accomplish a particular purpose, selection of parameters is often beset with difficulties arising from economical, mechanical and electrical constraints particular to the system on which it is integrated. For example, some hydrophone systems need to be inexpensive such as those employed on disposable sonobouys and some need to fit in the confined space offered by a torpedo [5]. The final design is achieved by trade offs and compromises. An example of a simple hydrophone design is illustrated in Figure 1.2.

Aside from acoustical performance, there are many additional factors to be considered when designing a hydrophone system. These include cost, reliability, lifespan, environment, temperatures, hydrostatic pressures, forces (turbulence, fluid flow, vibration and shock), electrical isolation, weight and dimensions [7, 8]. Some of these requirements are conflicting, and a compromise is usually accepted. However, in some cases, well designed structures may overcome some of these limitations. In recent years, high frequency hydrophone enclosure designs have progressed from simple housings to protect them from environmental factors into composite multi-element

structures containing matching and backing layers designed to optimize acoustical performance while protecting devices from mechanical and environmental loads. For many applications a simple design based on a supportive backing and protective front is acceptable. However, when a high performance design is desired techniques for synthesizing backings and matching layers are required [8].

1.2.1 Transducer Design

Transducers are often made of piezoelectric ceramic because of their low cost which enable them to be sintered from powders under high pressures and temperatures into a variety of shapes and then poled. Commercially available piezoelectric ceramics include plates, bars, rings, spheres and composite vibrators [7]. There are many considerations effecting the selection of transducers including the frequency range of the signals to be received, the need for a uniform sensitivity response across a range of frequencies, the sensitivity across large angles of incidence, the required sensitivity, and the amount of background noise expected [7, 8].

The design of a transducer is often centered around the response to a pressure field through a range of frequencies. This response has historically been modeled and designed using simplified lumped element mechanical, acoustical and electrical equivalent circuit models, combined with techniques of circuit analysis [9]. This method led to the use of quarter-wave matching layers with piezoelectric ceramic plates to produce high efficiency ultrasonic transducers for medical applications [10]. Unfortunately, for a complex system, the use of only equivalent circuits for modeling a transducer with many vibration modes can lead to huge errors [11]. However, recent development of computer technology and associated efficacy and speed of computer simulations makes the use of finite element methods (FEM) more attractive for the design of complex transducers. The flexibility available in FEM has led to its near

exclusive use in arbitrarily shaped transducers [12, 13]. Unfortunately, FEM is still time consuming and changes in geometry and materials often need to be modified manually. This is not ideal for a computer assisted optimization process [14].

Understanding the performance potential of different transducers is necessary for accurate sonar performance predictions [5]. An accurate prediction would allow for fewer prototyping iterations saving money and time for industries designing sonar systems.

1.2.2 System Design

While the piezoelectric element is an important part of the hydrophone, an accurate predictive design tool needs to consider the entire system. As discussed in Chapter 2, the system will perform significantly different when materials are added to the front or back of the transducer, whether they be introduced for acoustical or mechanical reasons. The final optimal design of a hydrophone is therefore a multi-objective optimization problem because the final outcome needs to satisfy several conflicting criteria [15].

With all of the layers in a system included in a model, Schroder et al. suggest using weighted cost functions to find o configuration that finds an optimal compromise between the system goals and constraints [11]. The cost functions considered by Schroder et al. were the maximum of the received electrical signal, frequency sensitivity coupling and maximum integrated out-of-plane displacement. Their work however was limited to only calculating the impedance at the center frequency of interest.

When designing a complex system Heikkola et al. suggested using a decision maker, or expert in transducer design, to find a preferred compromise between the

conflicting objectives [15]. This is best accomplished through repeatedly exchanging results to allow the decision maker to observe and comment on the pattern formation.

1.2.3 Material Selection

Wilson described formulae that may be used to analyze the response of the electrically and magnetically active materials in a hydrophone [7]. The design of the active portion of a hydrophone is considered at depth in a wide variety of papers. Unfortunately however, there is little in the way of design for the electrically inactive materials and their impact on hydrophone system performance.

Electrically inactive materials widely used in the construction of sonar systems include metals, elastomers and fluids. Metal parts are used as sound heads, as enclosures and mounting brackets. Elastomers are used as encapsulating materials, acoustic windows, transducer boots, spacers for vibration isolation, sound absorbers and o-ring seals [7, 16]. Fluids such as mineral and Castor oil are also often used in the electronics enclosures to maintain the volume shape under pressure and aid in temperature dissipation.

Material selection for any application is a daunting task since there are currently over 120,000 engineering materials at our disposal [3]. In order to narrow down the list of potential materials important variables must be considered. For example, elastomers should ideally be considered based on properties and processing including the curing time, additives, shape, cost, ease of mixing, strength requirements, acoustic properties, water permeability, elongation requirements, modulus of stiffness, oil resistance, low temp behavior, fatigue, mold-ability, tack, amenability to various cure systems, tear resistance, stress relaxation, service temperature, dynamic properties (hysteresis, damping, resilience, etc.), flammability and chemical resistance [16]. Due

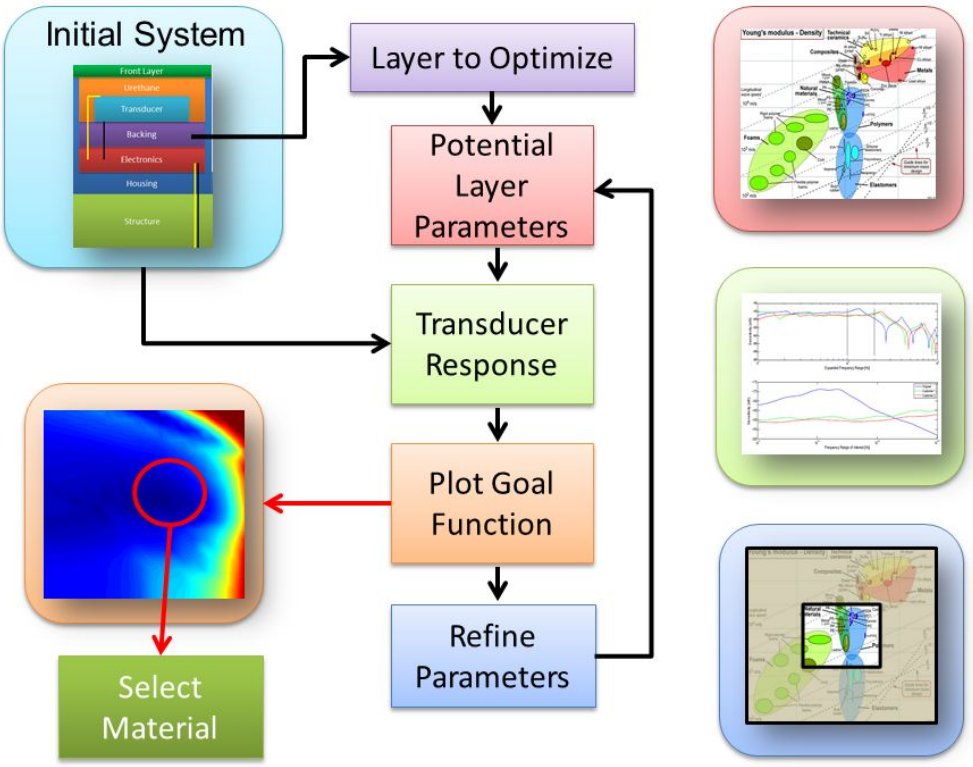

Figure 1.3: Block diagram depicting design process.

to the extensive nature of the important variables in elastomer selection designers must choose materials relying on documentation that is often incomplete [7].

1.3 Solution Developed

As indicated in the previous section, the optimal design of an ultrasonic hydrophone is a multi-objective optimization problem that depends on not only the sensing element, but also the transducer as well as the electrically inactive materials that surround it. The development of a simulation tool for a proposed hydrophone design will reduce the need for expensive and time-consuming experiments. An overview of this proposed work is depicted in Figure 1.3.

First, an understanding of the performance potential of different transducers

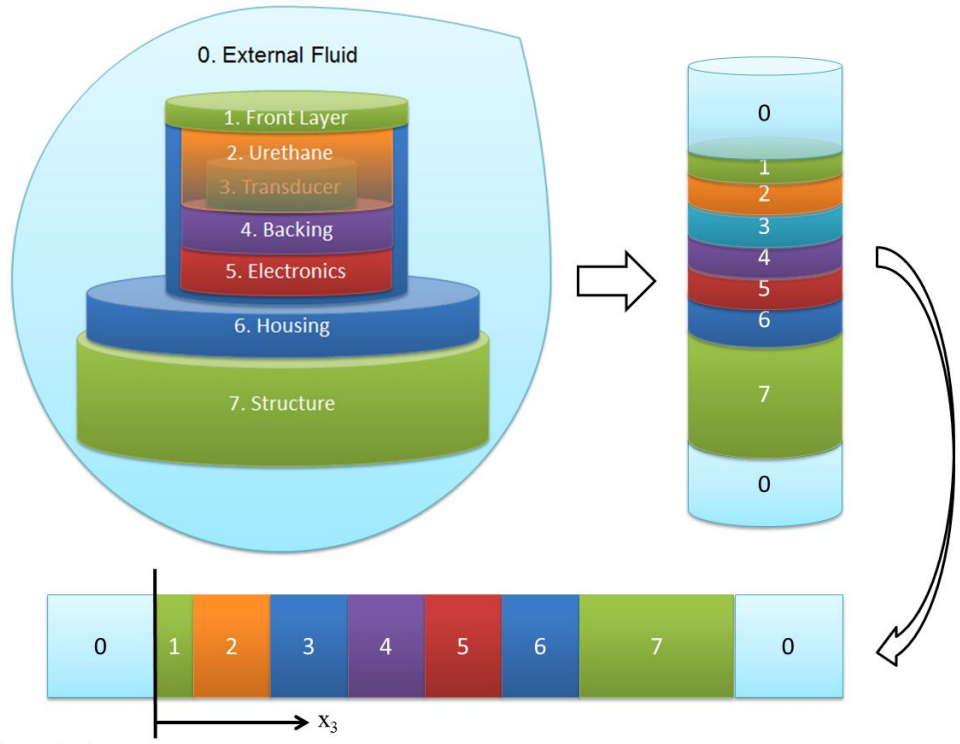

Figure 1.4: Illustrative transposition of a hydrophone system into a 1D array of layers.

is necessary for accurate sonar performance predictions [5]. This is accomplished by modeling a variety of transducers in air and comparing the results to known cases. Next, an analytical model has been developed to predict the receive response of a particular system by transposing it into a one-dimensional array of material layers as illustrated in Figure 1.4. This forward (predictive) model is then bench-marked with finite element models (FEM) and experiments. The FEM is composed using the finite element package Comsol Multiphysics, a commercially-available finite element software package[1]. Agreement between the two results for a variety of scenarios validated the simpler analytical models and increased confidence in the analytical model. By using analytical models the computational time required compared with finite element models was decreased significantly. For example, running a typical

[1]http://www.comsol.com

Comsol model used in this work took 30 minutes while the analytical calculations only took ten seconds per system. This much smaller computation time ultimately allowed for rapid analysis of many different cases.

Once the models had been validated, a more complex algorithm was developed that is independent of the properties and quantity of layers. The ability for the algorithm to handle any system defined allowed for a quick analysis with minimal troubleshooting. This model was then compared with a real multi-layer system for validation.

After the algorithm had been developed to handle any system of layers representing a hydrophone system, the model may be used in an inverse sense to find an optimal set of material properties for an individual layer taking into account customer needs and imposed boundary conditions. For example, a sonar designer may wish to know what transducer backing properties would provide a required response frequency range of interest. Combining the concepts developed by Heikkola and Schroder [15, 11], this work suggests developing a list of weighted goals with a decision maker. Potential solutions may then be shared with the decision maker to develop a working knowledge of the effective compromises until an acceptable solution is found as depicted in Figure 1.5.

To aid in the selection of an appropriate material, the use of a surface plot depicting the final goal value as a function of two material properties was combined with Ashby's material family plots as depicted in Figure 1.6. This utilized the advances in computation speed, which has propelled the growth in FEM, to perform a brute force approach to finding a solution to many potential material parameter sets. This wealth of information allowed for the recognition of patterns and then the application of an optimal material.

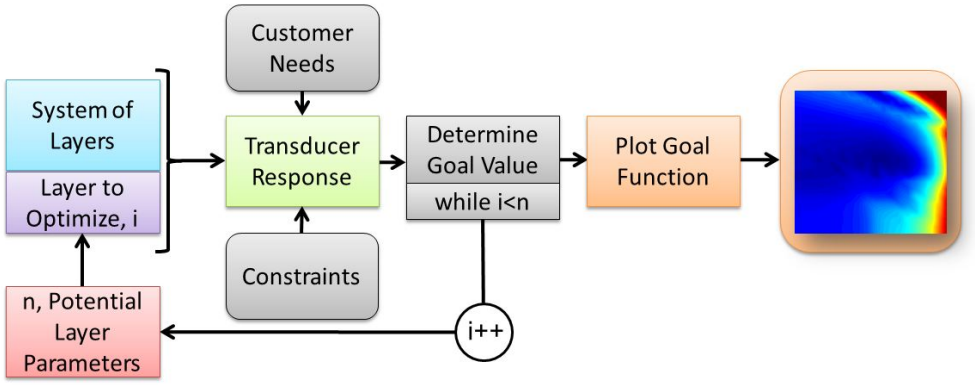

Figure 1.5: Schematic representation of the process used to translate an array of potential material properties into an easy to understand chart.

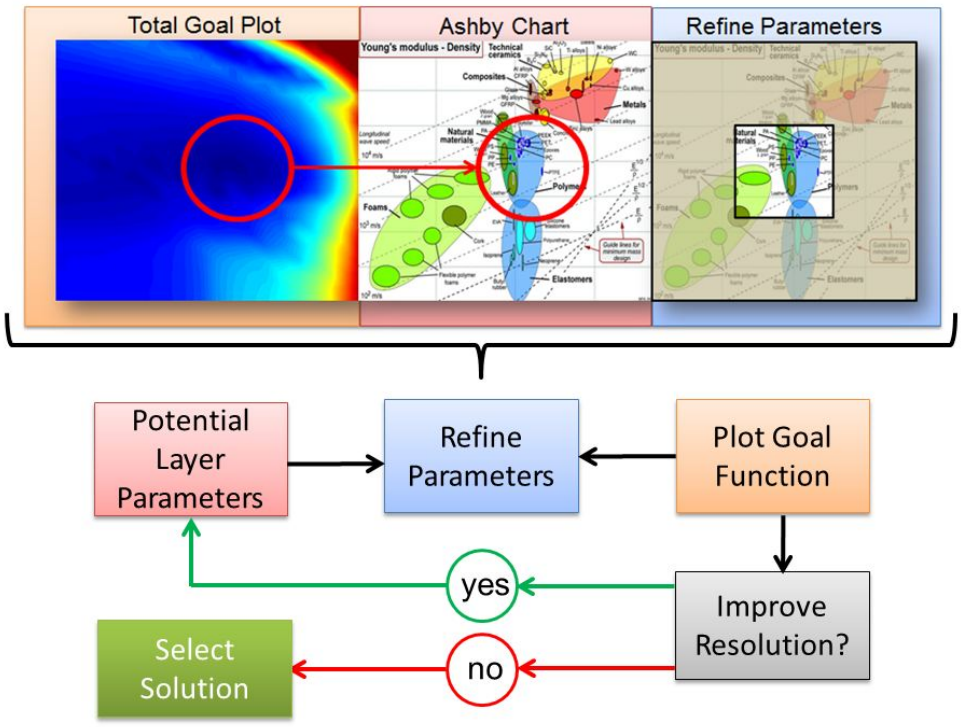

Figure 1.6: Schematic representation of the process used to refine a layer parameter set and selection of a final solution.

The data from the real system which was used to validate the generic algorithm was taken in an effort to find an optimal material to achieve a desired response. To illustrate the potential of this complete work, a real system was analyzed based on the preferences of two different decision makers. The final results were then compared to a base case and evaluated based on the choices made by the decision makers.

Chapter 2

Transducer Response

When designing a sonar transducer, the frequency response (also called the receiving response for a receiver) is usually the most important criteria. While largely a function of the piezoelectric material and shape, it is also significantly effected by materials both in front of and behind the piezoelectric material. In this work any layer in between the piezoelectric layer and the incoming pressure wave is referred to as a front layer. Any layer behind the piezoelectric layer with respect to the incoming pressure wave is referred to as a backing layer. The model *system* analyzed here is a one-dimensional cross section of the transducer housing parallel to the poled direction of the transducer.

2.1 Electromechanical Description

This work follows Wilson's notation that describes the basic mechanics behind a piezoelectric thickness vibrator [7]. These equations are used to examine an unloaded thickness mode resonator as an example. More complex examples follow to illustrate the transducer's response to an incident acoustic pressure for a variety of layer conditions. Modifications of the submerged model are then be described to account for the case of a submerged rigidly terminated transducer and a submerged transducer backed by a known generic impedance.

A mechanical description of the piezoelectric material response to an applied

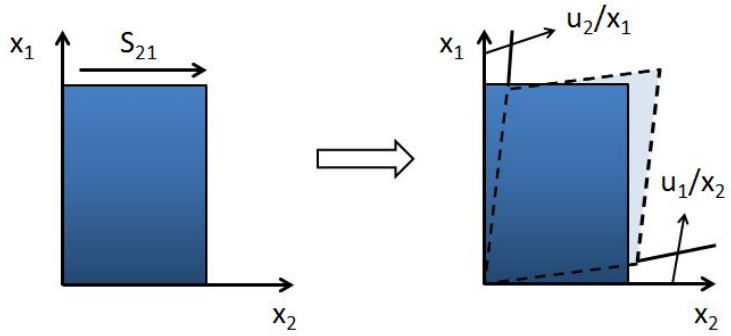

Figure 2.1: Example notation of a strain component using rectangular parallelepiped notation

force and electric field are examined first as they are used later to calculate the system response. It is shown that the response is a function of the stress, strain, dielectric effects and piezoelectric properties.

2.1.1 Stress, Strain and the Stress-Strain Relationship

To begin, the equations for stress and strain are described in a manner that allows for piezoelectric effects to be included. For a material displacement u_j, and coordinate system with axes x_k the strain, S_{jk}, can be expressed as a symmetric part of the gradient of the deformation field

$$S_{jk} = \left(\frac{1}{2}\right)\left(\frac{\partial u_j}{\partial x_k} + \frac{\partial u_k}{\partial x_j}\right). \tag{2.1}$$

In the above equation, S_{jk} is the component of strain described by a plane whose outward normal is parallel to x_j with a deformation along x_k. The strain can be expressed as acting along the axis of a rectangular parallelepiped using the common notation set illustrated in Figure 2.1. Therefore, for pure extension in x_1, x_2, or x_3 yields

$$S_{11} = \frac{\partial u_1}{\partial x_1},\ S_{22} = \frac{\partial u_2}{\partial x_2},\ S_{33} = \frac{\partial u_3}{\partial x_3}.$$

The strain components above are the components indicating the amount of stretch the material experiences when the deformation is parallel to a coordinate axis. For shear motion, the deformation is perpendicular to the coordinate axis yielding

$$S_{21} = S_{12} = \frac{1}{2}\left(\frac{\partial u_2}{\partial x_1} + \frac{\partial u_1}{\partial x_2}\right),$$

$$S_{31} = S_{13} = \frac{1}{2}\left(\frac{\partial u_3}{\partial x_1} + \frac{\partial u_1}{\partial x_3}\right),$$

$$S_{23} = S_{32} = \frac{1}{2}\left(\frac{\partial u_2}{\partial x_3} + \frac{\partial u_3}{\partial x_2}\right).$$

For convenience, this may be expressed using Voigt notation $S_{11} = S_1$, $S_{22} = S_2$, $S_{33} = S_3$, $S_{23} = S_4$, $S_{13} = S_5$ and $S_{12} = S_6$ [17].

$$\mathbf{S} = \begin{bmatrix} S_1 & S_6 & S_5 \\ S_6 & S_2 & S_4 \\ S_5 & S_4 & S_3 \end{bmatrix}.$$

Using symmetry this may be simplified to the 6×1 vector

$$S = \begin{bmatrix} S_1 & S_2 & S_3 & S_4 & S_5 & S_6 \end{bmatrix}. \tag{2.2}$$

The stress, T_{ij}, is the force per unit area as illustrated in Figure 2.2. Using the same notation discussed above for the indices allows the stress to be written as

$$T_{ij} = \begin{bmatrix} T_{11} & T_{12} & T_{13} \\ T_{21} & T_{22} & T_{23} \\ T_{31} & T_{32} & T_{33} \end{bmatrix},$$

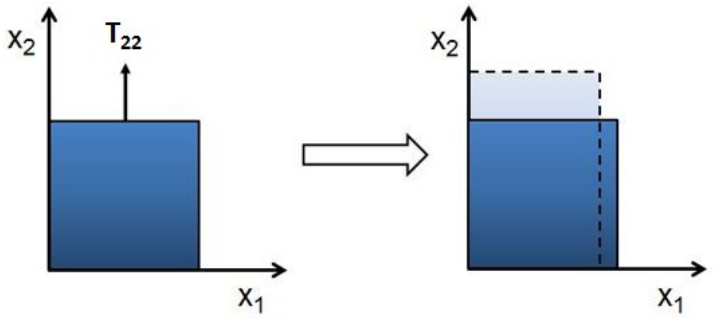

Figure 2.2: Example notation of a stress component using rectangular parallelepiped notation

$$\mathbf{T} = \begin{bmatrix} T_1 & T_6 & T_5 \\ T_6 & T_2 & T_4 \\ T_5 & T_4 & T_3 \end{bmatrix},$$

,

$$\mathbf{T} = \begin{bmatrix} T_1 & T_2 & T_3 & T_4 & T_5 & T_6 \end{bmatrix}. \tag{2.3}$$

According to Cauchy's theorem, the stress vector on any plane at a point can be found by knowing the stress vectors of three mutually perpendicular planes through that point [18]. This implies that any stress vector can be expressed as component tensors. Cauchy's stress principle is used to describe a material acted on by external forces as long as the surface forces are proportional to the area of contact and the body forces are distributed over the volume. Assuming an infinitesimal deformation of a continuum body Cauchy's stress tensor, Eq. 2.3, then completely defines the state of stress at a point.

Hooke's law is an approximation that can be used to relate the stress and strain for linear elastic materials. In general, the stress is proportional to the change in strain for small deformations, $u \ll x$, in a one dimensional system where x is the

length of the material in the x_1 axis. Hooke's law may be expressed as

$$\mathbf{T} = \mathbf{cS} \tag{2.4}$$

where $\mathbf{c}$ is the matrix of elastic stiffness. The elastic compliance matrix, $\mathbf{s}$, is the inverse of the elastic stiffness matrix, $\mathbf{s} = \mathbf{c^{-1}}$, and is used often to simplify notation.

2.1.2 Dielectric Properties

The thickness vibrator is assumed to be a piezoelectric material which is a non-conducting medium separated by two conductive plates. Describing the electric displacement vector $\mathbf{D}$ in terms of the material dielectric permittivity ϵ and the electric field vector $\mathbf{E}$

$$\mathbf{D} = \epsilon\mathbf{E}. \tag{2.5}$$

The electric displacement is the electric charge within a material per unit area.

2.1.3 Piezoelectric Effects

A piezoelectric material can be used as a transducer to convert acoustic signals into electric signals or vice versa. The piezoelectric effect is exhibited when there is a separation of the positive and negative charge centers, within the material lattice, as a result of electromechanical loading [2]. This effect is illustrated in Figure 2.3 using quartz as an example. The charge centers of the positive and negative charges are coincident when the quartz is un-strained. Strain the quartz however, and the charge centers move relative to each other creating surface charges. Many modern piezoelectric ceramics are made of fine powders of oxides in various proportions mixed together with a binder. Confined and heated, the powers form a dense solid material with a

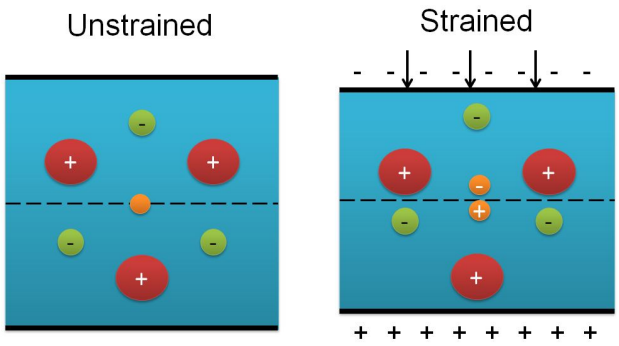

Figure 2.3: Piezo-electric action in quartz showing the centers of positive and negative charge centers (a) coincident and (b) separated when under stress, adapted from [2].

random crystalline structure consisting of multiple grains each of which contains many single crystal domains with randomly oriented electric dipoles. To align the random dipoles, the material is subjected to a high voltage, around 10 kV/m, while heated above the Curie temperature. With the voltage maintained as the material cools, the dipoles align. This process is called "poling" [19].

Once poling has been completed, the stress and electric field can then be expressed in terms of an independent strain and electric displacement by combining Eqs. 2.4 and 2.5 and noting that electro-mechanical coupling exists due to the non center-centric molecular structure of the material to yield the following stress-voltage forms of the piezoelectric relationships

$$\mathbf{T} = \mathbf{c}^D\mathbf{S} - \mathbf{h}_t\mathbf{D}, \tag{2.6}$$

$$\mathbf{E} = -\mathbf{h}\mathbf{S} + \beta^S\mathbf{D}. \tag{2.7}$$

Where the dielectric impermeability is equal to the inverse of the dielectric permit-

tivity, $\beta_{33}^S = 1/\epsilon_{33}^S$ and $\mathbf{h}$ is the matrix of the stress-voltage form of piezoelectric constants.. Unlike common notation, the transpose will be denoted in the subscript to avoid confusion with variables held constant which is indicated by a superscript. For example $\mathbf{c}^D$ is the elastic stiffness given a constant electric displacement and β^S is the inverse dielectric permittivity given a constant strain. With different transducer configurations it may be more convenient to use different combinations of independent variables leading to different combinations of the piezoelectric relationships [7].

When different variables are used as the independent variable, the above equations take the following forms. With $\mathbf{T}$ and $\mathbf{E}$ independent (strain-charge form)

$$\mathbf{S} = \mathbf{s}^E\mathbf{T} + \mathbf{d}_t\mathbf{E},$$

$$\mathbf{D} = \mathbf{d}\mathbf{T} + \epsilon^T\mathbf{E}.$$

With $\mathbf{S}$ and $\mathbf{E}$ independent (stress-charge form)

$$\mathbf{T}{=}\mathbf{c}^E\mathbf{S}{-}\mathbf{e}_t\mathbf{E},$$

$$\mathbf{D} = \mathbf{e}\mathbf{S} + \epsilon^S\mathbf{E}.$$

With $\mathbf{T}$ and $\mathbf{D}$ independent (strain-voltage form)

$$\mathbf{S} = \mathbf{s}^{\mathbf{E}}\mathbf{T} + \mathbf{g}_t\mathbf{D},$$

$$\mathbf{E} = -\mathbf{g}\mathbf{T} + \beta^T\mathbf{D}.$$

The variable $\mathbf{g}$, $\mathbf{h}$, $\mathbf{e}$, and $\mathbf{d}$ are piezoelectric constants when prefaced with the specific form (stress-charge, strain-charge, stress-voltage, or strain-voltage). Here $\mathbf{d}$ is the piezoelectric strain constant and $\mathbf{e}$ is the piezoelectric stress constant.

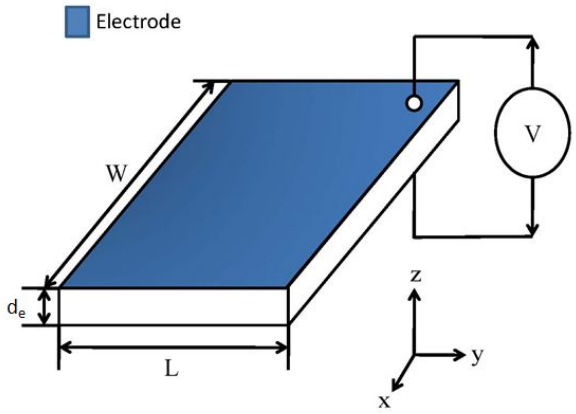

Figure 2.4: Thickness vibrator poled in z direction

2.1.4 Unloaded Thickness Vibrator

Consider the case of a thickness vibrator with electrodes applied on planes perpendicular to the poled direction as illustrated in Figure 2.4. Whenever plane-wave conditions exist, the particle displacement is considered one dimensional and occurs in the direction of the wave motion through the specimen [20]. The width W and length L are assumed to be much greater than the thickness t allowing the displacements perpendicular to the poled direction to be neglected which represents the plane strain condition. If the electrodes are assumed to be equi-potential, this leaves D_3 as the only non-zero component of the vector $\mathbf{D}$. When these assumptions are applied to Eqs. 2.6 and 2.7 one finds

$$T_3 = c_{33}^D S_3 - h_{33} D_3, \tag{2.8}$$

$$E_3 = -h_{33} S_3 + \beta_{33}^S D_3. \tag{2.9}$$

Where the superscript D indicates a constant obtained for a constant electric displacement and S a constant strain [7].

Assuming that the displacement consists uniquely of time-harmonic motion along the x_3 axis and is denoted as δ_3, Eq. 2.10 can be used to describe the field since it satisfies the wave equation for motion in the piezoelectric material

$$\delta_3 = (A \sin kx_3 + B \cos kx_3)e^{j\omega t}. \tag{2.10}$$

Where the wave number, k, is equal to the angular frequency, ω, divided by the speed of propagation of longitudinal waves in the thin plate with a constant electric displacement c_e^D.

$$c_e^D = \sqrt{\frac{c_{33}^D}{\rho}}.$$

Assuming the electric displacement in the x_3 direction is spatially uniform within the material for any instant in time once can write, $\mathbf{D} = D_3 = D_0 e^{j\omega t}$, to describe the electric displacement. Given displacement only along the x_3 axis

$$\mathbf{S} = S_3 = \frac{\partial u_3}{\partial x_3} = k(A \cos kx_3 - B \sin kx_3)e^{j\omega t}. \tag{2.11}$$

While the transducer is unloaded, $T_3 = 0$ at $x_3 = 0$ and that the element thickness is given by d_e. Equation 2.8 can be employed to find the unknown constants A and B,

$$A = \frac{h_{33} D_0}{c_{33}^D k}, \tag{2.12}$$

$$B = -\frac{h_{33} D_0}{c_{33}^D k} \tan(\frac{k d_e}{2}). \tag{2.13}$$

A solution for the electric field can then be found by substituting Eqs. 2.12 and 2.13 into Eq. 2.9 to give

$$E_3 = -\frac{h_{33}^2 D_0}{c_{33}^D}\left[\cos kx_3 + \tan(\frac{kd_e}{2})\sin kx_3\right] e^{j\omega t} + \beta_{33}^S D_0 e^{j\omega t}. \tag{2.14}$$

The potential between the electrodes is given by integrating Eq. 2.14 with respect to z from 0 to d_e

$$V = \int_0^{d_e} E_3 dx_3. \tag{2.15}$$

Substituting 2.14 into Eq. 2.15 and performing the integration yields the following expression for the potential difference between the top and bottom electrodes

$$V = \left[-\frac{h_{33}^2 D_0}{c_{33}^D k}\left(\sin kd_e + \tan\left(\frac{kd_e}{2}\right)(1-\cos kd_e)\right) + \beta_{33}^S D_0 d_e\right] e^{j\omega t}. \tag{2.16}$$

Since the electric displacement is a measure of the charge density of the material, it is possible to find the current, I, as the partial derivative of the electric displacement with respect to time

$$I = j\omega LW D_0 e^{j\omega t}. \tag{2.17}$$

The electrical impedance, Z_E, is a measure of the opposition a circuit presents to current flow when a potential is imposed across the circuit. In general it is expressed as the complex ratio of the voltage to the current

$$Z_E = \frac{V}{I} = \frac{\left[-\frac{h_{33}^2 D_0}{c_{33}^D k}\left(\sin kd_e + \tan\left(\frac{kd_e}{2}\right)(1-\cos kd_e)\right) + \beta_{33}^S D_0 d_e\right]\exp(j\omega t)}{j\omega LW D_0 e^{j\omega t}}.$$

The impedance can be simplified by using the clamped capacitance C_0 and thickness mode electromechanical coupling factor K_d^2 as described by Wilson [7]

$$C_0 = \frac{\epsilon LW}{d_e} = \frac{LW}{\beta d_e},$$

$$K_d^2 = \frac{h_{33}^2}{\beta_{33}^S c_{33}^D} = \frac{h_{33}^2 \epsilon_{33}^S}{c_{33}^D}.$$

This allows for the impedance to be rearranged to better illustrate the parameter limits

$$Z_E = \frac{jK_d^2}{\omega C_0} \frac{\tan\left(\frac{kd_e}{2}\right)}{\frac{kd_e}{2}} - \frac{j}{C_0 \omega}. \tag{2.18}$$

Notice that resonance occurs when the imaginary part of the impedance is equal to zero

$$\frac{\tan\left(\frac{kd_e}{2}\right)}{\frac{kd_e}{2}} = \frac{1}{K_d^2},$$

and anti-resonance occurs at the frequency of infinite impedance

$$\frac{kd_e}{2} = \frac{(2n-1)\pi}{2}.$$

Since $k = \omega / c_e^D$, where c_e^D is the material sound speed along the z-axis with a constant electric displacement, this leads to an anti-resonance frequency

$$f_a = \frac{(2n-1)c_e^D}{2t},\ n = 1, 2, 3....$$

Using the properties for a Navy Type Ceramic PZT 4 from Wilson [7] with a thickness of $t = 2\,\text{mm}$, the first f_a occurs at a frequency of 1.15×10^6 Hz. Plotting the impedance from Eq. 4.14 and phase with respect to frequency yields Figure 2.5.

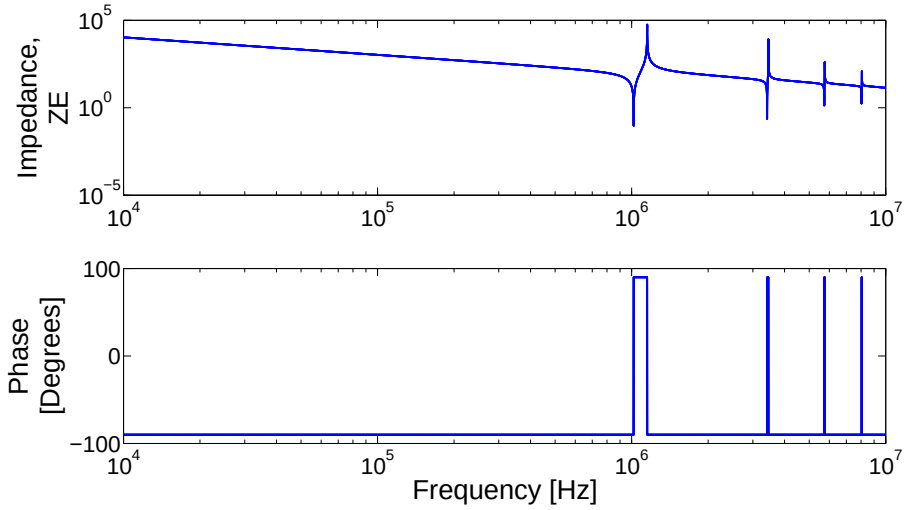

Figure 2.5: Unloaded impedance response

2.2 Examination of Special Cases

With this information, a simple sonar transducer design consisting of a piezoelectric element and a backing or front layer can be easily analyzed. A thickness vibrator in particular can be utilize when the external surface forces are not negligible. This transducer, whose length and width are much larger than the thickness, can be approximated with a 2D system of layers. The receive sensitivity M, of this system is then the ratio of the output voltage to the input pressure P_i,

$$M = \frac{V}{P_i}. \tag{2.19}$$

To determine the voltage output, the incident pressure first needs to be related to the velocity at each transducer face. By looking at a number of special cases the necessary components for a generic algorithm is realized that allows for analysis of more complex systems.

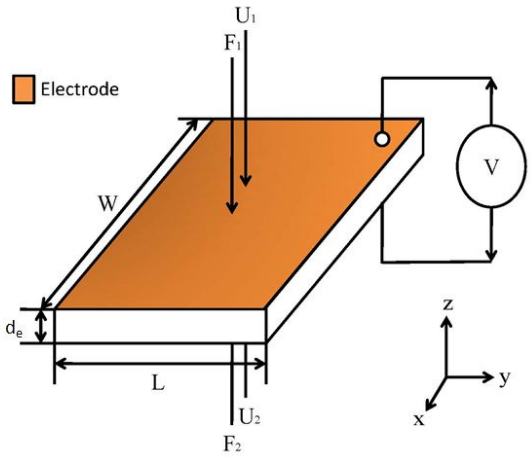

Figure 2.6: Submerged thickness transducer notation

2.2.1 Submerged Transducer

The first system considered is a thickness vibrator submerged in an infinite fluid with a plane pressure wave traveling in the x_3 direction. Assuming the deflection δ_{x_3} to be time harmonic allows the deflection, velocity and acceleration to be represented as

$$\delta_{x_3} = \delta_0 \exp(j\omega t),$$

$$\dot{\delta}_{x_3} = j\omega\delta_0 \exp(j\omega t),$$

$$\ddot{\delta}_{x_3} = -\omega^2\delta_0 \exp(j\omega t).$$

Rewriting δ_{x_3} in terms of the velocities at the transducer's faces U_1 and U_2 results in

$$\delta_e = \int \dot{\delta}_e dt = \frac{\delta_{x_3}}{j\omega} = \frac{(U_1 - U_2)}{j\omega}. \tag{2.20}$$

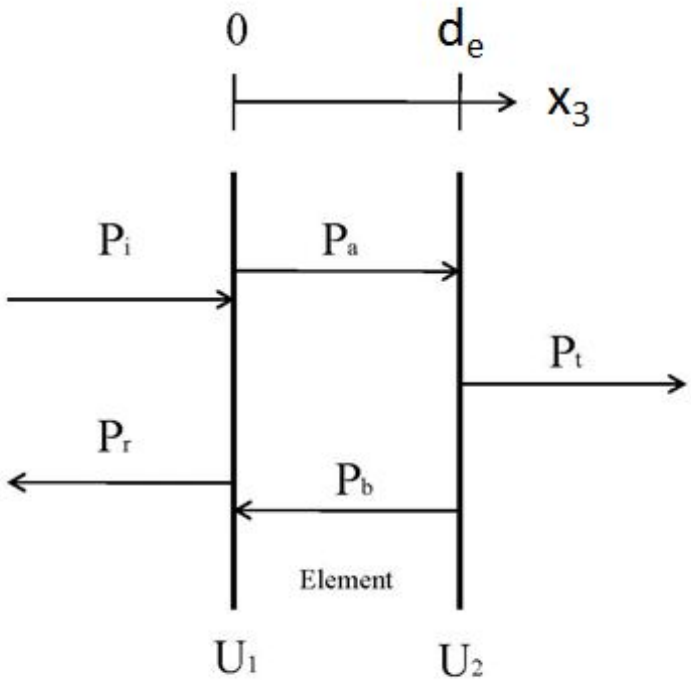

Figure 2.7: Components of the acoustic pressure field.

Again, assuming the electric displacement in the x_3 direction is uniform throughout the material, $D = D_3 = D_0 e^{j\omega t}$. By substituting Eqs. 2.11 and 2.20 into Eq. 2.14 allows for the voltage from Eq. 2.15 to be expressed as

$$V = \frac{-jh_{33}}{\omega} (U_1 - U_2) . \tag{2.21}$$

The velocity can now be related to the incoming pressure using acoustic impedance. Specific acoustic impedance is the ratio of pressure to particle velocity at a point

$$Z = \frac{P}{U}. \tag{2.22}$$

To determine the velocities, the pressure needs to be known at both the front and back face of the element. Using the notation in Figure 2.7 and assuming a constant

pressure at each interface yields $P_i + P_r = P_a + P_b$. Normalizing with the incoming pressure, P_i, yields the following notation $\frac{P_r}{P_i} = R$, $\frac{P_a}{P_i} = A$, $\frac{P_b}{P_i} = B$ and $\frac{P_t}{P_i} = T$. The above equations may then be used to express continuity of pressure at $x_3 = 0$ and $x_3 = d_e$ with Eqs. 2.23 and 2.24 respectively.

$$1 + R = A + B, \tag{2.23}$$

$$A \exp(-jk_e d_e) + B \exp(jk_e d_e) = T. \tag{2.24}$$

Here the subscript e indicates a property of the element. For example k_e is the wave number in the element and d_e is the element thickness. The velocity to the left and right of each face is also balanced and can be found by solving Eq. 2.22 for the velocity in terms of the pressure coefficients and substituting the result into Eqs. 2.23 and 2.24

$$1 - R = \frac{Z_0}{Z_e}(A - B), \tag{2.25}$$

$$(A \exp(-jk_e t) - B \exp(jk_e t)) = \frac{Z_e}{Z_0} T. \tag{2.26}$$

Where Z_e is the characteristic impedance of the element and Z_0 is the characteristic impedance of the surrounding medium. A, B, R and T describe the components of the pressure field normalized by the incident pressure and can be determined using

the set of linear equations that results from Eqs. 2.23–2.26.

$$\begin{bmatrix} 1 & 1 & -1 & 0 \\ \frac{Z_0}{Z_e} & -\frac{Z_0}{Z_e} & 1 & 0 \\ \exp\left(-jk_e d_e\right) & \exp\left(jk_e d_e\right) & 0 & -1 \\ \exp\left(-jk_e d_e\right) & -\exp\left(jk_e d_e\right) & 0 & -\frac{Z_e}{Z_0} \end{bmatrix} \begin{bmatrix} A \\ B \\ R \\ T \end{bmatrix} = \begin{bmatrix} 1 \\ 1 \\ 0 \\ 0 \end{bmatrix}. \tag{2.27}$$

The face velocities can then be determined by dividing the pressure on each face by the impedance. Remember that the equations above were normalized with the incoming pressure

$$U_1 = \left(\frac{1-R}{Z_0}\right) P_i = \left(\frac{A-B}{Z_e}\right) P_i, \tag{2.28}$$

$$U_2 = \left(\frac{T\exp\left(-jk_e d_e\right)}{Z_0}\right) P_i = \left(\frac{A\exp\left(jk_e t\right) - B\exp\left(jk_e d_e\right)}{Z_e}\right) P_i. \tag{2.29}$$

Now the response as described in Eq. 2.19 can be determined by substituting Eqs. 2.28 and 2.29 into Eq. 2.21 and dividing by the incoming pressure

$$M = \frac{-jh_{33}}{\omega} \frac{(U_1 - U_2)}{P_i}. \tag{2.30}$$

Response functions are typically illustrated with a logarithmic unit of measurement, the decibel (dB). This is the ratio of the actual sensitivity to a reference sensitivity, in this case $M_{ref} = 1\,\mathrm{V}/\mu\mathrm{Pa}$. The response can be expressed in decibels by using

$$M_{\mathrm{dB}} = 20\log_{10}\left(\frac{M}{M_{ref}}\right). \tag{2.31}$$

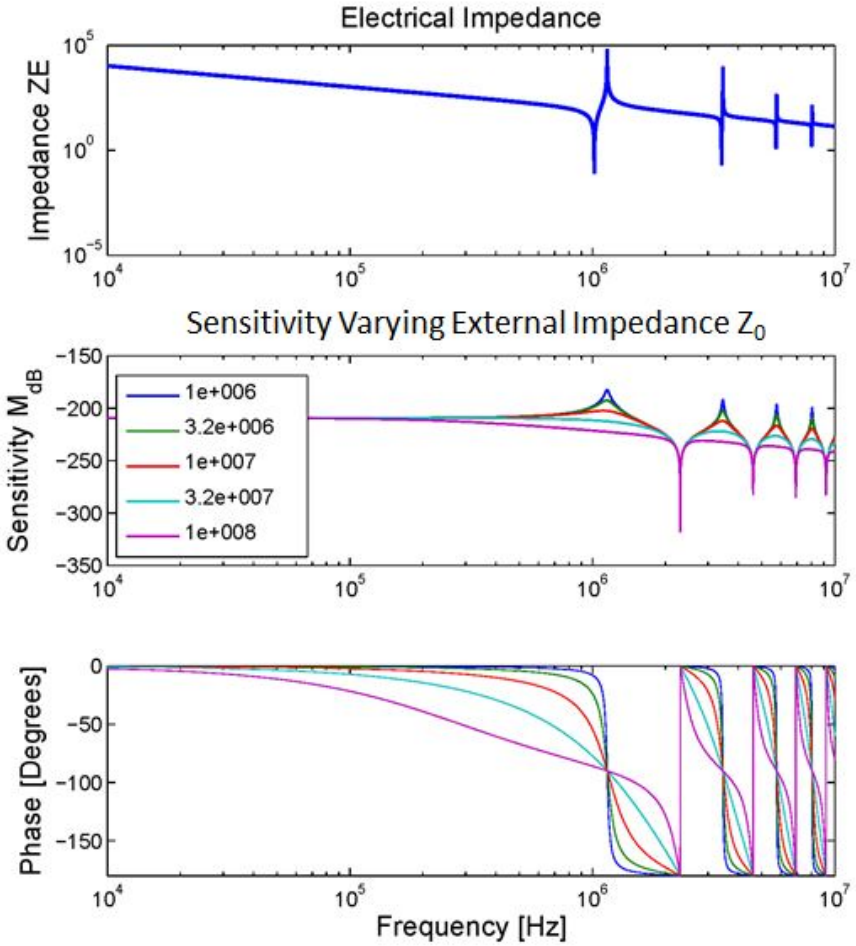

Figure 2.8: Element of 2 mm thickness submerged in fluids with varying Z_0.

In Figure 2.8 the electrical impedance, response, and phase of a 2 mm thick PZT4 element have been plotted as a function of frequency. The response has a sensitivity resonance when the reflection coefficient R of the element vanishes and the transmission coefficient T approaches -1. This occurs when the thickness corresponds to half wavelengths

$$f_r = \frac{(2n-1)\, c_e^D}{2d_e},\ n = 1, 2, 3.... \tag{2.32}$$

The response experiences anti-resonance when R vanishes and when T approaches $+1$ or when the thickness corresponds to a wavelength

$$f_{as} = \frac{n c_e^D}{d_e},\ n = 1, 2, 3.... \tag{2.33}$$

Note that the response's resonances correspond to the electrical anti-resonance, or when the electrical impedance goes to infinity. Taking the limit as the frequency goes to 0, we can see the amplitude is equal to the constant $h_{33} d_e / c_{33}^D$. As illustrated by Figure 2.8 the sharpness of the response's peaks are dependent on the external characteristic acoustic impedance.

2.2.2 Rigid Termination

A transducer backed by an infinitely thick rigid plate is simpler to solve than the submerged transducer because there is no motion at $x_3 = d_e$ and therefore one less variable to determine. A rigid termination reflects any incoming pressure reducing P_T to zero. This reduces Eq. 2.26 to

$$\left(A \exp\left(-jk_e d_e\right) - B \exp\left(jk_e d_e\right)\right) = 0,$$

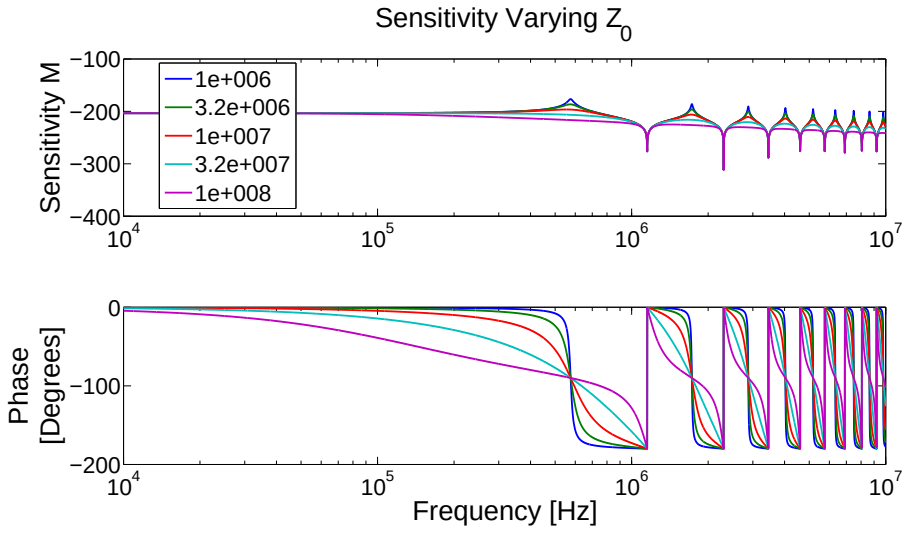

Figure 2.9: Element of 2 mm thickness rigidly backed and submerged in fluids with varying Z_0.

and simplifies Eq. 2.27 to

$$\begin{bmatrix} 1 & 1 & -1 \\ \frac{Z_0}{Z_e} & -\frac{Z_0}{Z_e} & 1 \\ \exp\left(-jk_e d_e\right) & -\exp\left(jk_e d_e\right) & 0 \end{bmatrix} \begin{bmatrix} A \\ B \\ R \end{bmatrix} = \begin{bmatrix} 1 \\ 1 \\ 0 \end{bmatrix}.$$

Following the steps above from Eq. 2.28 to Eq. 2.31 yields the response as illustrated by Figure 2.9.

The response has a resonance when $R = -1$. This occurs at thicknesses that correspond with quarter wavelengths

$$f_r = \frac{(2n-1)\, c_e^D}{4 d_e},\ n - 1, 2, 3.... \tag{2.34}$$

The response has an anti-resonance when the reflection approaches $+1$ or

$$f_a = \frac{n c_e^D}{d_e}. \tag{2.35}$$

It is interesting to note that there are twice as many resonances for a rigidly backed

transducer as compared to the submerged case due to the thickness corresponding to quarter wavelengths as opposed to half wavelengths. Also, every other resonance in the submerged case now corresponds to an anti-resonance in the rigidly backed case. This illustrates the need to carefully consider the backing choice when designing a transducer.

Taking the limit as the frequency approaches zero, we can see the amplitude is equal to the constant $2h_{33}d_e/c_{33}^D$, or twice the response of the submerged transducer. This doubling in response is similar to the pressure doubling seen at a rigid wall. Finally, notice that the curve is perfectly damped when the outside impedance approaches the element impedance, $Z_0 \to 3.45 \times 10^7$. When the outside impedance is less than the element, the response is under-damped leading to a sharper response.

2.2.3 Generic Impedance Backing

The surface impedance at the front and back surface of the transducer can be determined using the impedance translation theorem for a transducer backed by a material with a generic impedance Z_b, a known thickness d_b, and terminated with a known impedance. In general, this allows for the specific acoustic impedance to be determined at the end of an arbitrary number of layers as long as the impedance and thicknesses of the material is known along with the termination impedance. As illustrated in Figure 2.10, if we assume a rigid termination a distance d_b behind the transducer the acoustic impedance at the back surface, Z_2, can be found by analyzing the pressure and velocity in the backing.

For a rigid termination the pressure is reflected perfectly and can be expressed as

$$P = C\left(\exp\left(-jk_b d_b\right) + \exp\left(jk_b d_b\right)\right),$$

where C is a constant. Using Euler's identity, this can be simplified to

$$P = 2C\cos\left(k_b d_b\right).$$

Similarly using the impedance relation, Eq. 2.22, the velocity can be simplified to

$$U = j\frac{2A}{Z_b}\sin\left(k_b d_b\right).$$

The impedance at the back interface is then the ratio of the above pressure and velocity

$$Z_2 = -jZ_b\cot\left(k_b d_b\right).$$

To find the impedance at the front face, the ratio of the pressure and velocity inside the layer is again examined [21]

$$Z_1 = Z_e\left[\frac{Z_2\cot\left(k_e d_e\right) + jZ_e}{jZ_2 + Z_e\cot\left(k_e d_e\right)}\right].$$

Where $Z_e = \rho c_e^D = \sqrt{\rho c_{33}^D}$ and $k_e = \omega/c_e^D$. Since we know the impedance at the back of the element, again we do not need to solve for T. Our third equation is instead given by

$$Z_2 = \frac{\text{pressure}}{\text{velocity}} = \frac{A\exp\left(-jk_e d_e\right) + B\exp\left(jk_e d_e\right)^{jk_e d_e}}{\frac{A}{Z_e}\exp\left(-jk_e d_e\right) - \frac{B}{Z_e}\exp\left(jk_e d_e\right)},$$

or

$$\left(\frac{Z_2}{Z_e} - 1\right)A\exp\left(-jk_e d_e\right) - \left(\frac{Z_2}{Z_e} + 1\right)B\exp\left(jk_e d_e\right) = 0. \tag{2.36}$$

Now variables A, B, and R can be solved by combining Eqs. 2.23, 2.25 and 2.36

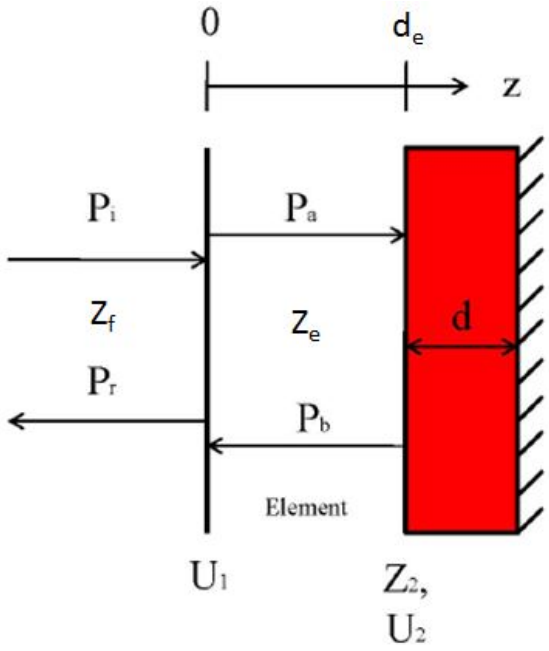

Figure 2.10: Element impedance backed with a rigid end condition

$$\begin{bmatrix} 1 & 1 & -1 \\ \frac{Z_0}{Z_e} & -\frac{Z_0}{Z_e} & 1 \\ \left(\frac{Z_2}{Z_e}-1\right)\exp\left(-jk_ed_e\right) & -\left(\frac{Z_2}{Z_e}+1\right)\exp\left(jk_ed_e\right) & 0 \end{bmatrix} \begin{bmatrix} A \\ B \\ R \end{bmatrix} = \begin{bmatrix} 1 \\ 1 \\ 0 \end{bmatrix}.$$

Following the steps above from Eq. 2.28 to Eq. 2.31 yields the response as illustrated by Figure 2.11 These results are similar to a combination of the rigid and submerged cases. At resonance, the peaks occur at the same frequency of the submerged case when the backing impedance is less than the element impedance. When the backing impedance is equal to the element impedance a perfectly damped response results. As the backing impedance increases the peaks occur at the same frequencies as discussed in the rigid cases.

In the low frequency limit the response switches between the submerged and rigid case as the backing impedance goes from less than to greater than the external

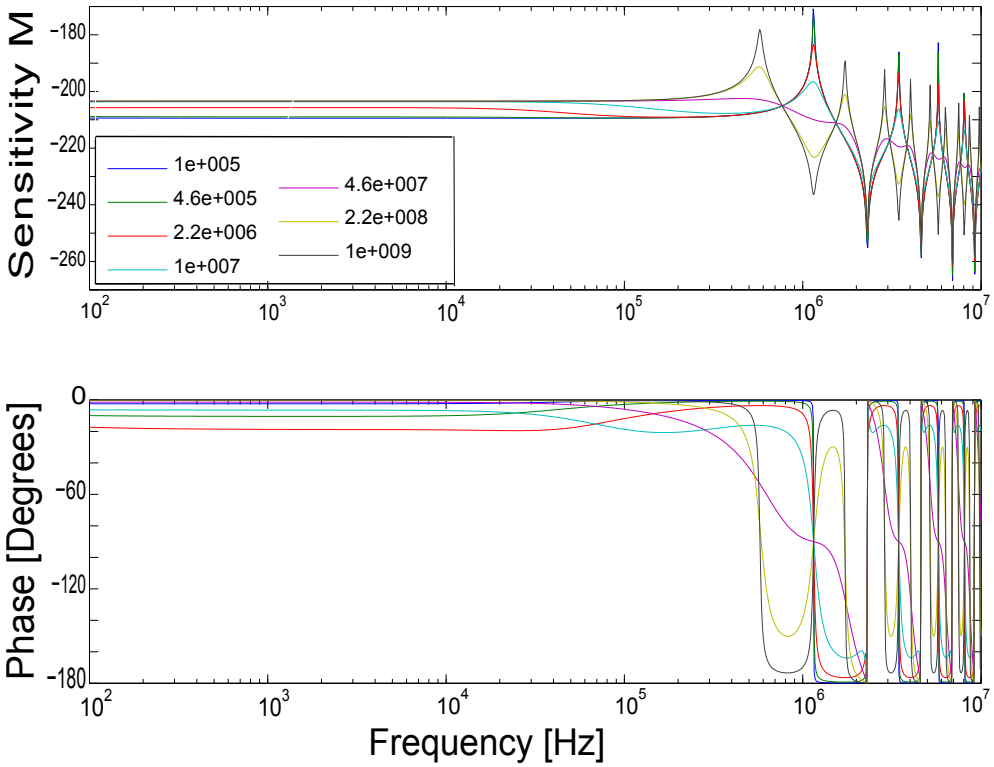

Figure 2.11: Element of 2 mm thickness backed with a varying impedance Z_b of 3 mm and a fixed $Z_0 = 1.5 \times 10^6$.

fluid impedance. This is an important result because a doubling in voltage response can be obtained at low frequencies when the backing impedance is greater than the external impedance and not the element impedance as is often cited in literature.

2.3 Parametrization

In Section 2.2.1, the response of a thickness vibrator was determined as a function of the external impedance. In this section, the effects of changing the element material type, thickness and backing thickness are investigated. Again, the effects of the system parameters on the response are illustrated and it is easy to see how choosing the wrong backing parameters when operating near resonance could result in poor acoustical performance.

2.3.1 Navy Transducer Materials

The commonly used materials considered are the Navy Type Ceramics PZT 4, PZT 5A and CERAMIC B [22, 7]. Varying the piezoelectric ceramics should not change the response shape, but instead should shift the curves and effect the low frequency limit due to the varying sound speed and densities. These shifts are illustrated for the submerged case previously discussed in Section 2.2.1 in Figure 2.12. All other trends discussed previously are maintained.

2.3.2 Transducer Thickness

Varying the thickness of the element also maintains the shape of the response curves while shifting the resonances and low frequency limit as described in equations 2.32, 2.33, 2.34 and 2.35. Figure 2.13 illustrates the shifting response as the thickness is increased.

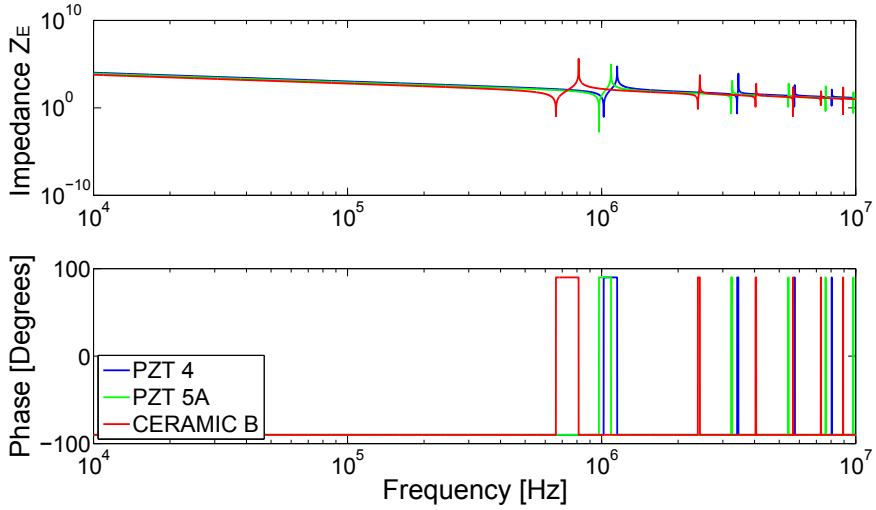

Figure 2.12: Thickness vibrator response in air with varying ceramic types.

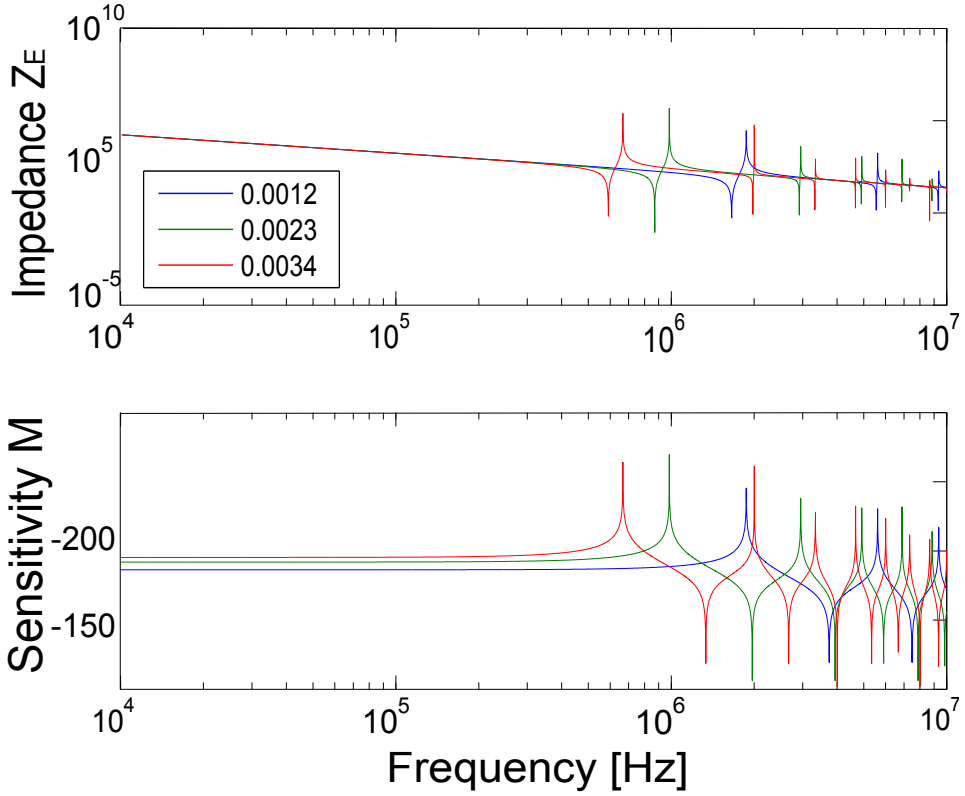

Figure 2.13: Element response in air with varying element thickness d_e [m].

2.3.3 Backing Thickness

By varying the thickness of the backing layer(s), the effective impedance can be increased or decreased. For example a thin backing has a negligible effect on the impedance while a thick backing significantly effects the response. Usually for a thin or thick backing in the low frequency limit this results in the cases discussed above for a rigid or submerged response, respectively. As seen in Figure 2.11, the amplitude of the low frequency limit is determined by the ratio of the backing versus external fluid impedance. Since the backing is assumed to be mounted on a rigid plate, as the backing thickness decreases the response approaches the rigid case. An interesting response results when the backing impedance is greater than the external fluid, yet less than the element. As seen in Figure 2.14, the resonance peaks shift from the rigid to pressure release case as the thickness varies from negligible to 10 cm.

To validate these models, they are compared to equivalent cases using finite element modeling software. Agreement between those two algorithms provided the base for developing a generic model that is independent of the layer quantity, thickness and material.

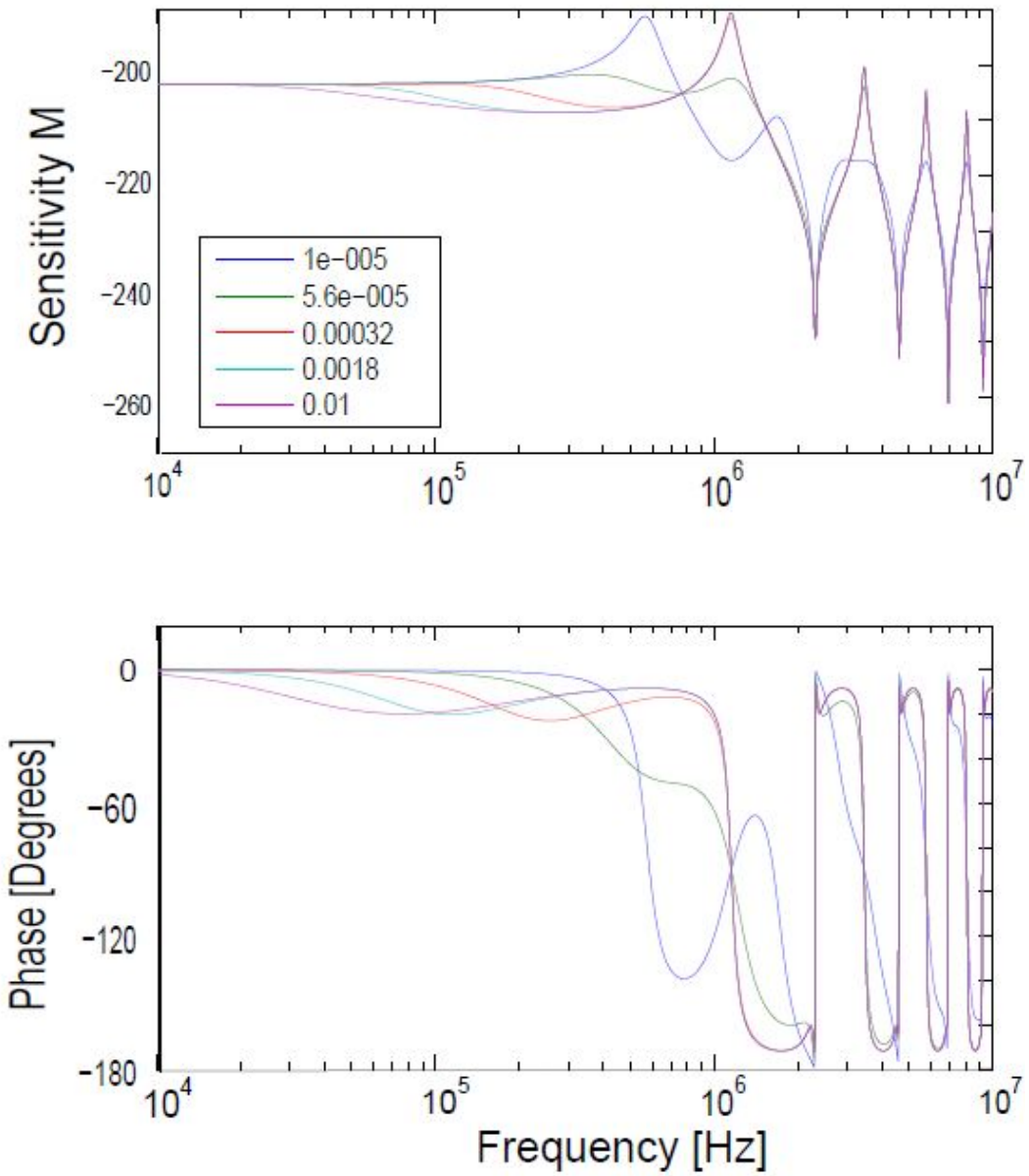

Figure 2.14: The sensitivity $\left[\text{dB re } \frac{1\text{V}}{\mu\text{m}}\right]$ of a thickness vibrator surrounded by air with backings of various thicknesses d_b [m].

Chapter 3

FEM Validation

Modeling the system using finite element modeling (FEM) software is useful for validating the analytical model described in the previous chapter before moving on to more complex examples. The finite element method uses numerical techniques to find approximate solutions to partial differential equations. To accomplish the validation, the commercial package Comsol was used, but the results given here should be the same regardless of software package. The objective of this section is to demonstrate agreement between the FE and analytical models for simple cases thereby establishing a benchmark for the analytical algorithm. Every case described in this paper uses the Comsol 2D Acoustics Piezo Plane Strain and Pressure Acoustics modules for which a detailed explanation can be found in Appendix A. To cover a wide variety of potential systems and increase the assurance level in the algorithm, multiple scenarios were considered. These scenarios consisted of a submerged transducer mounted to an impedance backing, mounted to a rigid backing, and sandwiched between an impedance backing and a front layer.

3.1 Submerged Transducer

For a submerged transducer, the piezoelectric layer is be sandwiched between two layers of the same external fluid. One fluid layer has a pressure applied at the top and the other has a Perfectly Matched Layer (PML) attached to the bottom. In order

to approximate an infinite acoustic domain in a FEM, it is insufficient to just impose just a condition of infinity at a boundary, instead a PML allows for the emulation of the Sommerfeld radiation condition such that no energy is radiated from infinity back into the system [23]. The PML utilizes a modified wave equation that is impedance matched to the adjoining domain and increases the absorption with distance. This results in waves that are absorbed only in the outward bound direction. For correct implementation of a PML, care needs to be taken to ensure that the PML is thick enough to completely absorb the pressure wave since any energy that reaches the boundary will be reflected back into the system.

The FEM implemented for this system consists of multiple layers as illustrated in Figure 3.1. The thickness, d, of the fluid layers depends on the sound velocity, c, in each material and the minimum frequency, f_{min}, of interest. A common rule of thumb for the layer thickness thickness is five wavelengths at the lowest frequency of interest [24] or

$$d = 5\lambda = 5\frac{c}{f_{min}}.$$

This guarantees the wave can be fully defined by the time it reaches the piezoelectric layer. For example, if the first layer is composed of water and the lowest frequency of interest is 500 kHz the minimum thickness is $5 \times 1500/500 \times 10^3$ or 0.0150 meters. This rule of thumb works well for layers in which the full field description is desired. The PML, on the other hand, only needs to absorb the pressure field completely making a small thickness possible. In this work, it was observed that setting the PML thickness to one wavelength worked well in every case where it was needed.

Since only propagation in the z direction is of interest, a minimal width is desired to guarantee lateral modes are not generated. Therefore, only one element is applied along the width axis approximating a 1D problem as modeled in the analytical

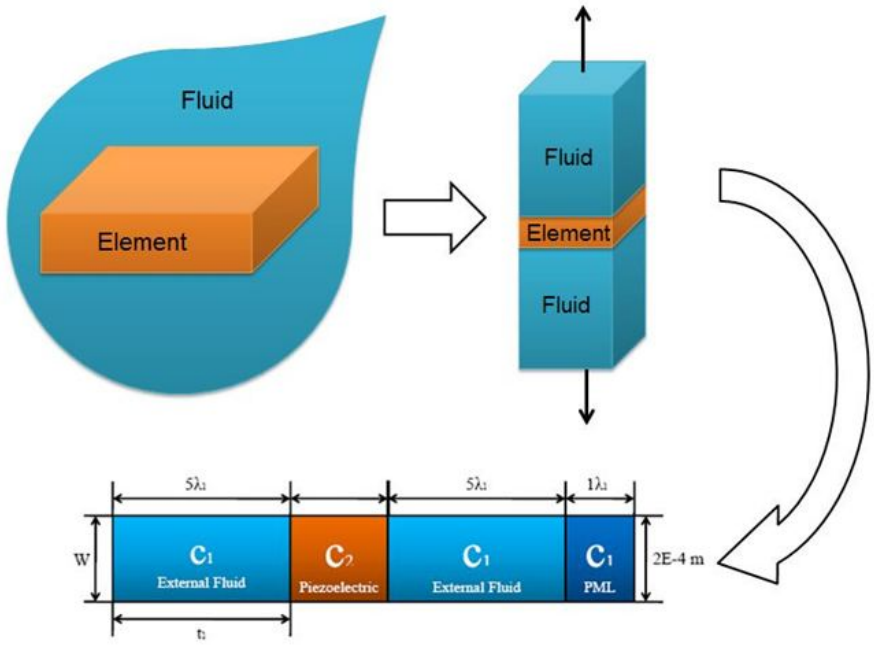

Figure 3.1: Illustration of the submerged transducer as it is represented in the FEM software.

code. We chose to make the width 2×10^{-4} m wide to facilitate selection of the boundaries. In this work, the guidelines mentioned above for thickness and width worked well when applied to every case considered.

After setting the boundary conditions and applying a pressure at the front face the sensitivity in dB is given by

$$M_{\mathrm{dB}} = 20 \log_{10} \left(\frac{V/p_i}{M_{ref}} \right),$$

where M_{ref} is $1\,\mathrm{V}/\mu\mathrm{Pa}$ and p_i [Pa] is the input pressure. The boundary conditions are illustrated in Figure 3.2 where the cross hatching represents a rigid boundary and the circles a rolling boundary. A fixed boundary prevents movement in all directions

$$u_1 = u_2 = u_3 = 0.$$

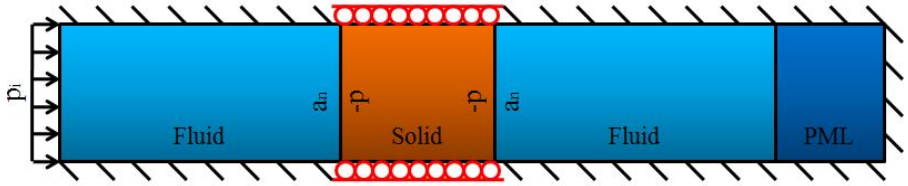

Figure 3.2: Illustration of the submerged transducer boundary conditions where the hash marks indicate a rigid boundary and the circles indicate a roller boundary.

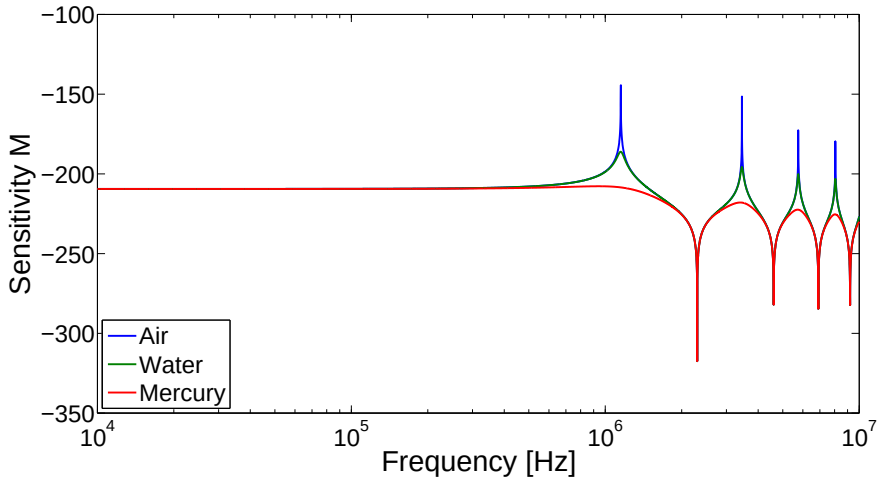

Figure 3.3: FE model predictions of the submerged transducer response for three external impedances detailed in Table 3.3.

A rolling boundary however, only prevents movement perpendicular to the applied surface. For example, a roller boundary applied to a surface described by x_1 and x_2 would result in no movement along x_3. The array of arrows on the left indicate a uniform time-varying pressure, $p = p_i \exp(j\omega t)$, applied to that boundary edge. Figure 3.3 plots this value at a point on the surface of the piezoelectric layer with the fluid properties detailed in Table 3.1. The frequency range was selected to illustrate the resonance, anti-resonance and low frequency asymptotic behavior. For the submerged case, the resonance occurs at 1.151 MHz, the anti-resonance at 2.302 MHz and the low frequency receive sensitivity level is -209.5 dB re 1V/μPa. These values can now be compared to other cases with different terminations, backings and front

Table 3.1: Values used to simulate and external fluid impedance.

Material	Density $\left[\frac{\text{kg}}{\text{m}^3}\right]$	Sound Speed $\left[\frac{\text{m}}{\text{s}}\right]$	Impedance $\left[\frac{\text{kg}}{\text{m}^2\text{s}}\right]$
Air	1.21	343	415
Water	1000	1500	1.5×10^6
Mercury	13600	1450	19.7×10^6

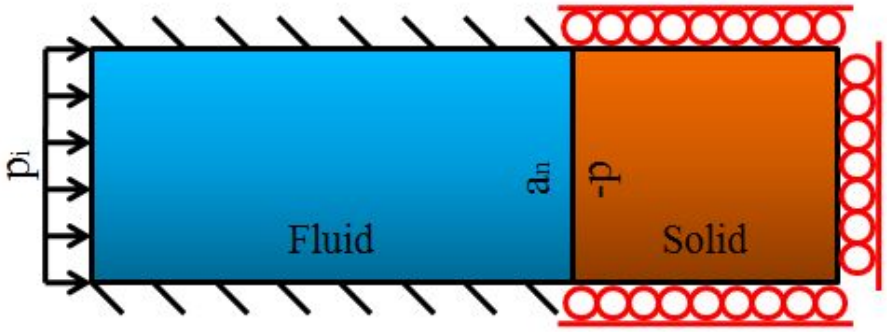

Figure 3.4: Illustration of the rigidly terminated transducer as implemented as a FEM.

layers.

3.2 Rigid Termination

Another simple canonical case of interest is that of a transducer submerged in a fluid whose back face experiences no motion, i.e. it is rigidly terminated. The rigid termination condition can be understood to represent a special case of the submerged condition discussed in Section 3.1 where the impedance at the back face of the piezoelectric domain approaches infinity. This rigid termination is achieved mathematically by setting a zero velocity condition at the surface and results in complete internal reflection in phase with the incident acoustic wave. The FEM model of this case is illustrated in Figure 3.4. The sensitivity as a function of the varying external properties described in Table 3.1 is illustrated in Figure 3.5.

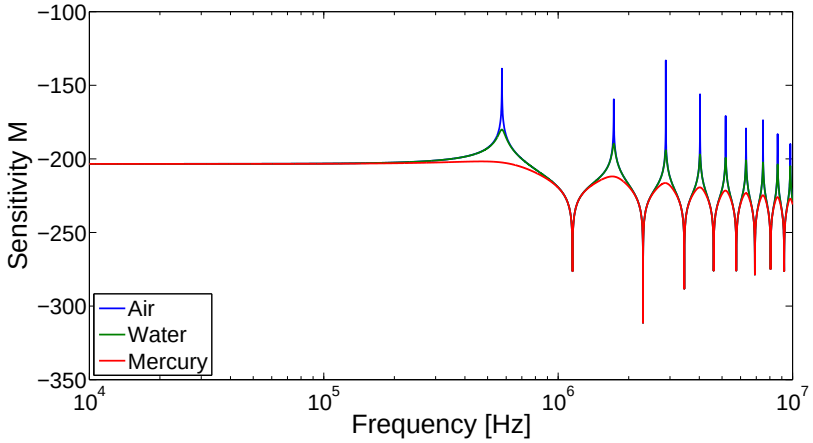

Figure 3.5: FE model predictions of the response of a rigidly backed transducer for the three external impedances detailed in Table 3.1.

Combining Figures 3.3 and 3.5 into Figure 3.6 illustrates the classic 6 dB gain [25] and doubling in number of resonances resulting from a rigid termination. This gain is the result of the entire pressure wave being reflected doubling the effective pressure at the front face at low frequencies. The difference in the low frequency levels and the resonance locations is again illustrative of the importance in proper backing selection.

3.3 Impedance Backing

The rigidly-terminated impedance backings investigated in this section. Impedance backings are more useful than the rigid backing of section 3.2, as it accurately represents the effects of a mounting material. A transducer operating near a backing's resonance has a highly frequency dependent response. If left unchecked, this may lead to an unexpected sensitivity variation. Therefore, it is important to know how the hydrophone is terminated. A model of the impedance backed system is illustrated in Figure 3.7.

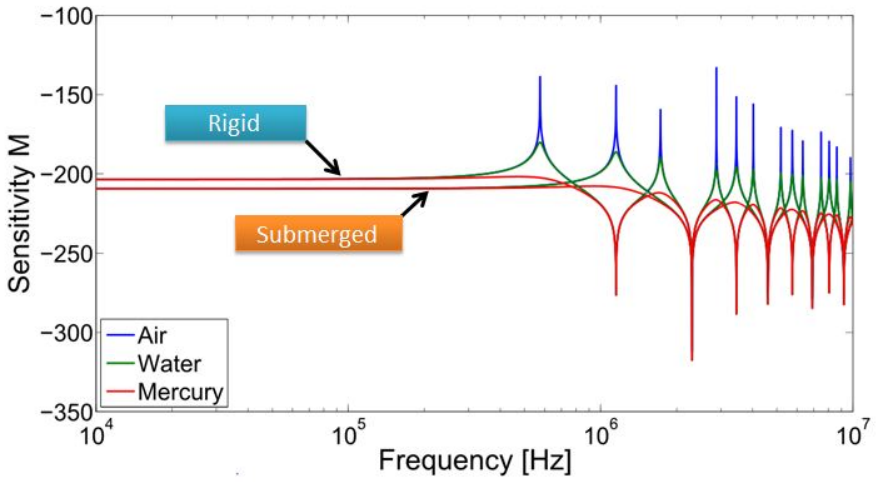

Figure 3.6: Figures 3.3 and 3.5 superimposed to illustrate the different location and number of resonances resulting from the different end conditions as well as differing low frequency sensitivity.

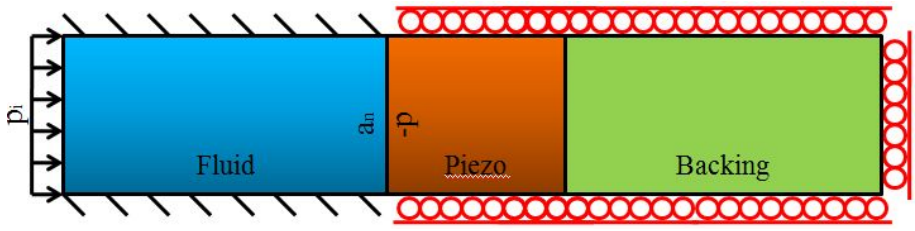

Figure 3.7: Illustration of an impedance backed thickness vibrator with rigid and roller boundary constraints as implemented as a FEM.

Table 3.2: Values to simulate a variety of materials for both backing and front layers. The back layers are 4 mm and the front layers are 2 mm.

Material	Young's Modulus [GPa]	Poisson's Ratio	Density $\left[\frac{\text{kg}}{\text{m}^3}\right]$
Cork	0.032	0	240
Nylon	2	0.3	1150
Steel	195	0.28	7700
Oak	12.4	0.3	630
FR-4	22	0.28	1900

Using the parameters in Table 3.2, Figure 3.8 depicts the sensitivity of a thickness vibrator transducer mounted on various materials 4 mm thick and submerged in water. Note the transition to a rigid termination in the lower frequencies as the wavelength becomes much larger than the backing thickness. Also, note the transition to the rigid resonance as the backing material impedance increases approaching the rigid case. As can be seen, the choice of backing material can have a significant effect on the frequency response.

3.4 Front Layers

A final model examines adding a front layer to the piezoelectric layer. Front layers may be used to protect the transducers from debris, damp out flow noise or smooth out the sensitivity. Whatever the purpose, a material in front of a transducer significantly effects its performance. An impedance-backed transducer with a front layer on top is illustrated in Figure 3.9.

Again using the same materials from Table 3.2, Figure 3.10 displays the sensitivity as a function of frequency. The front layer thickness is kept thin, 2 mm, to avoid completely damping the sensitivity. In Figure 3.10, nylon was used as the backing layer. Notice that cork reflects most of the higher frequency pressure wave before it

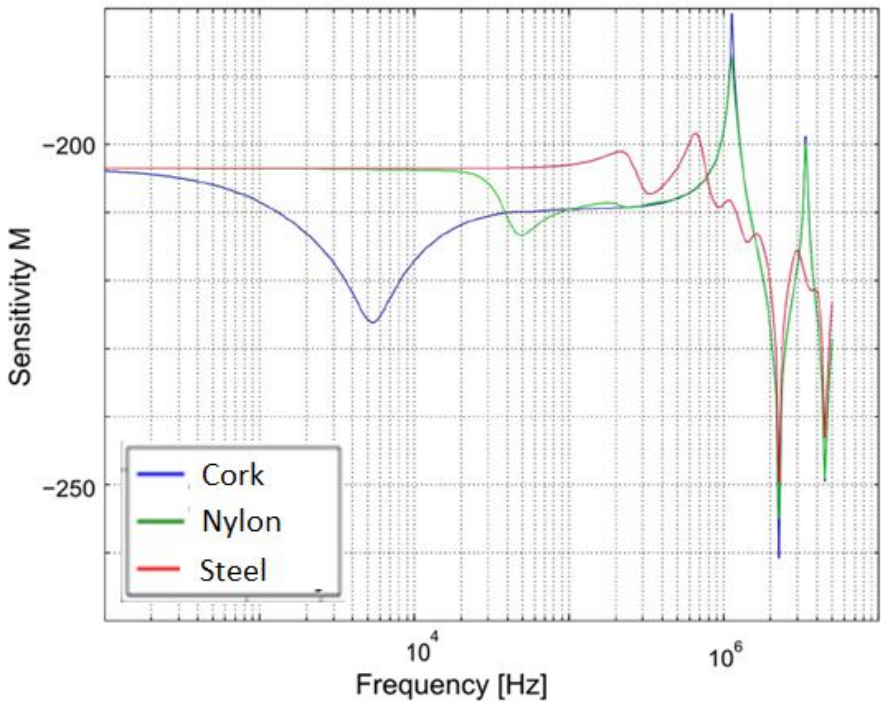

Figure 3.8: FE model predictions for a transducer submerged in water with three different backings 4 mm thick detailed in Table 3.2.

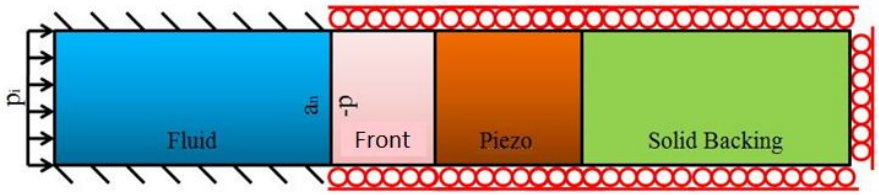

Figure 3.9: Illustration of a front layer and thickness vibrator as implemented as a FEM with hash marks indicating rigid boundary constraints and circles indicating rolling boundary constraints.

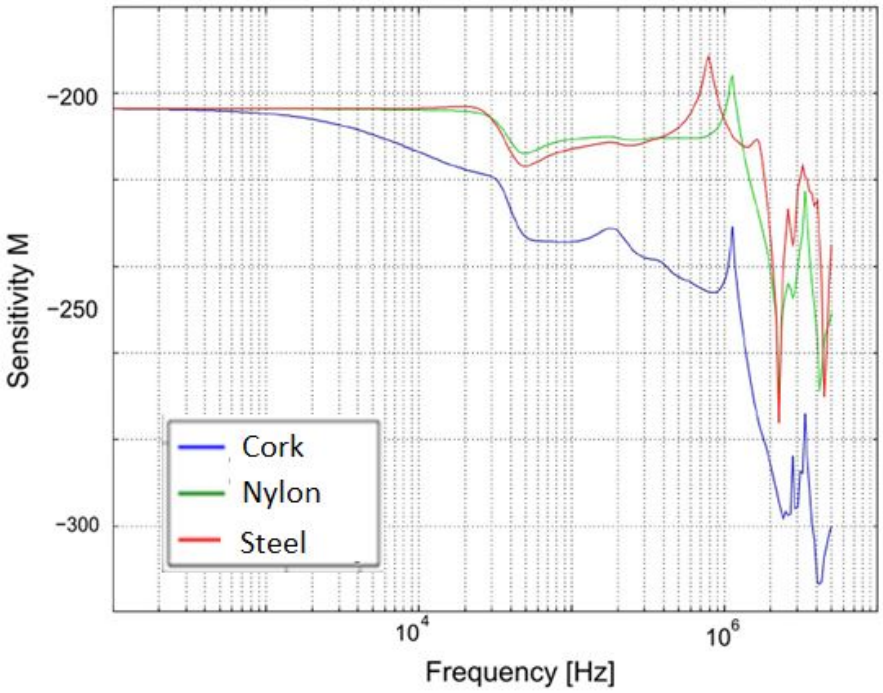

Figure 3.10: FE model predictions for a transducer backed with a 4 mm nylon layer, submerged in water, and with three different 2 mm front layers detailed in Table 3.2

reaches the transducer.

3.5 Comparing Models

The finite element and analytical models yield very similar results. There are very small differences in the frequencies of the resonances that results from different methods used to calculate the sound speed in the piezoelectric layer. Specifically, Comsol uses the full stiffness matrix as described in Chapter 2 to determine the stiffness in the piezoelectric material which is transversely isotropic in nature. The stiffness along the z-axis and density may then be used to calculate the sound speed

$$c = \sqrt{\frac{C_{33}^D}{\rho}}.$$

The analytical model makes use of the Young's Modulus, Poisson's ratio and damping ratio to determine the plane wave modulus

$$C_{33}^D = \frac{E\,(1-\nu)}{(1+\nu)\,(1-2\nu)}\,(1+j\eta)\,.$$

The Young's modulus, Poisson's ratio and damping ratio are used to calculate the velocity because is has been assumed that the piezoelectric material can be approximated as isotropic. Further, these properties are easier to obtain for a variety of materials than the full stiffness matrix. For common materials this step may be skipped if tabulated values can be found for C_{33}^D.

For the comparison, four systems were considered with different backing and front layers. Figure 3.11 compares the sensitivity of a transducer submerged in three different fluids; air, water and mercury. These plots match very well with only slight shift in the resonance frequencies due to slightly different values for the stiffness matrix. Figure 3.12 compares the sensitivity between the two models when a nylon

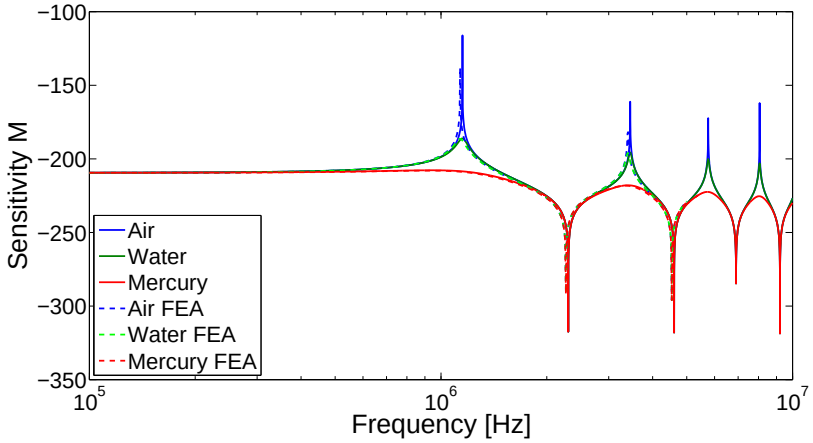

Figure 3.11: Comparing the analytical predictions from the model developed in Chapter 2 with the FE model predictions illustrated in Figure 3.3.

backing has been applied. Again, these plots match well with the same slight shift in the backing resonance frequency and amplitude. Figure 3.13 compares the sensitivity of a system with a element backed by 4 mm of nylon and followed by 4 mm of oak versus an oak and then nylon backing. Flipping the backing illustrates the significant effect of backing layering. For example, at a frequency range of 50 kHz to 100 kHz, the element backed with oak followed by nylon would have reduced response when compared to that of a nylon/oak backing. Finally, Figure 3.14 compares the sensitivity of a system with a nylon backing and FR-4 front layer. FR-4 is a glass reinforced epoxy sheet commonly used in printed circuit boards. As mentioned previously, front layers are sometimes used to broaden the receive sensitivity resonances. One of the simplest methods for achieving this is using a material with an impedance close to the mean of the materials to be matched. FR-4 happens to be similar to a material used in industry to broaden the response of PZT-4 ceramics. The gains may be seen by comparing the resonance peaks in Figures 3.14 and 3.12. Overall, these models compared very well with only slight differences in predicted resonance frequencies.

By developing an analytical model for the transducer response, it is easier to

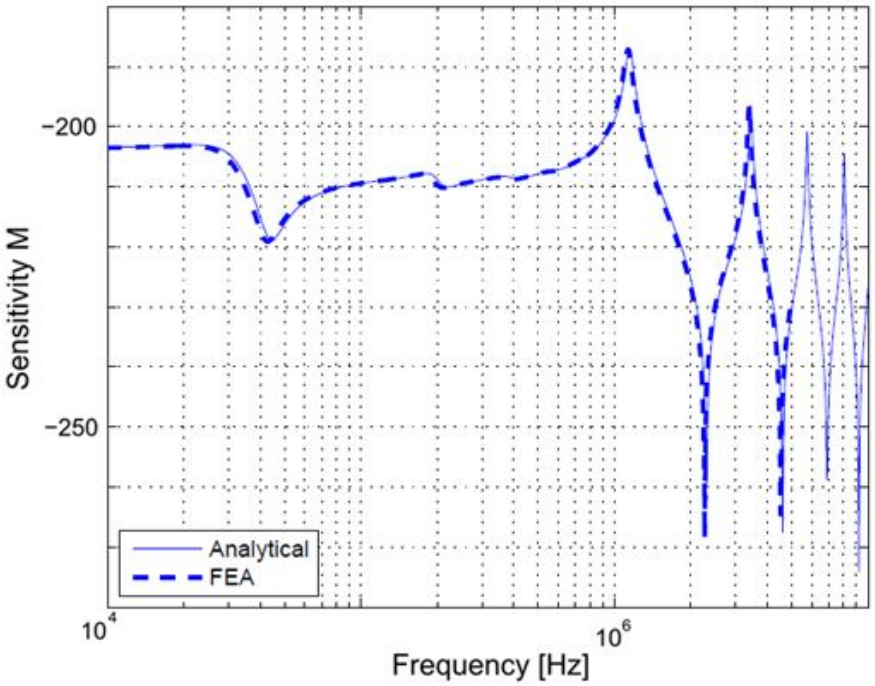

Figure 3.12: Comparing the predictions from the FE model and the analytical model developed in Chapter 2 for a transducer submerged in water with a nylon backing 4 mm thick. The values used to simulate nylon are detailed in Table 3.2.

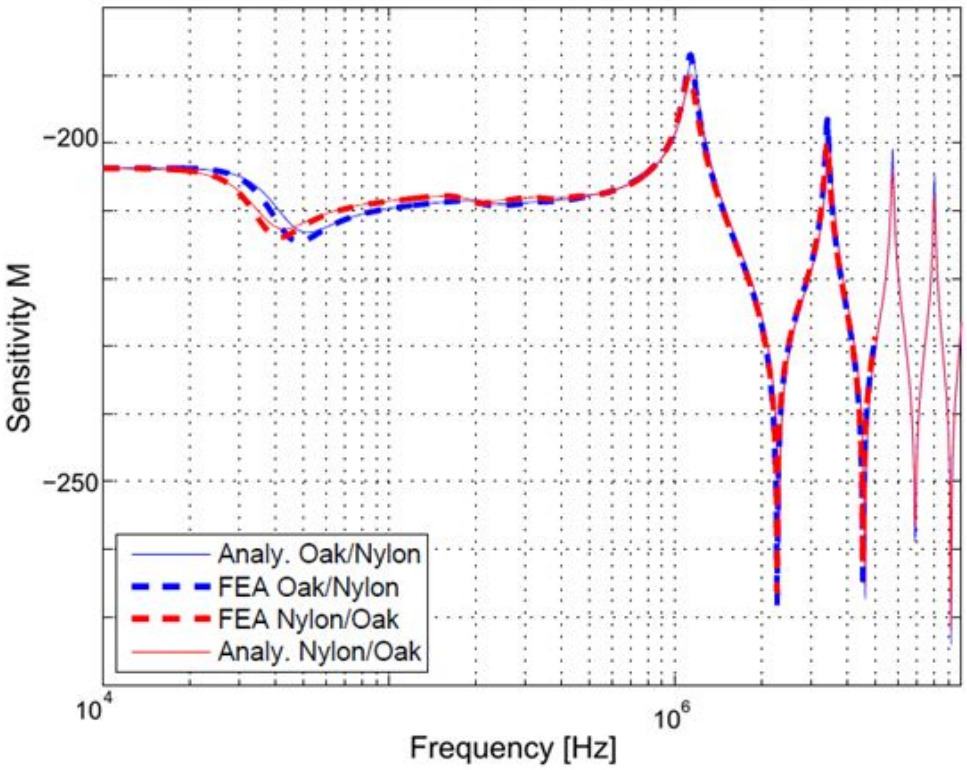

Figure 3.13: Comparing the predictions from the FE model and the analytical model developed in Chapter 2 for a transducer submerged in water with two backing layers. The blue lines indicate a system with a transducer followed by a 3 mm oak layer and finally a 4 mm nylon layer. The red lines indicate a system with a transducer followed by a 3 mm nylon layer and finally a 4 mm oak layer. The values used to simulate oak and nylon backing layers are detailed in Table 3.2.

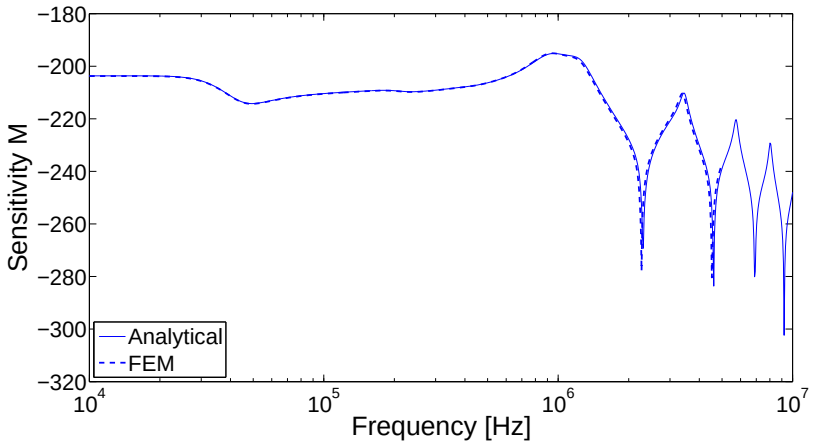

Figure 3.14: Comparing the predictions from the FE model and the analytical model developed in Chapter 2 for a transducer submerged in water with a 4 mm thick nylon backing and a 1 mm thick FR-4 front layer. The values used to simulate these layers are detailed in Table 3.2

determine the response given any layer material properties. Now that the analytical models have been validated, a generic model is designed to handle any number of backings and front layers. This model allows the layer's material to be varied over a range of material parameters and aids in the selection of an optimal response.

Chapter 4

Multilayer Transducer System Modeling

Using the solutions derived in Chapter 2, a generic algorithm has been developed to determine the receive sensitivity of a system regardless of the number of backing or front layers and and their parameters. The following solution employs the impedance translation theorem [21] in order to solve for a general configuration by using a transmission line approach to each layer. To determine the sensitivity, the system's interface impedances need to be calculated from a known termination to the front and then the pressure from the front needs to be translated to the element faces. Once the sensitivity has been determined, an optimization algorithm can be used to find optimal backing parameters for a given system over a given frequency range.

4.1 System Parameters

The system needs to be defined along one axis with each layer's thickness, sound speed, and impedance prescribed as illustrated in Figure 4.1 for a transducer consisting of a single piezoelectric layer and an arbitrary number of front and back layers.

The piezoelectric layer is described by its length L, width W, thickness d_e, sound speed $c_{d_e}^D$, and characteristic specific acoustic impedance Z_e. The transducer's sound speed and impedance may be calculated from the density ρ_e and the open

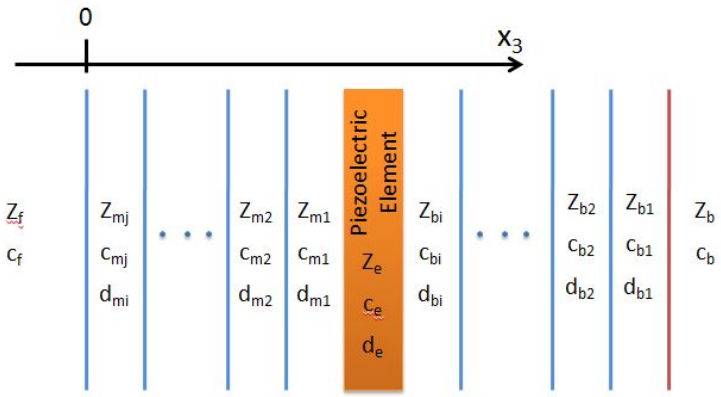

Figure 4.1: Notation used in the one-dimensional layered transducer model.

circuit plane wave modulus in the poled direction, C_{33}^D, using the following relations

$$c_e = \sqrt{\frac{C_{33}^D}{\rho_e}},$$

$$Z_e = \rho_e c_e.$$

Piezoelectric materials a usually anisotropic, so the values above will be tabulated and may not be related to an isotropic Young's modulus and Poisson's ratio.

Next the backing layers are defined with the thickness d_{bi}, sound speed c_{bi}, and impedance Z_{bi} where i is indicative of the layer location in relation to the piezoelectric layer as illustrated in Figure 4.1. Assuming the layers are isotropic, the sound speed and impedance may be determined by employing the material density ρ, Young's modulus E, Poisson's ratio ν and material loss factor η using

$$C_{33}^D = \left(E_{bi} \frac{1 - \nu_{bi}}{(1 + \nu_{bi})(1 - 2\nu_{bi})} \right) (1 + j\eta_{bi}),$$

$$c_{bi} = \sqrt{\frac{C_{33}^D}{\rho_{bi}}}, \tag{4.1}$$

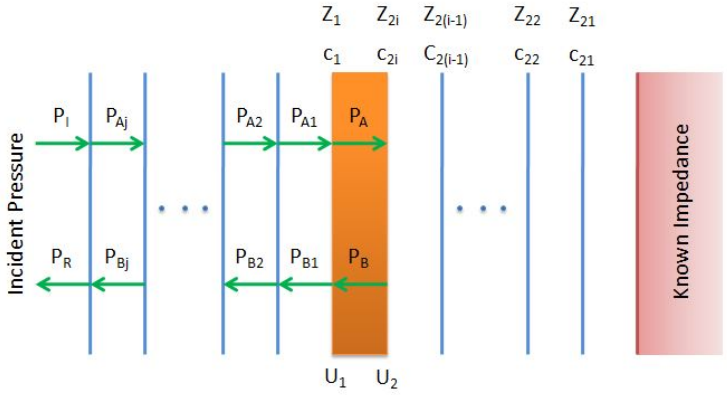

Figure 4.2: Notation used to describe the surface impedance and pressure translation.

$$Z_{bi} = \sqrt{\rho_{bi} C_{33}^{D}}. \tag{4.2}$$

Where C_{33}^{D} is the plane wave modulus. Similarly, the front layers are defined with the thickness d_{mj}, sound speed c_{mj}, and impedance Z_{mj} where j is indicative of the layer location in relation to the piezoelectric layer. For anisotropic layers, the plane-wave modulus will need to be measured or found in a table.

As shown in Chapter 2, the sensitivity is ultimately a function of the velocity at each surface of transducer. The velocity is then a function of the impedance and pressure at each surface as illustrated in Figure 4.2. A generic method for determining these values is described below.

4.2 Impedance Translation

Once the layers have been defined, translating from a known impedance to the input impedance at any surface of the system is fairly straightforward. The input impedance is the ratio of the pressure to the velocity at the surface of interest. Starting at the back of the system, we assume that the local input impedance is known and is

well approximated as either an infinite medium or rigid boundary. This is usually the case because most systems are terminated in a material that is orders of magnitude thicker or of greater impedance than any other layer. For example, hydrophones usually are often either terminated in the external fluid or be an effectively rigid mounting plate. Following the steps described in Chapter 2 and the notation used Figure 4.2, if the end condition is terminated in the external fluid [21]

$$Z_{21} = Z_{b1}\frac{Z_f \cot(k_{b1}d_{b1}) + jZ_{b1}}{jZ_f + Z_{b1}\cot(k_{b1}d_{b1})}, \tag{4.3}$$

where Z_0 is the external fluid impedance. A special case for which Eqn. 4.3 may be simplified is a rigid termination or as Z_b approaches ∞,

$$Z_{21} = -jZ_{b1}\cot(k_{b1}d_{b1}).$$

A second special case is when $Z_0/Z_{b1} \ll 1$ (pressure release case) which yields

$$Z_{21} = jZ_{b1}\tan(k_{b1}d_{b1}).$$

This case is useful for experiments in which the system is terminated with an air cavity.

For a system with only one backing, Z_{21} represents the interface impedance between the backing and the piezoelectric layer. For multiple layers, each input impedance at successive interfaces, Z_{2i}, needs to be calculated from the termination to the front of the hydrophone. Here the subscript i ranges from 1 to the number of backing layers nb, as illustrated in Figure 4.2. The impedance of each additional layer after the first is described by

$$Z_{2i} = Z_{bi}\frac{Z_{2(i-1)}\cot(k_{bi}d_{bi}) + jZ_{bi}}{jZ_{2(i-1)} + Z_{bi}\cot(k_{bi}d_{bi})}, \tag{4.4}$$

where $i = 2, 3, ..., nb$. In the case where there are no backings, the impedance at the back of the piezoelectric element is dependent on the termination. If terminated in an infinite medium, the rear surface impedance Z_{n_b}, is equal to the external fluid's impedance.

Once the impedance at the back surface of the piezoelectric layer has been determined the impedance at the front can be calculated. The front surface impedance as a function of frequency can be determined using the piezoelectric layer properties and the back surface impedance.

$$Z_1 = Z_e \frac{Z_{2n_b} \cot(k_e d_e) + jZ_e}{jZ_2 + Z_e \cot(k_e d_e)}. \tag{4.5}$$

If there are no backing layers and the piezoelectric layer is rigidly terminated, the rear surface impedance approaches infinity. In this special case, the front impedance reduces to

$$Z_1 = -jZ_e \cot(k_e d_e).$$

In practice, this is difficult to obtain since is requires $Z_{2nb} \gg Z_e$. Since piezoelectric materials already have a high impedance value the number of appropriate backing materials to simulate a rigid case is limited.

Now the local input impedance may be determined for any front layer included in the system. For a generic number of front layers j, the first front layer can be expressed as

$$Z_1 = Z_{m1} \frac{Z_1 \cot(k_{m1} d_{m1}) + jZ_{m1}}{jZ_1 + Z_{m1} \cot(k_{m1} d_{m1})}. \tag{4.6}$$

Each additional layer interface impedance can be calculated with

$$Z_i = Z_{mi} \frac{Z_{(j-1)} \cot(k_{mj} d_{mj}) + jZ_{mj}}{jZ_{(j-1)} + Z_{mj} \cot(k_{mj} d_{mj})}. \tag{4.7}$$

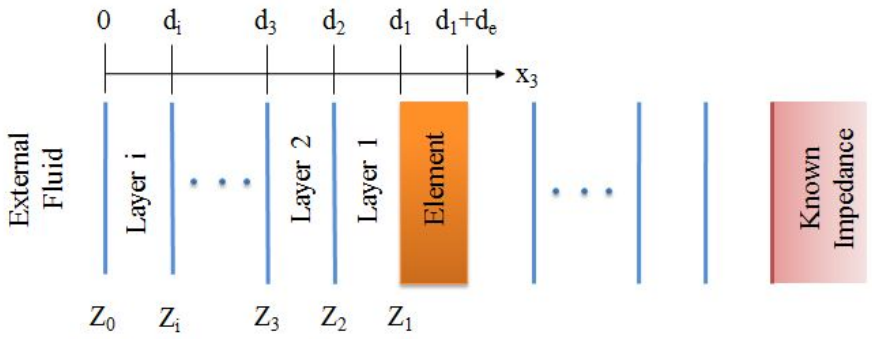

Figure 4.3: Notation used to describe the interface location.

The remaining solution only needs the interface impedance exposed to the external fluid is needed

$$Z_0 = Z_j.$$

If the hydrophone contains no front layers

$$Z_0 = Z_1.$$

4.3 Pressure Translation

The second portion of the equation requires knowing the pressure field acting on the front and back surfaces of the piezoelectric layer. First, all of the interfaces are defined starting from the surface facing the initial pressure field. The notation used to identify each interface is illustrated in Figure 4.3. For each frequency, the pressure at each interface is a function of the layer's sound speed, c_i, location with respect to the external surface, z_i, impedance, Z_i, and the previous layer's pressure field.

To determine the pressure field within the first layer, the external field needs to be defined first. For a time varying pressure field incident upon an interface, the wave will be partly reflected and partly transmitted. As illustrated in Figure 4.4,

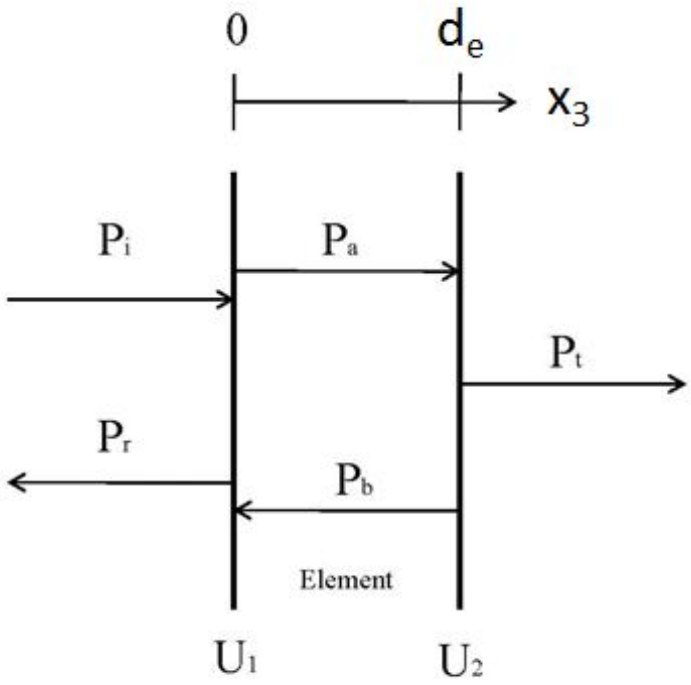

Figure 4.4: Notation used to define the acoustic pressure field.

the incident pressure field P_i generated a reflected field P_r and a transmitted field within the first layer. Using the notation in Figure 4.4 yields $P_i + P_r = P_a + P_b$. Normalizing with the incoming pressure P_i yields the following notation $\frac{P_r}{P_i} = R$, $\frac{P_a}{P_i} = A$, $\frac{P_b}{P_i} = B$ and $\frac{P_t}{P_i} = T$. The reflection coefficient may now be written in terms of the external fluid characteristic impedance and the initial boundarys specific acoustic impedance [26]

$$R_f = \frac{Z_0 - Z_f}{Z_0 + Z_f},$$

where the subscript f indicates a property of the external fluid. For each layer, the previous layer's pressure field is defined as A_i for the incident pressure and B_i for the reflected pressure. The full external pressure field can then be represented as

$$A_f = 1,$$

$$B_f = \frac{Z_0 - Z_f}{Z_0 + Z_f}.$$

The first layer's pressure field A_i and B_i can now be solved using

$$C = \begin{bmatrix} \exp(-jk_i d_{i+1}) & \exp(jk_i d_{i+1}) \\ \exp(-jk_i d_{i+1}) & -\exp(jk_i d_{i+1}) \end{bmatrix}, \tag{4.8}$$

$$D = \begin{bmatrix} A_{i+1}\exp(-jk_{i+1}d_{i+1}) + B_{i+1}\exp(-jk_{i+1}d_{i+1}) \\ \frac{Z_i}{Z_{i+1}}\left(A_{i+1}\exp(-jk_{i+1}d_{i+1}) - B_{i+1}\exp(-jk_{i+1}d_{i+1})\right) \end{bmatrix}, \tag{4.9}$$

$$\begin{bmatrix} A_i \\ B_i \end{bmatrix} = C^{-1}D. \tag{4.10}$$

For the first layer z_{i+1} is 0 and Z_{i+1}, k_{i+1}, A_{i+1} and B_{i+1} refers to Z_f, k_f, A_f and B_f respectively. The process described above is repeated from the front interface to the sensing element until the pressure field in the element is determined A_e and B_e.

4.4 Generic Solution

The values determined for the impedance and pressure translation may now be combined to find the velocities at the front and back surfaces, U_1 and U_2 respectively

$$U_1 = \frac{A_e\exp(-jk_e d_1) + B_e\exp(jk_e d_1)}{Z_1}, \tag{4.11}$$

$$U_2 = \frac{A_e\exp(-jk_e(d_1+t)) + B_e\exp(jk_e(d_1+t))}{Z_2}. \tag{4.12}$$

Substituting these velocities into the previous equation yields the sensitivity

$$M = \frac{-jh_{33}}{\omega}(U_1 - U_2). \tag{4.13}$$

Now the sensitivity can be calculated for a variety of backings and front lay-

ers. The layers can be defined with just five variables; thickness, Young's modulus, density, Poisson's ratio, and damping ratio. These five variables may now be used in an iterative algorithm that attempts to find an optimum set which satisfies a goal function determined by a customer. This is described further in Chapter 5 which discusses layering optimization to achieve the desired hydrophone response.

Before beginning the optimization, an attempt is made to validate the above analytical model by comparison with experimentally obtained data. This validation is useful in illustrating the strengths and weaknesses of the one-dimensional model.

4.5 Experimental Validation

To provide additional validation that the analytical model provides a good approximation of real-world transducer behavior, results from this 1-D model are compared with the results from the experimental data. The experiments were designed to be simple consisting of a few layers and elements. Comparing these results to the output of the generic algorithm illustrates the strengths and weaknesses of the analytical algorithm.

4.5.1 Experimental Apparatus

This system architecture limited the design of the system form factor to a four inch diameter and two inch height. Within this framework, a variety of layers have been explored using a 1.27 cm thick piezoelectric element with a square cross-section normal to the thickness direction. The elements used in this system are 2.54 cm $\times$ 2.54 cm $\times$ 1.27 cm piezoelectric 3-1 composite. The in-air electrical impedance of five individual elements was measured and are compared to the analytical model in Figure 4.5. The electrical impedance, Z_E, is a measure of the opposition a circuit

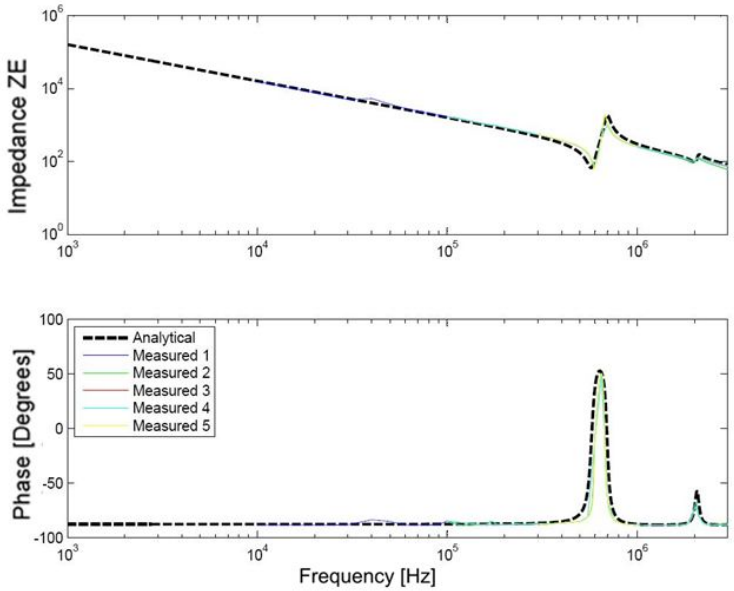

Figure 4.5: Measured and modeled electrical input impedance for five individual specimens of 3-1 composite piezoelectric elements.

presents to current flow when a potential is imposed across the circuit. In general it is expressed as the complex ratio of the voltage to the current

$$Z_E = \frac{V}{I} = \frac{\left[-\frac{h_{33}^2 D_0}{c_{33}^D k}\left(\sin kd_e + \tan\left(\frac{kd_e}{2}\right)(1-\cos k_e d_e)\right) + \beta_{33}^S D_0 d_e\right]\exp(j\omega t)}{j\omega LW D_0 e^{j\omega t}}.$$

The impedance can be simplified by using the clamped capacitance C_0 and thickness mode electromechanical coupling factor K_d^2 as described by Wilson [7]

$$C_0 = \frac{\epsilon LW}{d_e} = \frac{LW}{\beta d_e},$$

$$K_d^2 = \frac{h_{33}^2}{\beta_{33}^S c_{33}^D} = \frac{h_{33}^2 \epsilon_{33}^S}{c_{33}^D}.$$

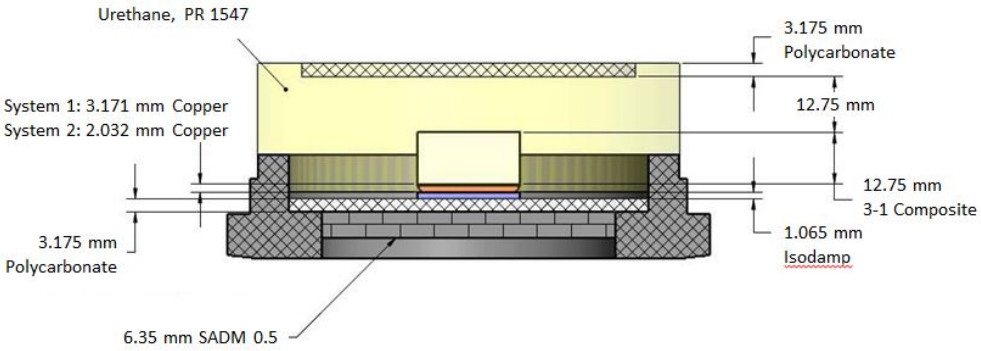

Figure 4.6: SolidWorks cutaway of the experimental transducer setup

This allows for the impedance to be rearranged to better illustrate the parameter limits

$$Z_E = \frac{jK_d^2}{\omega C_0} \frac{\tan\left(\frac{kd_e}{2}\right)}{\frac{kd_e}{2}} - \frac{j}{C_0\omega}. \tag{4.14}$$

This calculation required information about the material properties of the 3-1 composite elements which was obtained using in-house analytical homogenization models. As can be seen in Figure 4.5, very accurate results can be generated using the above system of equations when the material properties are well defined.

For testing purposes, the backing construction was designed to be inexpensive and modular. This was accomplished by using a generic PVC tube as the housing for the electronics with a common connection for a variety of hydrophones. Figure 4.6 is a cutaway of a SolidWorks model depicting the hydrophone and electronics housing. Note that Figure 4.6 illustrates the two different systems to be tested composed of Isodamp, polycarbonate, and SADM backings. System 1 contains element 1 backed by a 3.175 mm copper plate and System 2 contains element 2 backed by a 2.032 mm copper plate. The generic algorithm though, only sees this system as a combination of layers of different thicknesses as illustrated in Figure 4.7.

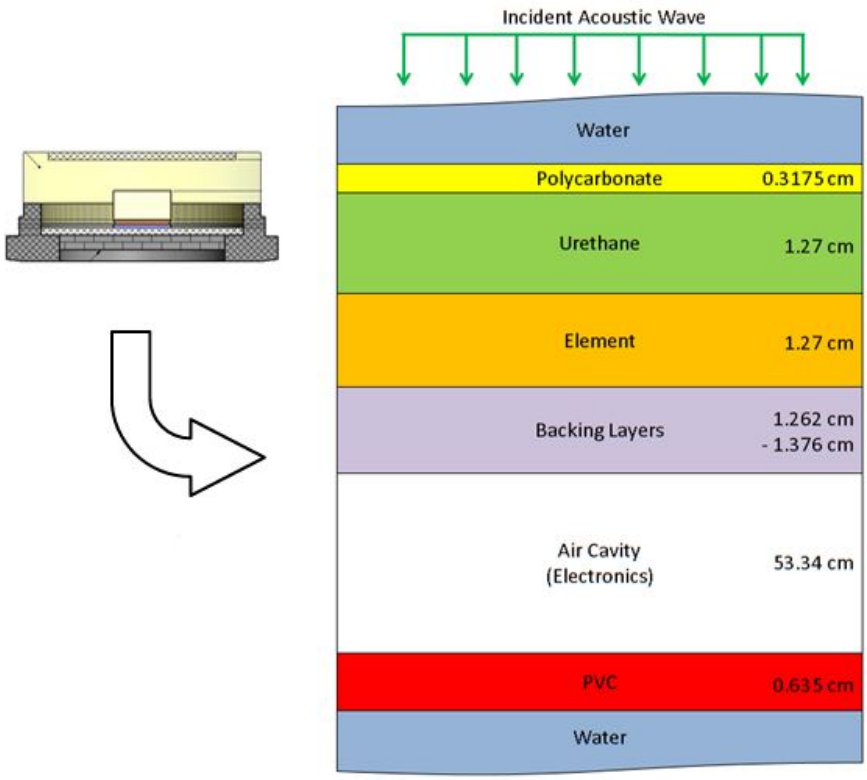

Figure 4.7: Illustration of the conversion from the experimental setup into a system of layers.

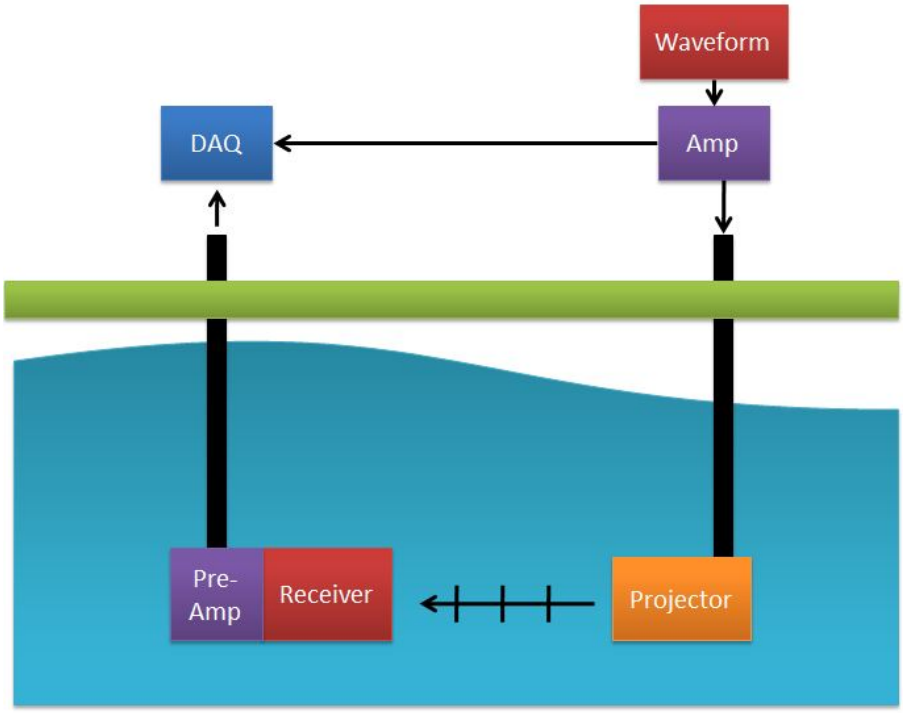

Figure 4.8: Illustration of the experimental system setup.

The response of the system, illustrated in Figure 4.8, using the different backing layer schemes were tested at Applied Research Laboratories Lake Travis Test Station (LTTS), which is a large open water test facility[1]. Each system was lowered down to a depth of 6.1 m and 9.14 m away from a calibrated projector which was also 6.1 m below the surface. The projector was fed an amplified signal from a waveform generator. The voltage response from the test hydrophone was then amplified voltage with 12 dB of gain and digitized with a LabView based data acquisition system.

4.5.2 Results

Table 4.1 details the material properties for each layer used in the generic algorithm. Elements 1 and 2, as illustrated in Figure 4.6, are both terminated by a

[1]http://www.arlut.utexas.edu/researching/facilities.html

Material	Density $\left[\frac{\text{kg}}{\text{m}^3}\right]$	Young's modulus [Pa]	Poisson's ratio	Loss Factor
Polycarbonate	1210	2.2×10^9	0.37	0.05
Urethane PR-1547	1050	3×10^8	0.48	0.18
Copper	8700	1.1×10^{11}	0.35	0.001
Isodamp C-1002-06	1002	23×10^7	0.4	0.1
SADM-0.5	2200	4×10^8	0.3	0.05

Table 4.1: Material properties of the layers in the experimental setup.

SADM backing, 1.27 cm thick, before the air cavity housing the electronics. The only difference between the two systems is the copper plate thickness placed immediately behind the element. Applying these parameters to the generic algorithm developed above yields the predicted receive sensitivities illustrated in Figure 4.9. Compared with the experimental results, there is generally a good agreement between the levels as well as the resonant and anti-resonant behavior across a broad range of frequencies.

As expected, element 1 has a higher resonance frequency. This is due to the thicker copper backing which increased the rigidity of the system. The high frequency character in the response seen lacking in the analytical prediction was expected as well. These resonances can not be predicted by the generic model in its current one dimensional form. These resonances, near 40 through 70 kHz, are the result of in-plane resonances (modeled with FEA) that this model cannot predict. This is the result of an element which is to thick for the ideal use of a 1-D model at these frequencies. Work has been started in improving the model with respect to these three-dimensional modes and is discussed in the Future Work section in Chapter 7.

Even given the shortcomings, this is a fairly accurate model of the expected system especially given the number of layers in the experimental setup. Use of this generic algorithm allows for a quick analysis of experimental systems given a large

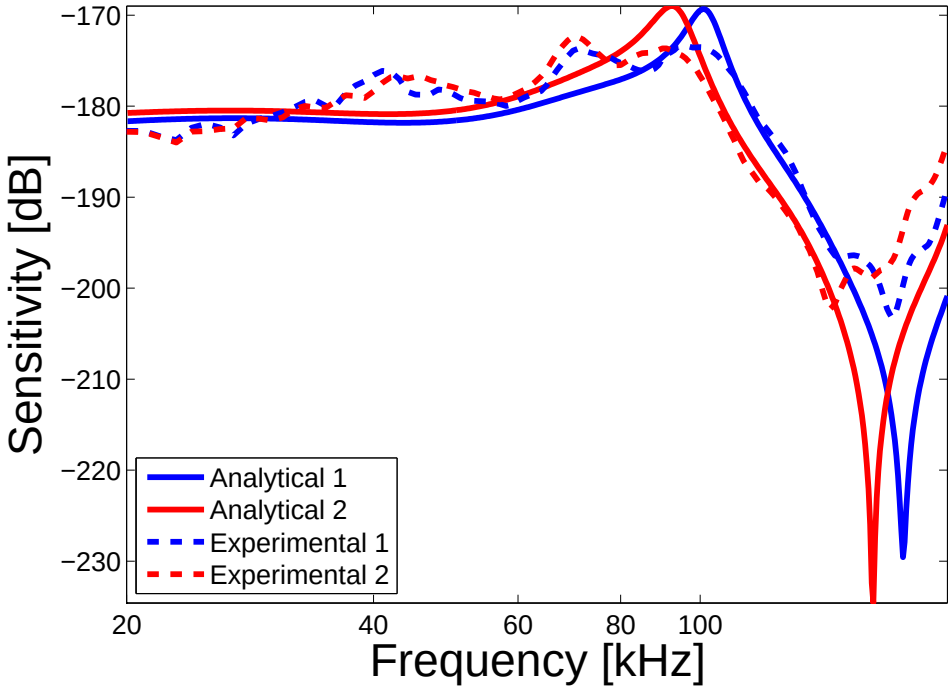

Figure 4.9: Comparison of the receive sensitivities predicted by the generic analytical algorithm and the experimental results of the system described above.

number and variety of layers. This significantly decreases the time spent traditionally prototyping and hydrophone systems testing.

The generic algorithm has also proven to be a useful tool in running many simulations of an experimental setup with incremental changes. This paves the way for an algorithm to analyze multiple backing materials which can aid in the development of a solution with optimal properties which is the topic of Chapters 5 and 6.

Chapter 5

Layer Optimization

Transducer elements in a sonar systems are generally mounted to a material, known as a backing. The backing may be designed to help isolate the receiver from unwanted acoustic or vibrational noise or improve the bandwidth of the transducer. The geometry of the backing material is often heavily influenced by system constraints, leaving the material parameters as the only option for optimization. To illustrate, the optimization methodology employed in this work a system is studied as illustrated in Figure 5.1. In this system it was desired that an optimal backing be found which was limited to a thickness range between 3.175 and 12.7 mm composed of a single or multiple layers of any solid material(s).

In order to completely characterize the engineering properties of an elastomer, it is necessary to know two of the following parameters, the Poisson's ratio ν, dynamic bulk modulus, dynamic shear modulus, and Young's modulus E [20]. In this work, the materials were assumed isotropic, and defined by their Young's modulus and Poisson's ratio. This optimization algorithm started by considering six variables Young's modulus, density ρ, Poisson's ratio, damping ratio η, element thickness d_e, and backing thickness d_b. The hydrophone's receive sensitivity response was then calculated for specific combinations of these input parameters. In order to reduce the computation time, the two parameters that least effect the response were held constant. Use of the generic algorithm developed in the last chapter allows for many combinations of the important parameters. These results may then be compared to

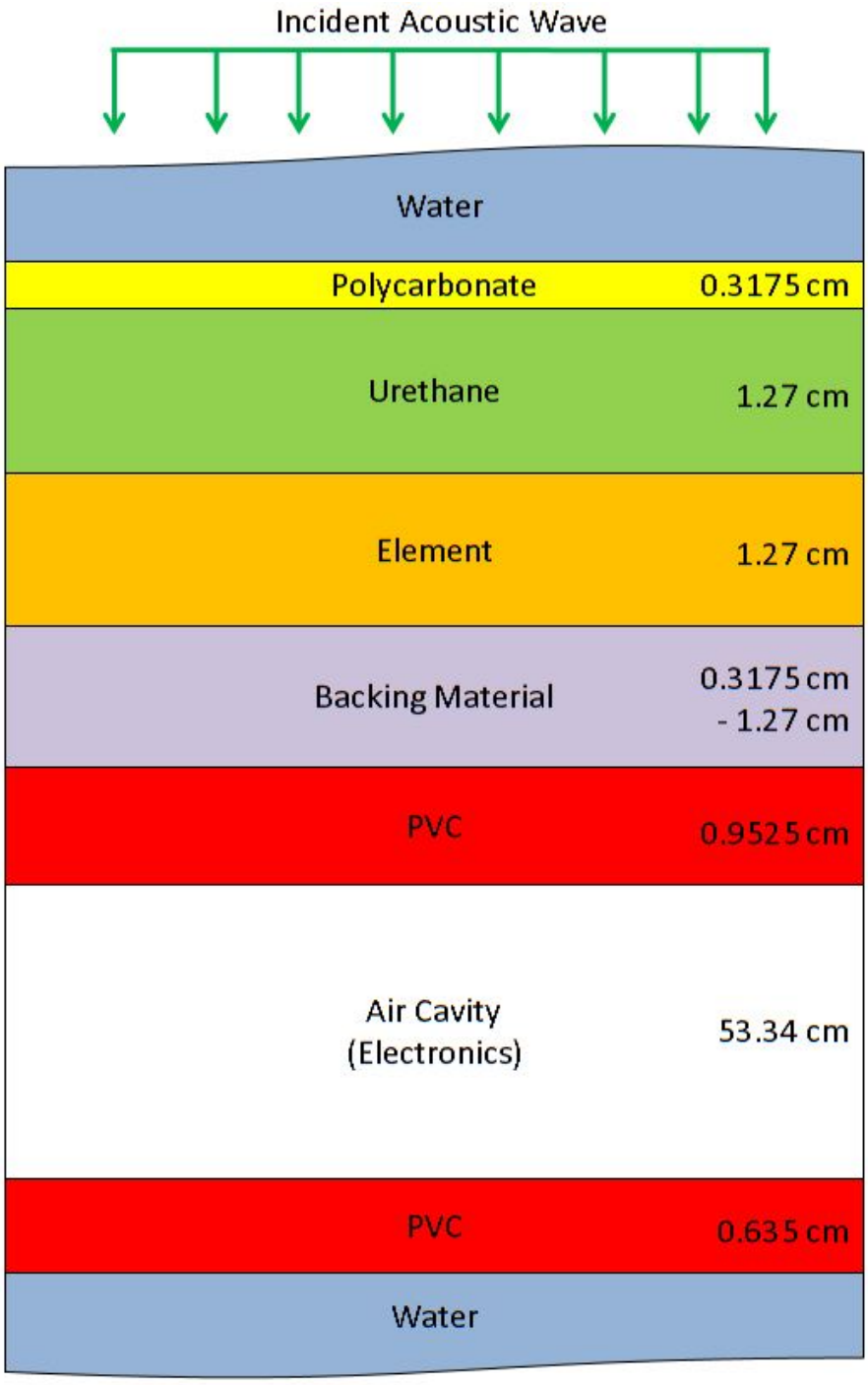

Figure 5.1: Test system cross section

aid in the selection of a final optimal material.

5.1 Goal Parameters

Every real backing material will require some compromise. This was illustrated in Chapter 2, where it was shown that the choice of backing material could cause the sensitivity response function to exhibit either a local minimum or maximum at a given frequency. The first step in developing a backing was to determine the required frequency parameters. For this work, the center frequency was given as 110 kHz with a bandwidth of 90 kHz. The center frequency and bandwidth are used to define the frequency range of interest, and in practice would generally be determined by the customer.

There are many important hydrophone characteristics including a flat magnitude and phase response, mean output level, receive bandwidth, and directional response characteristics. Comparison of different hydrophone designs centers around the value of the above characteristics in the frequency range of interest. The flatness can be measured using the standard deviation of the sensitivity over a given range of frequencies. For a set of values $\mathbf{x}$, the standard deviation σ may be expressed as

$$\sigma = \sqrt{\frac{\sum (x_i - \bar{x})^2}{N}},$$

where $\bar{\mathbf{x}}$ is the mean of the parameter set $\mathbf{x}$ and N is the number of values in set x. As the standard deviation approaches zero, the system approaches a flat response. The receive bandwidth parameter is determined by finding the bandwidth around the maximum response, in the frequency range of interest, with a response 3 dB less than the maximum response. The final parameter is meant to illustrate the ability of the backing to reduce the level of noise generated from behind the baffle. This

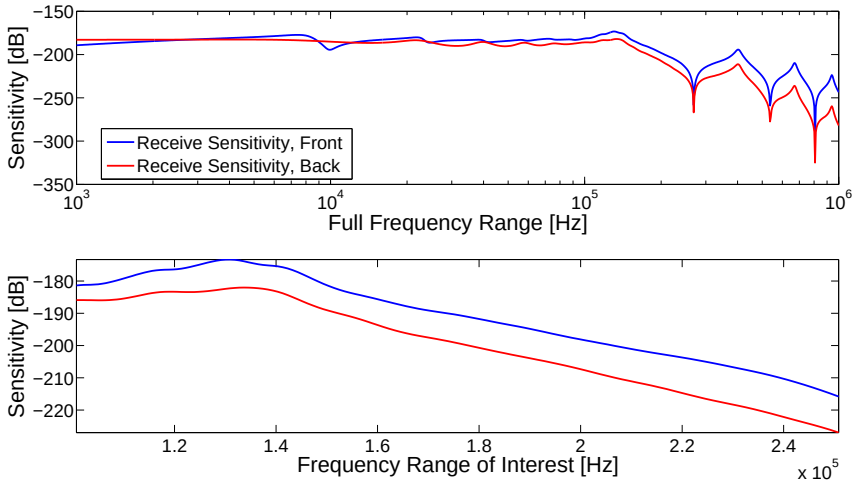

Figure 5.2: Receive response of the system described in Figure 5.1 with a 1.27 cm SADM backing.

may be valuable in preventing acoustic noise generated be electric components from interfering with the receive response. The difference is found by subtracting the mean response from an incident acoustic wave originating behind the hydrophone from the mean response of an incident acoustic wave originating in front of the hydrophone. To illustrate, consider the system illustrated in Figure 5.1 with a backing material of SADM, a material commonly used in hydrophone design, about a frequency range from 100 to 250 kHz. Applying a Young's modulus of 4×10^8 Pa, density of 2200 kg/m^3, Poisson's ratio of 0.3, and thickness of 1.27 cm to the generic algorithm developed in Chapter 4 yields the results in Figure 5.2. In the frequency range of interest, the standard deviation of the receive sensitivity from the front is 12.12. The maximum sensitivity is -173.3 dB at 131 kHz, and the receive bandwidth occurs at the -176.3 dB responses above and below at frequencies of 143.3 kHz and 120.5 kHz respectively. Thus the receive bandwidth is 22.8 kHz. The mean receive response from the front is -188.3 dB, and the mean response from the back is -196.8 dB, leading to a difference of 8.5 dB. Note that some of these metrics may be more important than others

Constraint	Value
Center Frequency	110 kHz
Bandwidth	90 kHz
Element Thickness	$d_e < 1.27$ cm
Total Thickness	$d_e + d_b < 2.54$ cm
Maximum SG	3

Table 5.1: Frequency, receive response and physical parameter constraints.

depending of the requirements of the specific application.

Geometric and other physical parameters must also be considered when designing a transducer backing layer. The thicknesses of the piezoelectric element and baffle do not exceed 2.54 cm in the present study. Weight and density are usually a large concern in underwater acoustic applications. In this work, the density of the backing material is evaluated using its specific gravity, or the ratio of the backing material density to the density of water. In this case, a total system specific gravity near one is desired in order to negligibly effect the buoyancy of the system. However, a maximum specific gravity of three is acceptable as long as the performance gains are sufficiently large. For applications at depth, the Young's modulus may also be an important parameter to prevent the backing from deflecting significantly under pressure, which is undesirable as a change in thickness can lead to a change in system performance.

As mentioned above, the system studied here has five constraints, repeated in Table 5.1 for convenience. This system also has a variety of design goals. In this work, five parameters were considered the most important; sensitivity flatness, mean sensitivity, backing weight, difference in sensitivity between the front and back, and the receive bandwidth.

It is important to understand which parameters are the most important to the

Design Goals	Weighted Value, w_i [%]
Mean Sensitivity	30
Receive Bandwidth	25
Sensitivity (Front - Back)	20
Flat Sensitivity	15
Weight	10

Table 5.2: Weighted values assigned to the important values

customer as the results can vary significantly. One method is to assign each design goal a weight w_i where

$$w_i \geq 0,$$

$$\sum_{i=1}^{n} w_i = 1,$$

for n design goals. This design approach is known as the Archimedian weighted deviation function, and is common in engineering design. For the system studied it was determined that the mean sensitivity was the most important value followed by the receive bandwidth, a flat response, a large sensitivity difference between the front and back, and a low weight. Table 5.2 details the values of the assigned weighting factors, w_i. It should be noted that these parameters are not independent, and assigning a particular weighting factor to one parameter may skew the results for others. For example, the receive bandwidth and a flat response are closely related. These relationships are explored before determining the final weighting factors.

A metric is needed that characterizes the effectiveness of a design given a parameter set with respect to the customer's weighted values for the multiple design goals. This may be accomplished by calculating the normalized difference d_i between the desired goal for a design goal D_i, and the attained value A_i of a design goal for a given parameter set where i denotes a particular design goal. For n design goals the difference function normalized with respect to the maximum difference between the

Material	$A_5\left[\frac{\text{kg}}{\text{m}^3}\right]$	d_5
Aluminum	2700	1.000
Nylon	1150	0.139
Cork	240	0.367

Table 5.3: Difference values calculated using Eq. 5.1 for three different materials given a desired density of $900\,\text{kg/m}^3$.

desired design goal and the attained value may be expressed as

$$d_i = \frac{|A_i - D_i|}{|A_i - D_i|_{max}};\ i = 1, 2, ..., n. \tag{5.1}$$

As the actual value approaches the desired value, the deviation function d_i approaches zero. This is a simple case of optimization in which the minimum deviation function is desired. For example a desired density of $D_5 = 900\,\text{kg/m}^3$ leads to the following difference functions for the three materials listed in Table 5.3.

Increasing the number of objectives to the optimization problem increases the complexity. For example, an optimal hydrophone design may desire a maximum sensitivity and a flat response. Often these objectives will be in conflict with one parameter set offering a maximum sensitivity and another a flat response. In between are an infinite number of solutions involving a compromise between these two. A compromise can then be determined by summing the weighted individual goals into a final goal function,

$$G = \sum_{i=1}^{n} w_i d_i;\ i = 1, 2, ..., n.$$

As the current system solution approaches the desired system solution G approaches zero. This value may now be used to compare an array of parameters in order to find a final optimal solution.

5.2 Backing Parameters

There are a variety of important material parameters that can be varied, but careful selection is needed since each additional parameter increases the computational time exponentially. For example, if a parameter range was examined over ten values it would require ten runs through the generic algorithm. If that first parameter was compared to a second with ten values the computation would require 100 runs through the generic algorithm. Given a number of values per parameter n, and a number of parameters m, the number of runs through the generic algorithm is equal to n^m.

For numerical efficacy, optimization was done iteratively. First, multiple parameters were compared to each other at a low resolution. This allows for a comparison between the parameters, with minimal computation, in order to determine which have the greatest influence on the Goal function. The parameters with greatest influence on the behavior of the system are retained and the resolution increased in order to find an optimal combination of material parameters. Further, rather than comparing the influence of all parameters simultaneously, we compared only two parameters at a time to ease visualization of the goal function of those particular parameters. For example the Goal was plotted as a function of E and d_e, E and ν, E and ρ, etc. Each parameter was compared with the others allowing for the most influential parameters to be determined. The ranking of these parameters in importance is different depending on the system boundaries and weighting. In this work the parameters which had the greatest influence on the Goal function in decreasing order of importance, are the Young's modulus E, the element thickness d_e, the backing thickness d_b, the density ρ, the Poisson's ratio ν, and finally the damping ratio η.

The system depicted in Figure 5.1 after applying the weights listed in Table 5.2

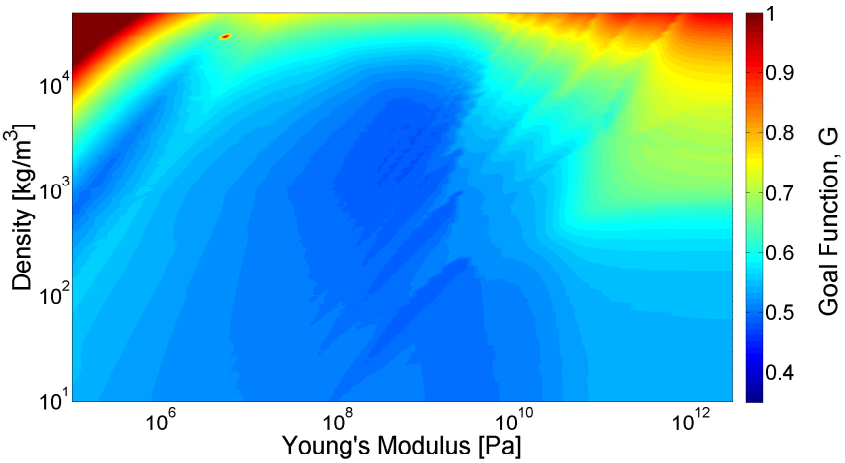

Figure 5.3: Total Goal solution dependence on the Young's modulus and density of the backing material.

yields two total Goal function plots illustrated by Figures 5.3 and 5.4. These plots illustrate the difference in parameters that are highly influential on the Goal value and those that are not. As can be seen in Figure 5.3, the Goal function varies significantly with both the Young's modulus and density. However, in Figure 5.4 the Goal function varies significantly with the Young's modulus but only slightly with the Poisson's ratio. This lack of influence is a reason for not including analysis of the Poisson's ratio in future higher resolution analysis of the system. Computational power is better allocated by using variables that more influential on system performance.

5.3 Solutions

Optimization problems with multiple objectives often have multiple configurations that yield a desirable overall response. These can be parameters that provide a goal function minimum in either a local or global sense. Since the objective of most optimization algorithms is to only find the best global solution, the users may find themselves with a lack of knowledge of other possibilities. This argument led to the

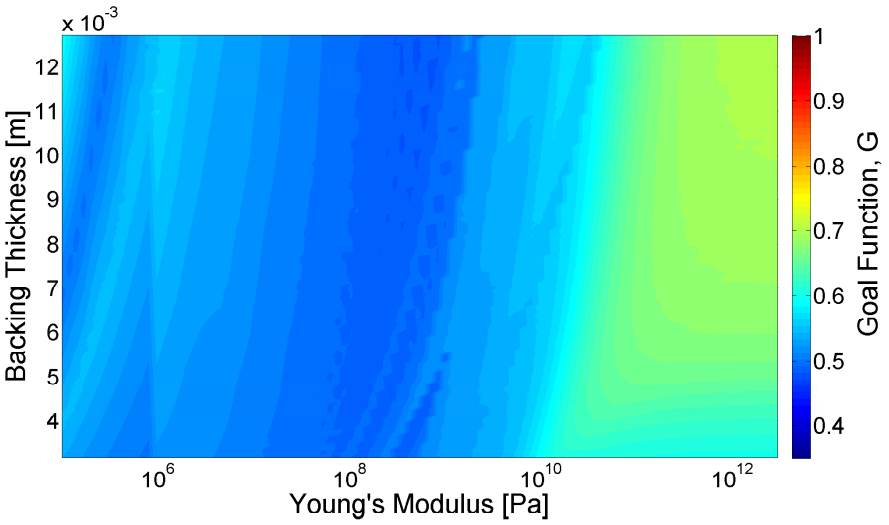

Figure 5.4: Total Goal solution dependence on the Young's modulus and Poisson's ratio of the backing material.

Parameter	Value
Young's modulus	1×10^9 [Pa]
Density	3000 $\left[\frac{\text{kg}}{\text{m}^3}\right]$
Poisson's Ratio	0.3
Thickness, d_e	1.27 [cm]

Table 5.4: Seed parameters for the system.

solution method employed for this work. Instead of solving for a single global solution the following method displays the local minima in a 2D space allowing the designer to compare the different potential solutions with their corresponding location with respect to material families. While this method does not guarantee the user will find a global minimum to the design space, the simple nature allows for the total goal values to be calculated quickly and the compared to existing plots of material families. Details of this approach are given in the following paragraphs.

The optimization algorithm is seeded with the starting values detailed in Table 5.4. These values were the starting point for the algorithm. When two parameters

Parameter	Range
Young's modulus	$1 \times 10^5 < E < 3x \times 10^{12}$ [Pa]
Density	$10 < \rho < 5 \times 10^4 \left[\frac{\text{kg}}{\text{m}^3}\right]$
Poisson's ratio	$-0.95 < \nu < 0.45$
Thickness	$0.3175 < d_e < 1.275$ [cm]

Table 5.5: Initial system parameter ranges.

are varying the other two parameters are held constant at these values. Once a parameter range has been found that better satisfies the design goals, these seed values were changed to fall within the new parameter range.

Initially, parameters are given a large range in order to cover a wide variety of possible materials. The initial range used in this work is listed in Table 5.5 This range should include most engineering materials available including possible material combinations. Using these parameter ranges through the optimization program yields the results illustrated in Figure 5.5.

The first step is to narrow the range of the geometric parameters. As seen in the Figure 5.5 in the graphs illustrating the thickness effects, the Goal function is minimized when the thickness ranged from 0.635 through 1.111 cm. This range was selected to cover all of the global solutions in each graph.

The next step was to a smaller parameter range that encompasses the area with a minimized Goal function in order to increase the resolution. First though, the solution was compared with existing material families that lie on the same range. This is the point at which a local solution may prove more valuable than a global solution. For example when Figure 5.3 is compared to Ashby's [3] Young's modulus versus density in Figures 5.6, some solutions have simple material analogs while others would require a composite material. This is the point at which a choice needs to be made that takes into account the eventual material and configuration of the backing.

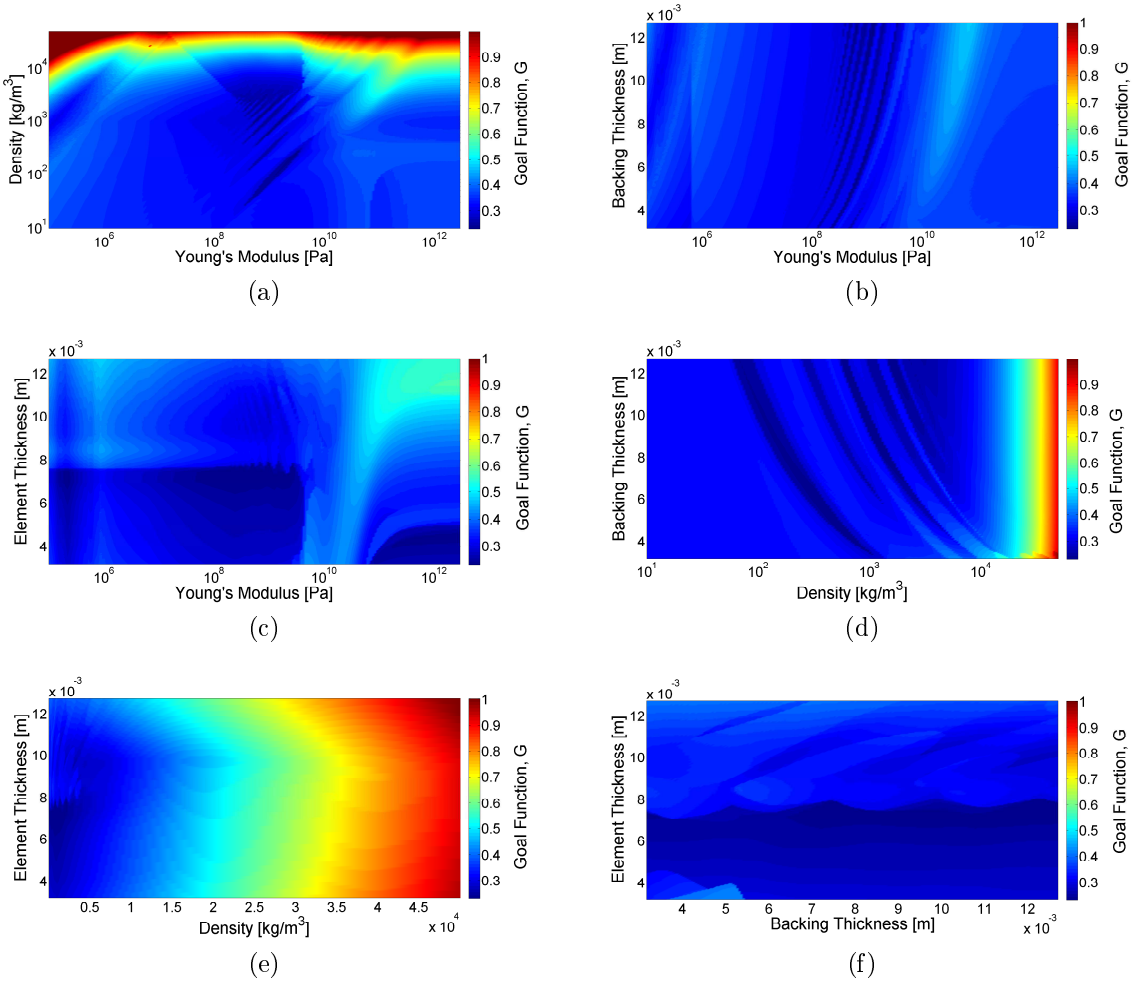

Figure 5.5: Total Goal solutions to the system (a) varying the Young's modulus and density, (b) varying the Young's modulus and backing thickness, (c) varying the Young's modulus and element thickness, (d) varying the density and backing thickness, (e) varying the element thickness and density, and (f) varying the backing thickness and element thickness.

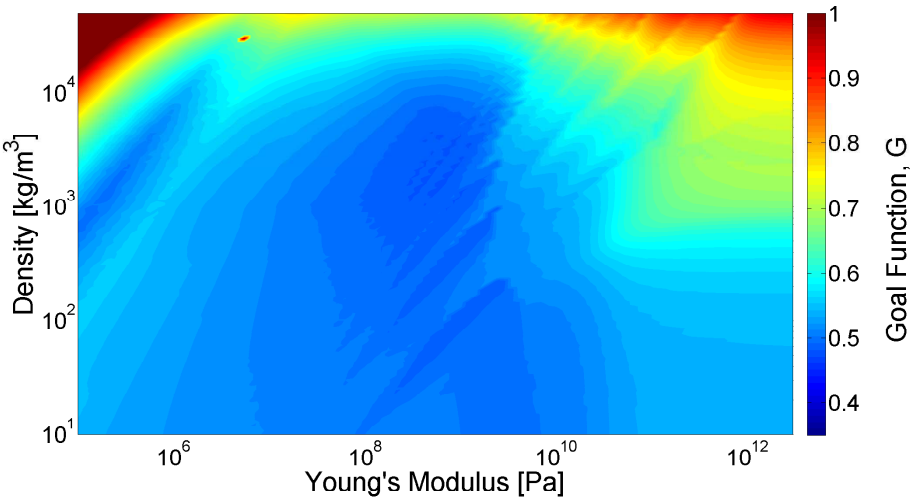

(a)

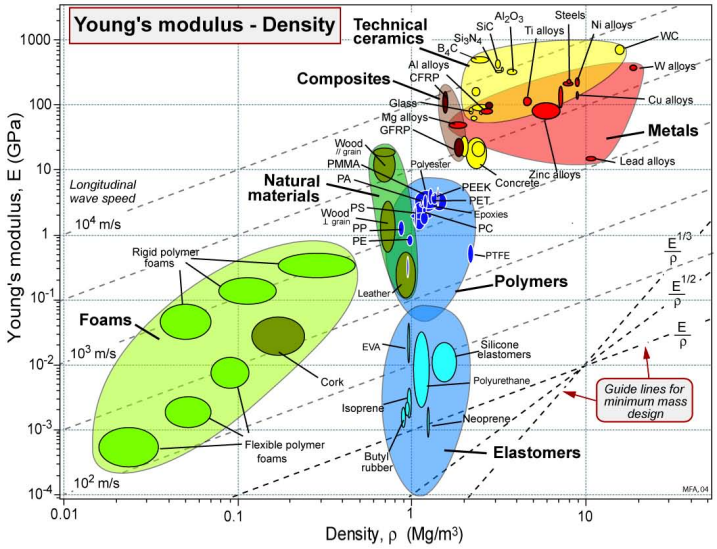

(b)

Figure 5.6: Illustration of the ease of comparing the (a) plot of the goal value as a function of a varying Young's modulus and density and (b) Ashby's Young's modulus vs density plot of common engineering material families [3].

Chapter 6

Material Selection

In this section, the selection of materials for optimal mechanical and acoustical performance while considering the constraints of the system is achieved by applying a method similar to that described in Ashby's publications on materials and material selection [1, 3, 27]. Since there are over 120,000 materials at an engineer's disposal [1], selection begins with a narrowing of the field. To accomplish this, the design requirements need to be translated into functions, constraints, design goals and free variables in order to implement the methods introduced in Chapter 5. While initially large, the list of potential materials may be reduced by first eliminating everything outside of the system bounds. The remaining material parameters may then be utilized to scope the optimization algorithm discussed previously. The results allow for the remaining materials to be ranked based on how well they minimize the difference from the system goals. The values assigned to the materials with specific parameter sets may then be plotted and compared to the corresponding Ashby chart as illustrated at the end of Chapter 5. This approach aids designers in easily recognizing potential promising parameter sets. Alternatively, if an ideal material is not available, a composite of multiple materials may offer an acceptable compromise.

6.1 Bounds and Constraints

An upper bound for a set of numbers is a value which is greater than or equal to every value within the set. A lower bound is dually defined as value which is less than or equal to every value within the set. These boundaries may be set as those physically possible material properties described in the last chapter. A constraint is a condition that a solution to an optimization program must satisfy. Common constraints in material selection include stiffness, strength, fracture toughness, thermal conductivity, electrical resistivity, optical transparency, cost, and mass [27]. Passive sonar systems include elastomers used to a large extent in transducer boots, isolation spacers, sonar domes and sound absorbers, reflectors and transmitters. Common polymers constraints include water permeability, elongation, oil resistance, low temperature performance, tear resistance, service temperature, and chemical resistance [16, 20, 7]. Constraints may be imposed based on the needs and requirements of the customer. Another constraint in the use of this model is the assumption that a one-dimensional model captures the resonances in the frequency range of interest. That is, this model only captures resonances due to in-plane excitations and in-plane displacements created by out-of-plane excitations. The primary assumption behind this model is that the layers in-plane are much larger than they are out-of-plane.

The boundaries do not need to include every possible material and combination, but a wide range is desirable. The larger the initial range, the more likely it is to discover unexpected highly ranked area. The work uses the range described for the seed parameters in the previous chapter as the set of boundaries. These ranges are reprinted in Table 6.1 for convenience.

Another constraint is commonly placed on the density. One of the goals of our project is to develop a lightweight baffle so it would be desirable for the baffle

Parameter	Range
Young's modulus	$1 \times 10^5 < E < 3 \times 10^{12}$ [Pa]
Density	$10 < \rho < 5 \times 10^4 \left[\frac{\text{kg}}{\text{m}^3}\right]$
Poisson's ratio	$-0.95 < \nu < 0.45$
Thickness	$0.3175 < d_e < 1.27$ [cm]

Table 6.1: Parameter ranges of the system under consideration.

to be buoyant in water. This would be very limiting as seen in Figure 6.1 where almost half of the materials available would be eliminated by placing the boundary at $1000\,\text{kg/m}^3$. Depending on the response gains, for this project the customer is willing to accept a maximum density of $3000\,\text{kg/m}^3$.

A final example customer requirement for this work is a minimal thickness change under pressure. For example, at littoral depths, a sonar baffle may be required to stay within 1% of its nominal thickness. Given a depth of 152 m

$$P = \rho g h = 1.489 \text{ [MPa]}.$$

The plane wave modulus M, can be understood to represent the ratio of normal stress to the corresponding thickness change of a thin plate

$$M = \frac{\text{normal stress}}{\text{normal strain}} = \frac{F/A}{\triangle t/t_0} = \frac{P}{\%\triangle} = 0.149 \text{ [GPa]}.$$

The plane wave modulus may also be expressed as a function of the Young's modulus and Poisson's ratio

$$M = \frac{E\,(1-\nu)}{((1+\nu)\,(1-2\nu))}.$$

This leads to a Young's modulus that may be expressed as a function of the Poisson's

ratio and plane wave modulus

$$E = \frac{M\left((1+\nu)\left(1-2\nu\right)\right)}{(1-\nu)}.$$

The maximum value for E occurs when ν equals zero which leads to $E = M = 0.149$ [GPa]. As the Poisson's ratio goes from zero to -1 or 0.5, the Young's modulus decreases and approaches zero itself. To satisfy the customer constraint in the worst case scenario when $\nu = 0$, the Young's modulus must be greater than or equal to 0.149 [GPa].

The constraints developed above are illustrated in Figure 6.1 as boundaries along with the solution to the goal function developed in Chapter 5. Figure 6.1b depicts Young's modulus constraint which eliminates most of the Foams and all of the Elastomers, and the density constraint eliminates most of the metals and heavier ceramics. The remaining materials in the top left quadrant may now be compared using the solutions generated by the optimization program.

6.2 Design Goals

Now that constraints on possible material properties have been placed, and there is some sense as to where an optimal material may lie, the design objectives may be taken into account. These values are choices or preferences made by the designer or customer that would be desirable but are not system constraints. For example, the customer may ask for a material that is injection mold-able to allow for an inexpensive manufacturing. This request would significantly narrow the material families available. Another potential customer request may be for a material that can be purchased off the shelf in order to minimize time spent on designing and testing a composite system. Common design goals include minimizing cost, mass, volume,

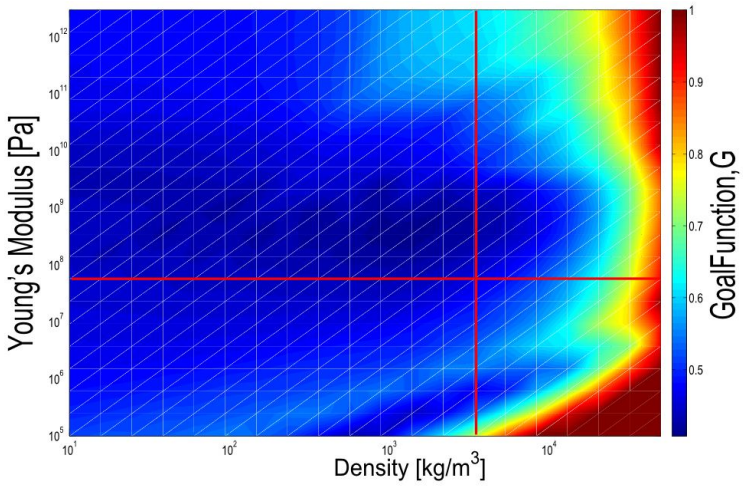

(a)

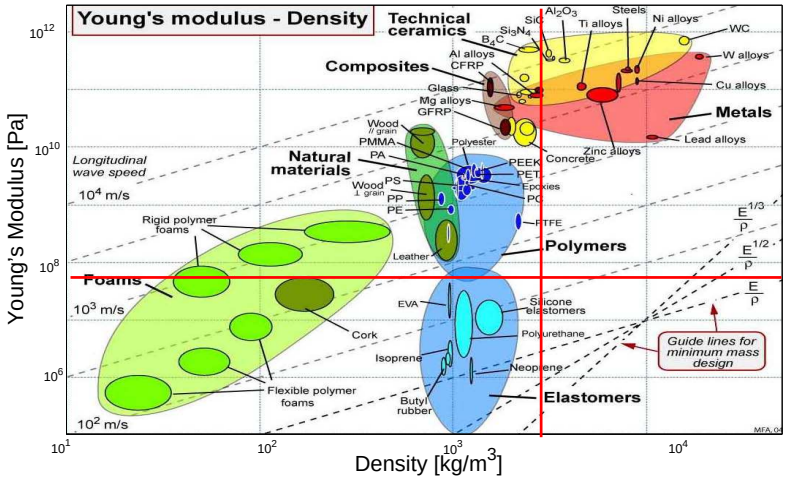

(b)

Figure 6.1: Comparison of the (a) Design area constraints for Young's modulus and density overlaid on the total goal function, G, results and (b) the design area constraints for the Young's modulus and density overlaid on Ashby's Young's modulus vs density chart adapted from Ref. [3].

environmental impact, heat loss and transmissibility, and maximizing absorption, ruggedness, pressure tolerance, and shock tolerance [27, 8, 20].

Design goals often involved with the selection of polymers include mold-ability or flow, tack and amenability to various cure systems [16]. These are constraints that can be answered in part with the use of Ashby charts [1]. Ashby charts, named after the Cambridge professor Michael Ashby, illustrate the placement of many materials and classes of materials along the axis of two often conflicting properties. The bottom plot in Figure 6.1 is an example of an Ashby plot comparing the Young's modulus and density of a wide range of materials.

As seen in Figure 6.2, when the total Goal solution is plotted with Ashby's charts, a decision may be made depending on where local minima occur with respect to the material families. For example, there is a local minimum that falls on both the natural and polymer material families. It is this point at which Heikkola recommends collaboration with a "decision maker", which for this application would be an expert in transducer design [15]. The decision maker is able to narrow the materials down given multiple minima from optimization map utilizing their experience, knowledge of the systems design parameters, and preferences. Some solutions may be discarded for manufacturing reasons, and others may be included that are not at a minima. Once these materials have been narrowed down, the constraints may be reset at these new boundaries and another iteration run through the optimization program with an increased resolution. This interactive method gives the decision maker a chance to recognize pattern formation, and help aid in the selection of an optimal material.

There were multiple areas in the goal function depicted in Figure 6.2a that approached a local minimum. These areas circled in red were then transcribed to Ashby's Young's modulus - density plot in Figure 6.2b. The local minimum around

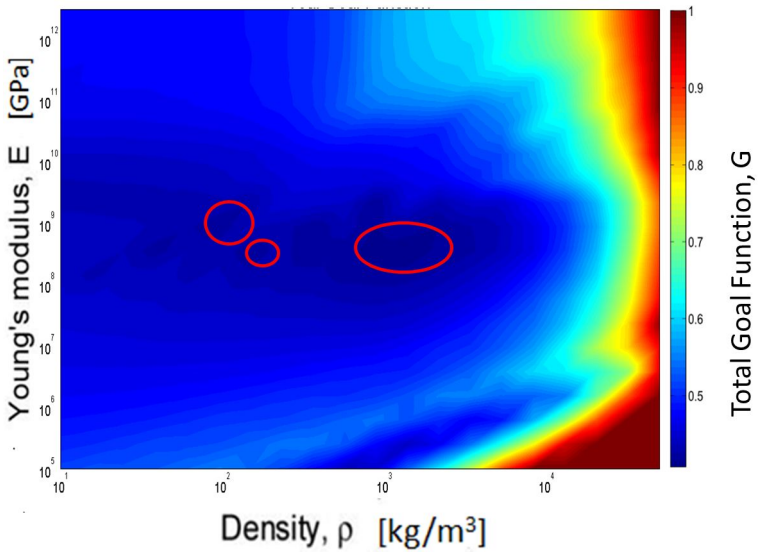

(a)

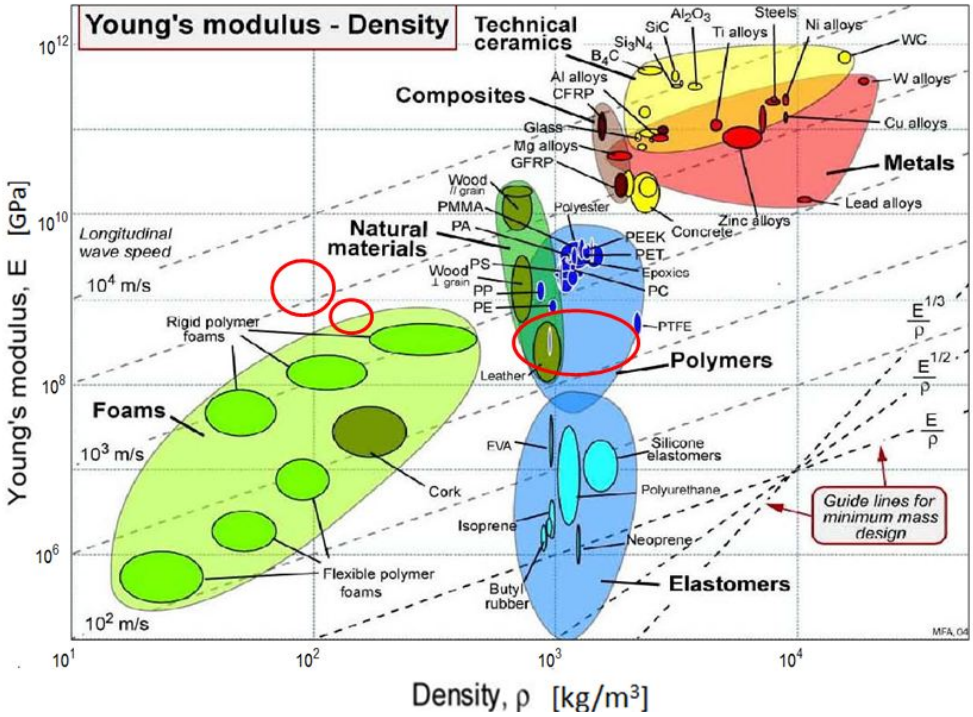

(b) Locations of local minima from the total goal function transcribed to Ashby's material properties plot of Young's modulus and density adapted from Ref. [3].

Figure 6.2: Comparison of the (a) areas approaching a local minimum within the original total goal function boundaries (circled in red) and (b) the locations of local minima from the total goal function transcribed to Ashby's material properties plot of Young's modulus and density adapted from Ref. [3].

the density of $100\,\mathrm{kg/m^3}$ covers a wide range of possible materials that may not be available off the shelf. In this case, the designer has the option of an off the shelf solution with a less than desired response or attempting to find a way to stiffen the material without increasing the density; a difficult proposition. These conflicts are an illustration of the benefits of comparing the Goal function to the corresponding Ashby charts as opposed to finding just the global minimum.

Often an ideal solution falls outside a material family or material available off the shelf as seen in Figure 6.2. In this case, a combination of two or more materials to create a custom composite material may yield the desired material properties. While often a time consuming process, composite material design for a specific application has lead to many innovative materials such as carbon fiber and galvanized steel.

6.3 Composite Material Design

When a desirable solution falls in the white space outside of the material families, a composite material may be designed through the combination of two or more readily available materials in order to produce an overall response that meets the specified design needs. A composite is a material in which a discrete amount of contrast material, known as phase B, is distributed within a continuous matrix , phase A. The expected mechanical behavior can then be derived from the different constituent materials properties, geometry and or boundary properties [3]. In designing a composite material, Ashby utilizes a method paraphrased as, "A + B + configuration + scale" [1]. That is: the properties of the composite material are a function of two different materials A and B as well as the configuration, relative volume fraction and scale of the contrast phase.

The selection of the two materials A and B is dependent upon many consid-

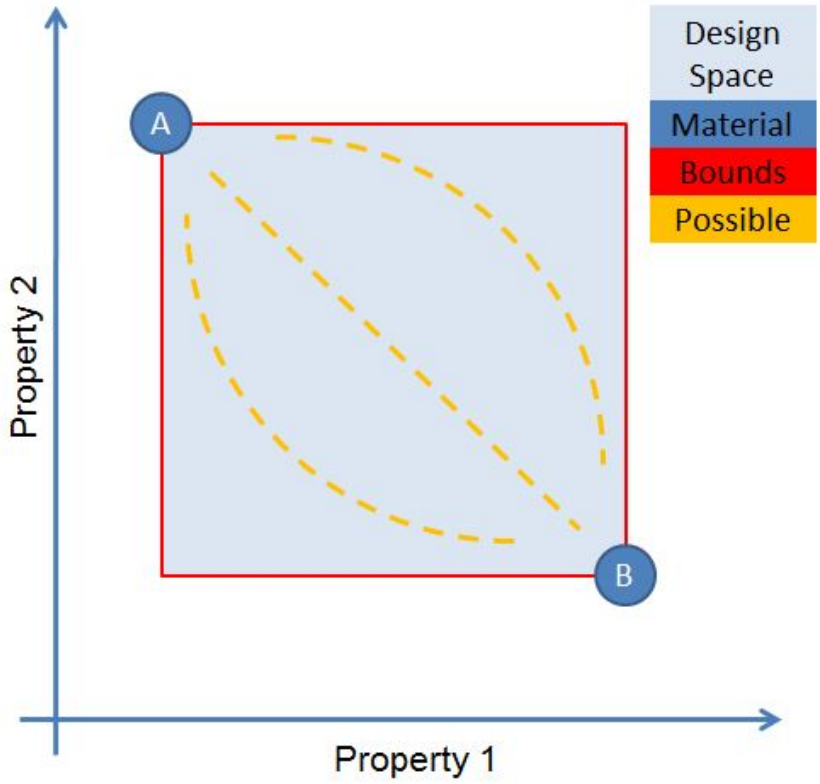

Figure 6.3: Composite design space given two materials

erations. First, the selection is obviously dependent upon the material properties desired. Figure 6.3 illustrates the entire possible design space given two materials. The light blue area is the space in which the desired material properties should land. The selection of A and B is also dependent on the configuration. The dotted orange lines illustrate a few possible scenarios the composite properties track as more or less of the second material is added. Note that the scale and configuration (geometry) of the phase B dictates which track is followed.

There are many possible ways of combining the two constituent materials in order to provide different functionality. Common configurations organized in Figure 6.4 include composites, sandwich, lattice or segments. The functionality commonly pro-

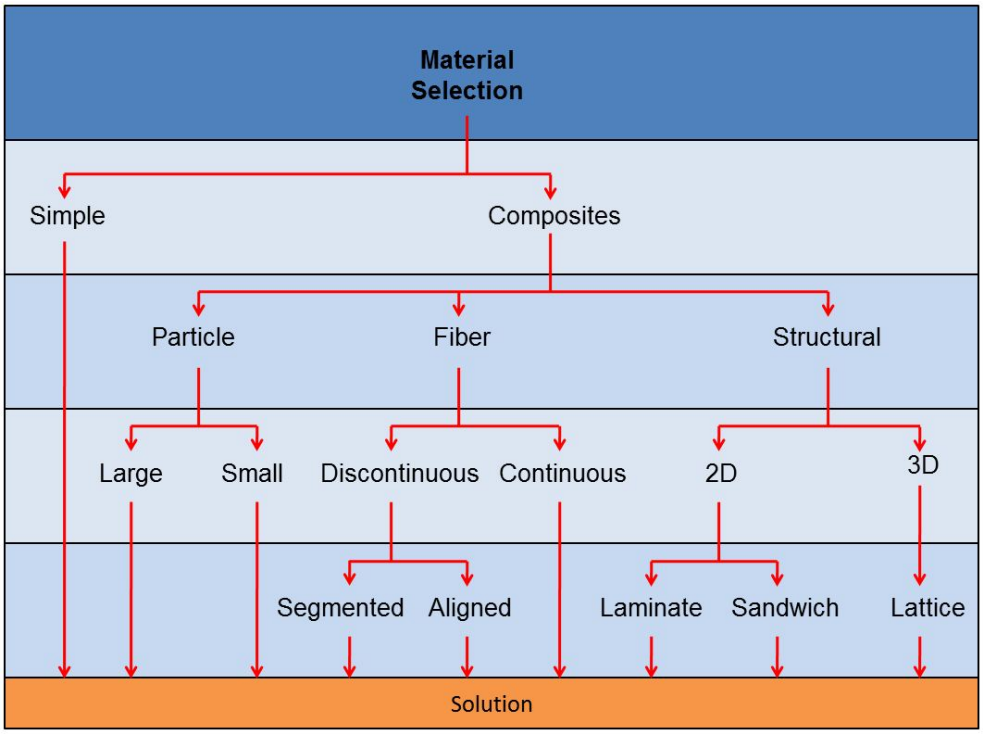

Figure 6.4: Organization chart of common material configurations.

vided by each configuration is detailed in Table 6.2.

6.3.1 Composite Analysis

Composite materials made from a reinforcing particle or fiber inside a polymer matrix are common due to their ease of manufacturing. As seen above in Table 6.2 these materials are stiff, strong, tough, insulative, and light. These are all characteristics often desired in a sonar. In Chapter 5, the optimization algorithm found a minimum to the goal function around a Young's modulus of 3.48×10^8 Pa and a density of 1385 kg/m^3 as seen in Figure 6.5. This corresponds to a point on the Ashby material plot with few potential solutions as illustrated in Figure 6.6. To find a suitable material, a composite material with optimal density and Young's modulus is needed.

Table 6.2: Configurations often used to achieve a particular function are marked with a red dot in this Table adapted from Ref. [1].

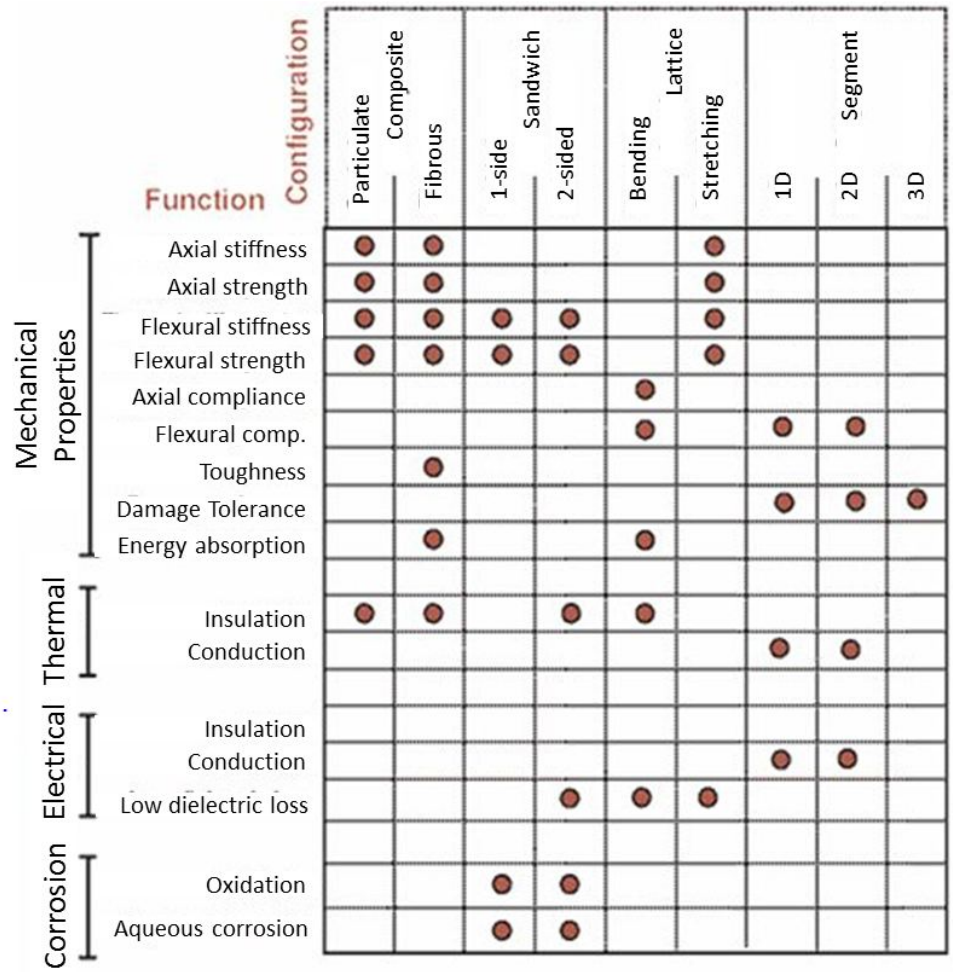

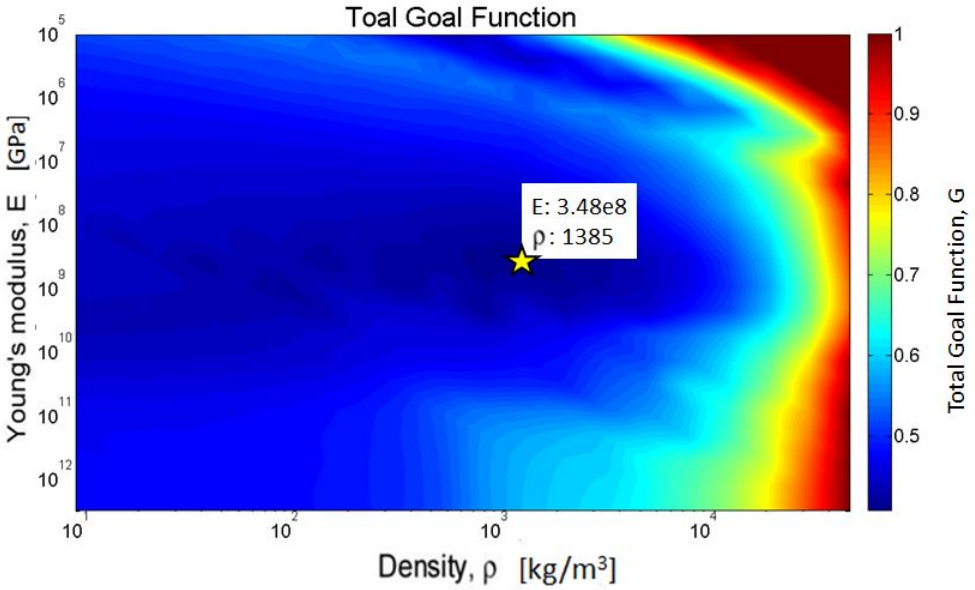

Figure 6.5: Results of the Goal as a function of Young's modulus and density.

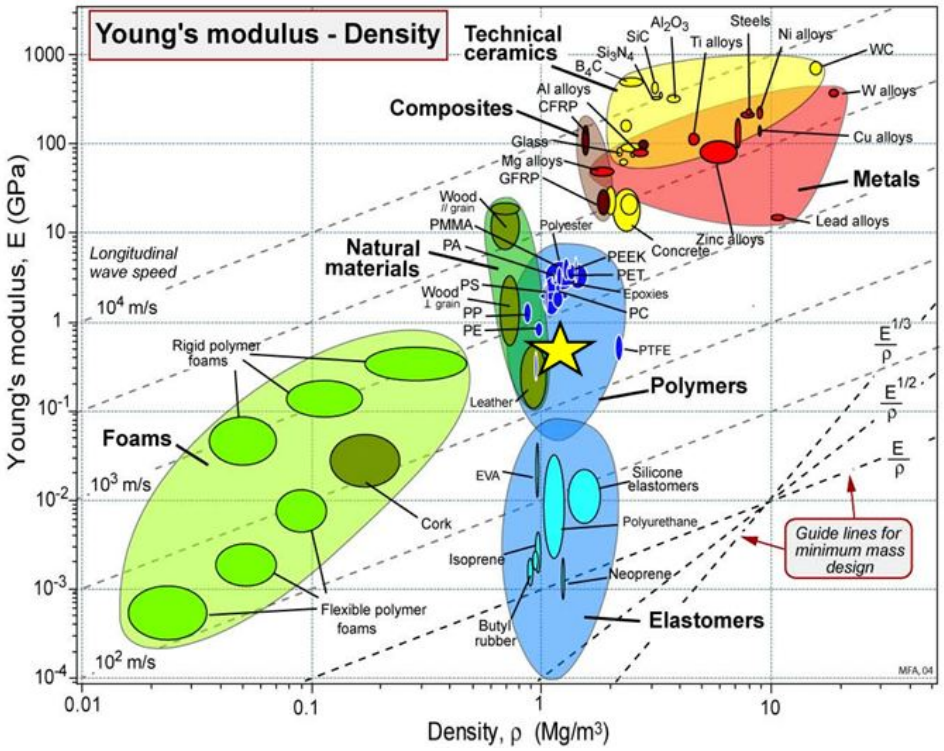

Figure 6.6: Corresponding location of the goal function on the Ashby material plot adapted from Ref. [3].

The density of a composite material is the sum of the masses divided by the sum of the volumes [1, 28]. The composite density, ρ, is a function of the reinforcement particle density, ρ_r, matrix density, ρ_m, and fraction of the reinforcement, f. The reinforcement fraction may range from zero to f_{max} which is determined by the maximum packing fraction. The composite density is given by

$$\rho = f\rho_r + (1 - f)\,\rho_m, \tag{6.1}$$

which is simply the volume average of the densities of the constituents.

A simple method for calculating the Young's modulus is with the Voigt and Reuss bounds [28, 1]. The upper bound, E_u, assumes both the matrix and reinforcement experience the same strain when loaded. This then leaves the stress as a function of the volume average and the composite Young's modulus follows the rule of mixtures solution

$$E_u = fE_r + (1 - f)\,E_m. \tag{6.2}$$

Where E_r and E_m are the Young's modulus of the reinforcement and matrix, respectively. This upper bound on the Young's modulus is sometimes termed the rule of mixtures solution. The lower bound, E_l, assumes both the matrix and reinforcement experience the same stress. In this case the composite strain is a function of the volume average, and the composite Young's modulus may be expressed as the inverse of the rule of mixtures

$$E_l = \frac{E_m E_r}{fE_m + (1 - f)\,E_r}. \tag{6.3}$$

This constraint on the composite Young's modulus assumes a full density or no residual porosity between the matrix and reinforcement particles. While Voigt and Ruess bounds are good starting points, much better predictive models exist. The bounds produced by the Voigt and Ruess models are far enough apart for composites that

often that offer little practical value. A variational approach derived by Hashin and Shtrikman offers a solution with tighter bounds without specifying the phase geometry [29].

Finding an appropriate set of materials for the system studied above starts with the selection of a matrix material. In this case polyurethane, specifically PR-1547, is assumed. PR-1547, manufactured by PRC Desoto International, and distributed by Bergdahl Associates Inc[1], is a two part epoxy that may be easily worked at room temperatures. It is commonly found in hydrophones as an encapsulant of electronics and piezoelectric elements. PR-1547 has a density of $1050\,\mathrm{kg/m^3}$ and a Young's modulus of $3 \times 10^8\,\mathrm{Pa}$ for the expected operating temperatures and frequencies of the application of interest.

Finding a reinforcement material may be accomplished with an algorithm similar to the optimization algorithm in Chapter 5. In this case however the goal function is a simple one or zero based on the constraints above. To maintain uniformity with the previous goal function zeros be used to indicate a material set that satisfies the goal, and one for a material set that does not. Searching through a material set with a Young's modulus ranging from 1×10^5 Pa to $3 \times 10^{12}\,\mathrm{Pa}$, and a density from $10\,\mathrm{kg/m^3}$ to $5 \times 10^4\,\mathrm{kg/m^3}$ covers most common engineering materials. The fiber reinforcement material percentage is set as a range from $1\,\%$ to $99\,\%$. Setting the desired Young's modulus and density to

$$E_d = 3.48 \times 10^8\ [\mathrm{Pa}]\,,$$

$$\rho_d = 1385\ \left[\frac{\mathrm{kg}}{\mathrm{m^3}}\right].$$

Using Eqs. 6.1–6.3 the goal program then finds every reinforcement material Young's

[1] http://www.bergdahl.com

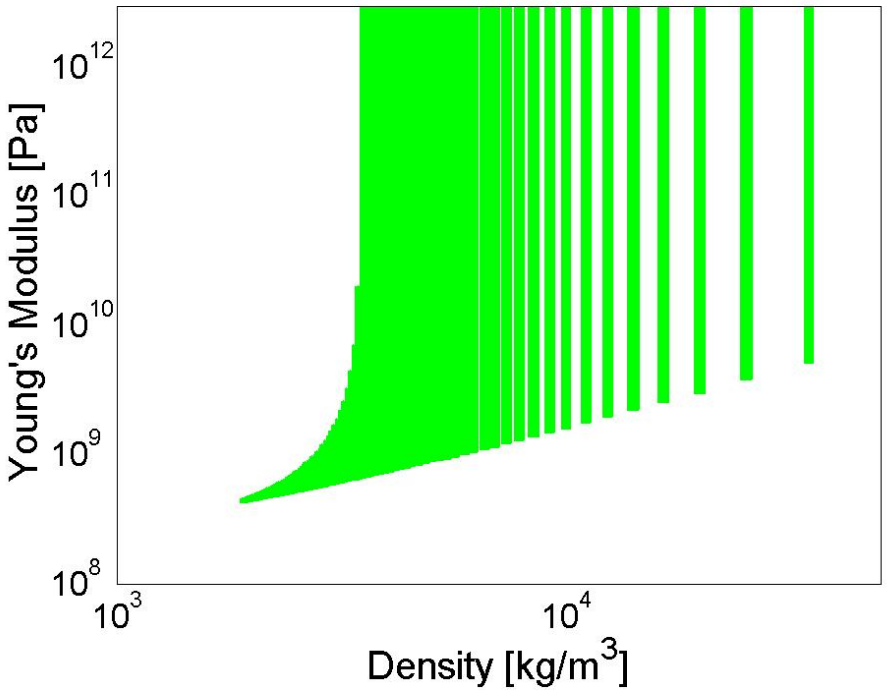

Figure 6.7: The range of parameter values that satisfy the goal condition are shaded green.

modulus and density as a function of reinforcement percentage set that satisfies

$$|\rho_d - \rho(f)| \leq 10 \left[\frac{\text{kg}}{\text{m}^3}\right],$$

$$E_l \leq E(f) \leq E_u.$$

Here $10\,\text{kg/m}^3$ is the range found acceptable from difference between the calculated composite density and the desired composite density. The results of this algorithm are illustrated in Figure 6.7. After selecting a material that satisfies the goal function, the fiber fill percentage is a function of the above constraints as well. For this example, brass particles with a Young's modulus of 104×10^9 Pa and density of $8500\,\text{kg/m}^3$ falls within the acceptable region. This material satisfies the above constraints when the reinforcement fraction f falls between $0.044 \leq f \leq 0.046$.

Combining the methods developed above to screen materials, and analysis of possible material combinations with the optimization method described previously allows for a baffle to be considered with respect to a wide variety of possible layer materials. This use of repetitive computational analysis saves considerable time compared to the traditional method of analyzing systems through trial and error and even finite element analysis. Once a material has been narrowed down to a few promising possibilities would be the ideal time to build a prototype. To illustrate the combination of these methods, the next chapter considers a representative problem with real consumer preferences and constraints.

Chapter 7

Optimal Layer Design for an Example System

It is illustrative to design an example hydrophone system by combining the generic algorithm, optimization algorithm and material selection methodology developed in previous chapters by using the approach schematized in Figure 7.1. Applying an initial layering configuration to the generic algorithm and then running the optimization algorithm based on the customers needs allows for the refinement of the backing layer parameters and material selection. In Chapter 4, an example system is detailed in which the experimental results are compared to the results from the generic program. Using this system as an example, two sonar designers will be interviewed for real customer needs and a material layer will be found that may replace the current backing layers to produce an improved sensitivity through the desired frequency range. This specific case, in which only the backing layer is considered, will be examined to illustrate the combination of the methods described in the previous chapters. Elaboration and improvements of the method are simply a matter of including more variables in the optimization scheme, which is numerically more time-consuming, but conceptually simple.

7.1 System Description

The system considered is a generic version of the experimental setup first seen in Chapter 4. The system layer materials and thicknesses are illustrated in Figure 7.2.

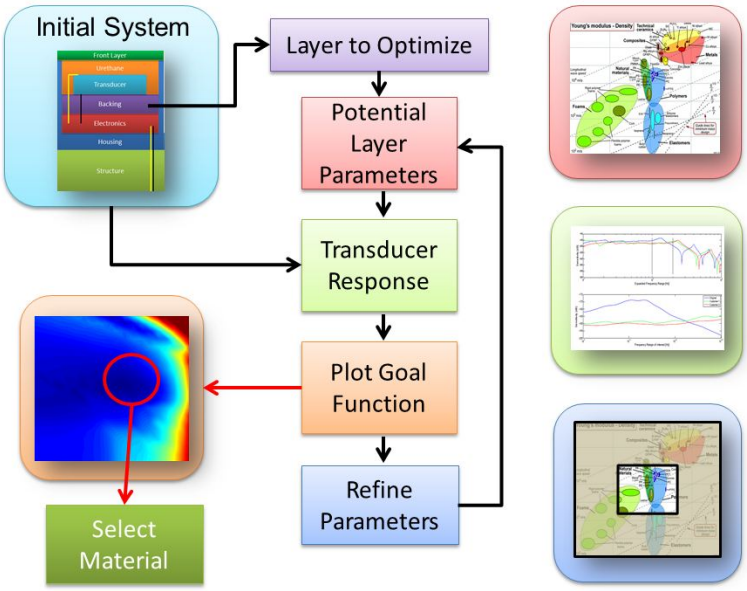

Figure 7.1: Block diagram depicting design process.

Table 7.1: Material properties of the layers in the experimental setup.

Material	Density $\left[\frac{\text{kg}}{\text{m}^3}\right]$	Young's Modulus [Pa]	Poisson's Ratio	Loss Factor
Polycarbonate	1210	2.2×10^9	0.37	0.05
Urethane PR-1547	1050	3×10^8	0.48	0.18
PVC	1390	4×10^7	0.28	0.01
SADM-0.5	2200	4×10^8	0.3	0.05

The material properties used are listed in Table 7.1. The backing material to be designed is compared with a SADM backing 1.27 cm thick sourced from Syntech[1]. The constraint applied to the geometry is a height range from 1.27 cm to 0.3175 cm for the baffle and an element maximum height of 1.27 cm.

The element being considered for potential modification is a 2.54 cm square

[1]http://www.syntechmaterials.com

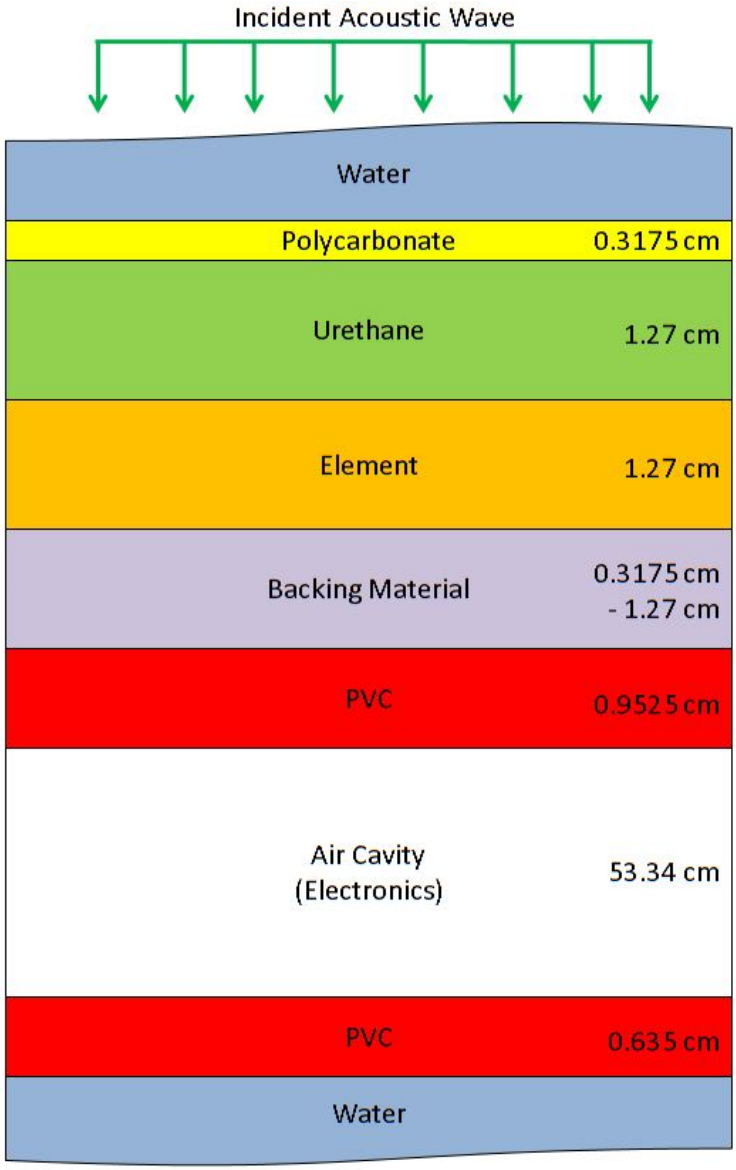

Figure 7.2: Experimental setup illustrated as a system of layers.

Constraint	Value
Center Frequency	150×10^3 [Hz]
Bandwidth	50×10^3 [Hz]
Element Thickness	$d_e < 1.27$ [cm]
Total Thickness	$d_e + d_b < 2.54$ [cm]
Maximum Density	3000 $\left[\frac{\text{kg}}{\text{m}^3}\right]$

Table 7.2: Limiting values for system parameters of the example system.

by 1.27 cm tall 3-1 composite produced by Material Systems Inc. (MSI)[2]. It is noted that there is potential for modification of the element thickness as an optimal response may be found that requires a smaller thickness when considering customer needs and system constraints. These elements may be easily cut to size with a diamond tipped blade and re-electroded with a thin layer of silver epoxy.

7.2 Optimization and Material Selection

The constraints and objectives of the current study were developed using input from real customers with the goal of developing commercially viable sonar systems. The system constraints from Chapter 5 are repeated in Table 7.2 for convenience.

Two experienced sonar designers from the Applied Research Laboratory at the University of Texas (ARL:UT)[3] were interviewed as the customers for this system. They were both given the system design requirements and constraints and a variety of objectives. The input from two designers is utilized in order to illustrate the difference in outcomes which may occur when attempting to satisfy different goals.

Most of the material properties listed are those that were substituted into the generic algorithm developed in Chapter 4. The customers were given the following

[2]http://www.matsysinc.com
[3]http://www.arlut.utexas.edu

Objectives	Customer 1 [%]	Customer 2 [%]
Mean Sensitivity	40	20
-3dB Bandwidth	25	20
Front - Back Isolation	10	15
Flat Sensitivity	20	30
Weight	5	15

Table 7.3: Weighted values assigned to the design goals

metrics as design objectives: (i) maximum sensitivity from the front, (ii) maximum -3dB bandwidth, (iii) isolation between the front and back, (iv) maximally flat sensitivity, and (v) minimum weight. The customers then weighted each objective according to their interpretation of the design requirements. These weighted objectives are compared in Table 7.3. As can be seen, the first customer's main concern is the mean sensitivity while the second customer feels a flat response and lighter system are more important to the design requirements. Care should be taken when deciding on the weighted values as minimizing one or more parameter may lead to undesirable solutions minimizing the goal function. Since the choice of requirements can lead to poor performance, the selection of design goal weights is an important step in the process. These weights may now be applied in the optimization algorithm to determine an optimal baffle configuration meeting the needs of each customer.

The parameters considered for optimization the element thickness and the thickness, density, Young's modulus, Poisson's ratio, and loss factor of the backing. The initial ranges for these materials are listed in Table 7.4. After a quick low resolution scan as described in Chapter 5, the four most influential parameters were fully considered with a higher resolution and multiple iterations at increasing levels of detail. As noted previously, the Poisson's ratio and loss factor for this system minimally effect the response compared to the other parameters.

Parameter	Range
Young's Modulus	$1 \times 10^5 < E < 3 \times 10^{12}$ [Pa]
Density	$10 < \rho < 5 \times 10^4 \left[\frac{\text{kg}}{\text{m}^3}\right]$
Poisson's Ratio	$-0.99 < \nu < 0.49$
Loss Factor	$0.01 < \eta < 0.3$
Element Thickness	$0.3175 < d_e < 2.54$ [cm]
Backing Thickness	$0.3175 < d_b < 2.54$ [cm]

Table 7.4: Example system parameter ranges.

7.2.1 Customer 1

Applying the weighted goals of the first customer to the optimization algorithm generates the goal function plots for various parameter combinations shown in Figure 7.3. The insights and information gained from these plots may be used to narrow the parameter ranges and number of parameters varied for the next design iteration.

When considering the Young's modulus and density, the location of material families needs to be considered as well. The data from Figure 7.3a are compared with Ashby's density-Young's modulus plot in Figure 7.4. An optimal design would be the selection of parameters which will yield the best overall performance. In this field however the optimal design may fall within an inappropriate or unacceptable parameter set. The optimal design may also be a point in the parameter space with little tolerance for variation. The goal of refining the parameter set is not necessarily to find the best solution, but to find a solution that performs well, falls within an acceptable parameter set, and is tolerant of parameter variation. There are multiple local minima as illustrated in Figure 7.4, however within optimal area bounded by a density of $600\,\text{kg/m}^3$ through $4000\,\text{kg/m}^3$ and Young's modulus from $1.4 \times 10^8\,\text{Pa}$ through $5.3 \times 10^9\,\text{Pa}$ lies a large collection of elastomers and natural materials. This is beneficial because if a material can be found off the shelf it will facilitate the design by

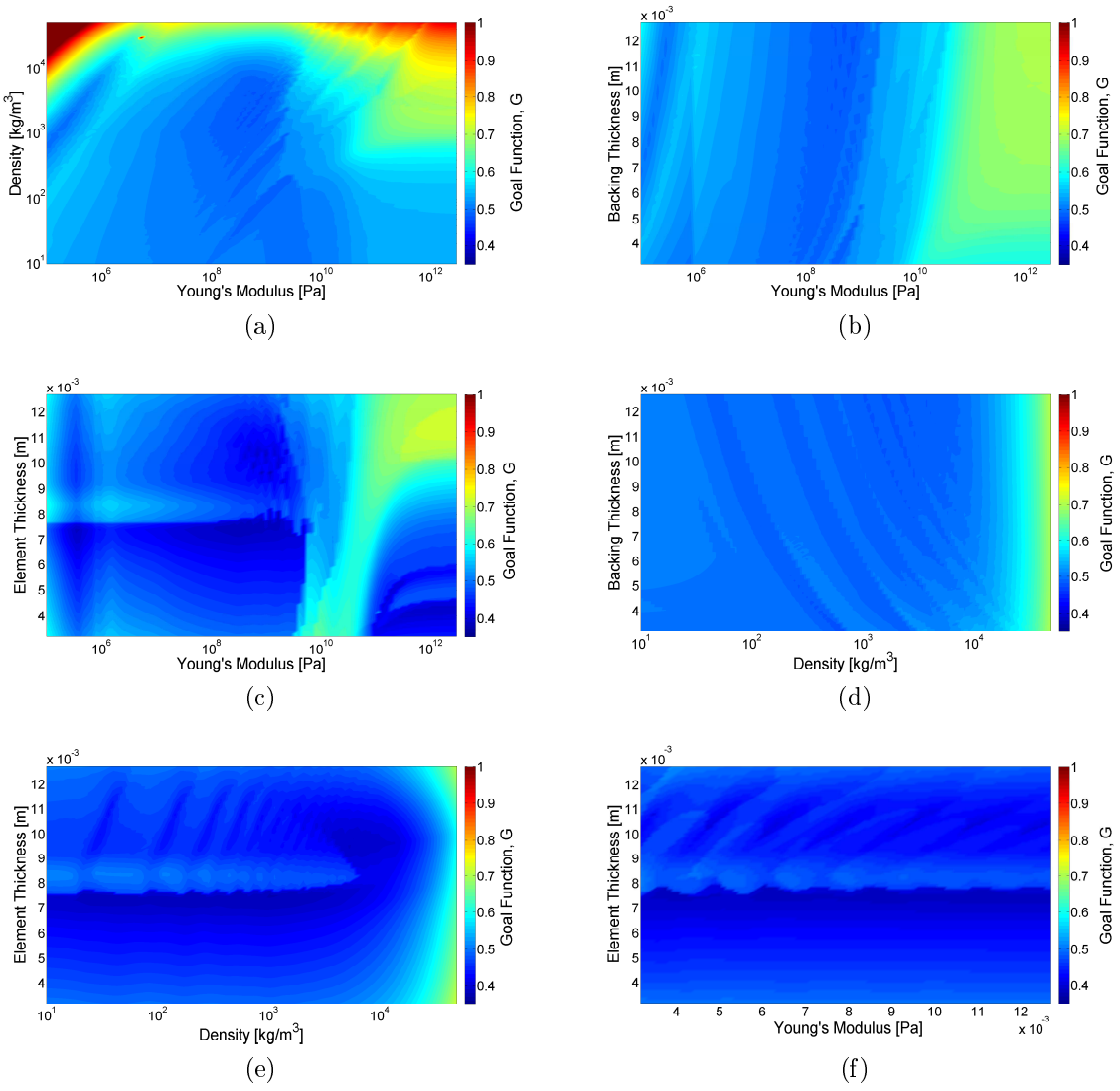

Figure 7.3: Total goal function as a result of the first customer's specifications (a) varying the Young's modulus and density, (b) varying the Young's modulus and backing thickness, (c) varying the Young's modulus and element thickness, (d) varying the density and backing thickness, (e) varying the element thickness and density, and (f) varying the backing thickness and element thickness.

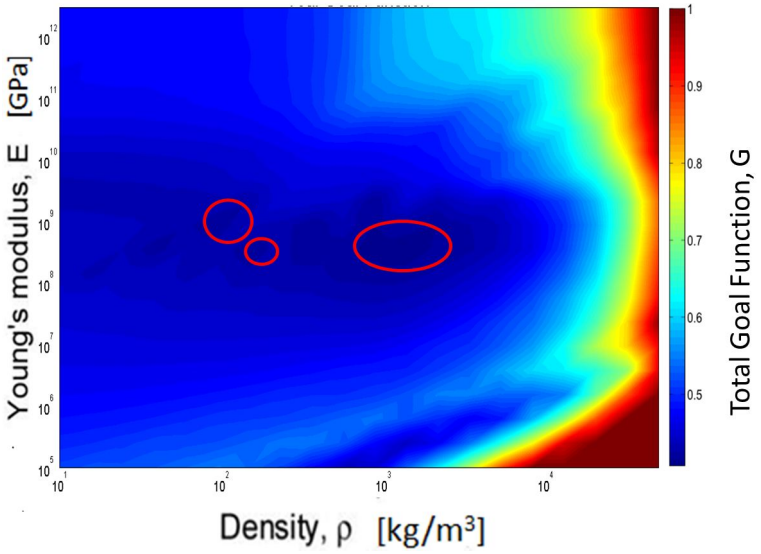

(a)

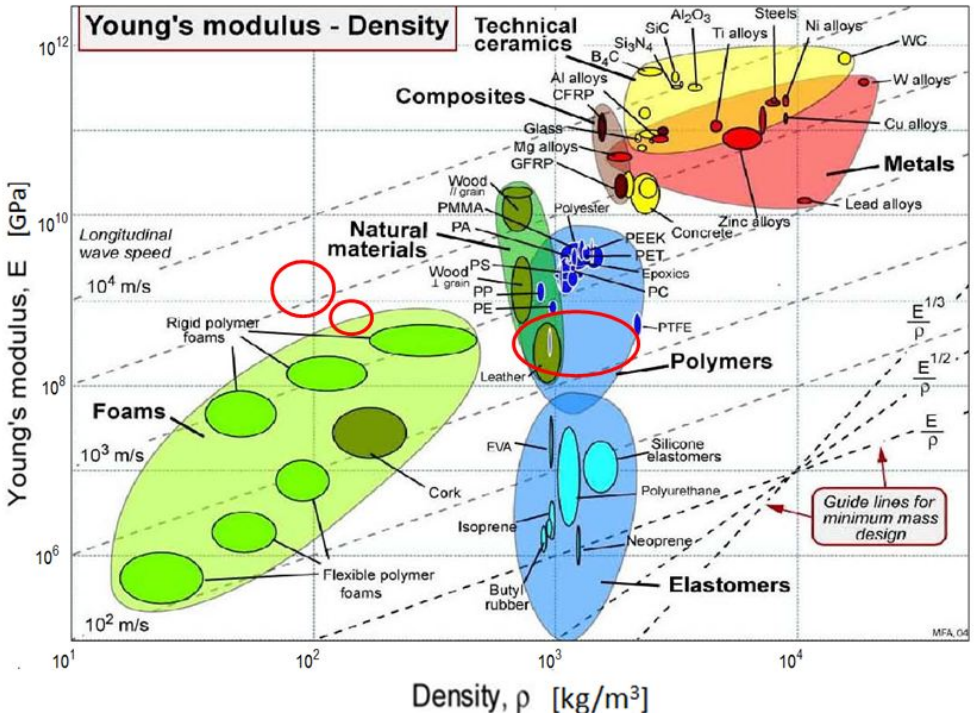

(b)

Figure 7.4: Comparison of the (a) Locations of local minima within the original total goal function boundaries and (b) Locations of local minima from the total goal function transcribed to Ashby's material properties plot of Young's modulus and density adapted from Ref. [3].

greatly decreasing the time to prototype. Next, the bounds above may now be applied to the element thickness in Figures 7.3c, 7.3e, and 7.3f. There are a couple areas that seem to provide good results so both are included in the next iteration. This leads to a new thickness range of 0.00668 m through 0.0102 m. Figures 7.3b, 7.3d, and 7.3f compare the backing thickness with the other parameters. Again considering only the density and Young's modulus range developed above, a backing thickness range of 0.004 m through 0.0127 m encompasses the area with the best results.

Changing the boundaries from Table 7.4 to those determined above allows for the next iteration of the optimization algorithm to further refine an optimal solution. This second iteration yields Figure 7.5. When selecting the next parameter range for system optimization, it is important to consider which area yields the best results. This may be accomplished by selecting a chart whose range varies greatly and whose total goal function is the lowest. For example, Figures 7.5c, 7.5e, and 7.5f which compare the element thickness vary significantly more than the others. These charts also have areas with the best goal function. Note that even though the range over which the element thickness varies has been refined, there is still a large difference between solutions that are relatively close to each other. From these figures, the optimal range for the element thickness may now be set at 0.007 m through 0.011 m. This is the most important parameter because an increase of only 11 mm in the thickness would almost double the final goal result. The rest of the Figures (7.5a, 7.5b and 7.5d) do not stand out in terms of range or minimum goal so the easiest parameter to vary should be selected. The backing thicknesses in Figures 7.5b and 7.5d have the best goal total in the top half of the results leading to a new range of 0.0108 through 0.0127 m. In this backing thickness range the best density falls within 1600 $\mathrm{kg/m^3}$ through 1800 $\mathrm{kg/m^3}$ and a Young's modulus between 1×10^9 Pa through 1.3×10^9 Pa.

The optimization algorithm was run once more to yield the results for cus-

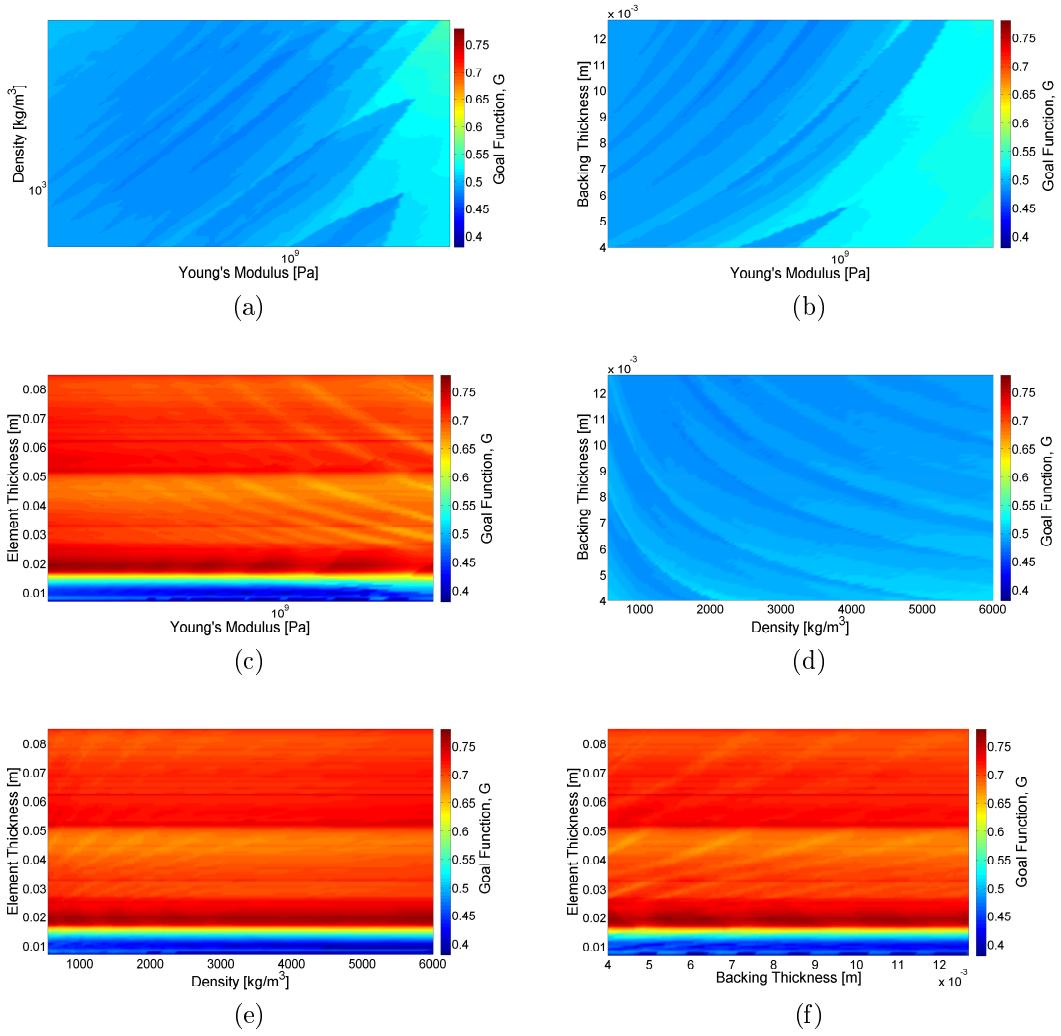

Figure 7.5: Refined total goal function as a result of the first customer's specifications (a) varying the Young's modulus and density, (b) varying the Young's modulus and backing thickness, (c) varying the Young's modulus and element thickness, (d) varying the density and backing thickness, (e) varying the element thickness and density, and (f) varying the backing thickness and element thickness.

Table 7.5: List of potential materials that correspond with the first customer's specifications.

Material	Supplier	Part #	E [Pa]	$\rho \left[\frac{\text{kg}}{\text{m}^3}\right]$	G_F
Ideal Material			1×10^9	1800	0.381
Polyvinylidene Fluoride (PVDF)	RTP Company	RTP 3300	1.38×10^9	1770	0.483
Fluoropolymer Resin	DuPont	Tefzel 210	1.2×10^9	1700	0.476
Fluoropolymer Resin	DuPont	HT-2183	1×10^9	1700	0.382
SADM (Reference)	Syntech	SADM-0.5	4×10^8	2200	0.393

tomer 1 shown in Figure 7.6. By narrowing down the results again as seen in the first and second iteration, the element thickness proves the be the most significant parameter. Setting the element thickness at 0.0777 m leads to a backing thickness of 0.01095 m. At this backing thickness, the optimal density is $1800\,\text{kg/m}^3$ and a Young's modulus of $1 \times 10^9\,\text{Pa}$. Applying these values to the generic algorithm yields a total goal function, G_f, or 0.381.

Based on the results developed above, Figure 7.7 shows an area in which any density and Young's modulus combination provides the desired results. These values fall in the middle of the polymer material family and on edge of maximum density for the material family. A quick look through some material suppliers yields potential solutions for the backing which are in Table 7.5. These materials were sourced by first searching Matweb[4] with the material properties and then reading through the supplier literature until a close match was found. Matweb is an on-line material property database with over 83,000 metals, plastics, ceramics and composites. Also

[4]http://www.matweb.com/

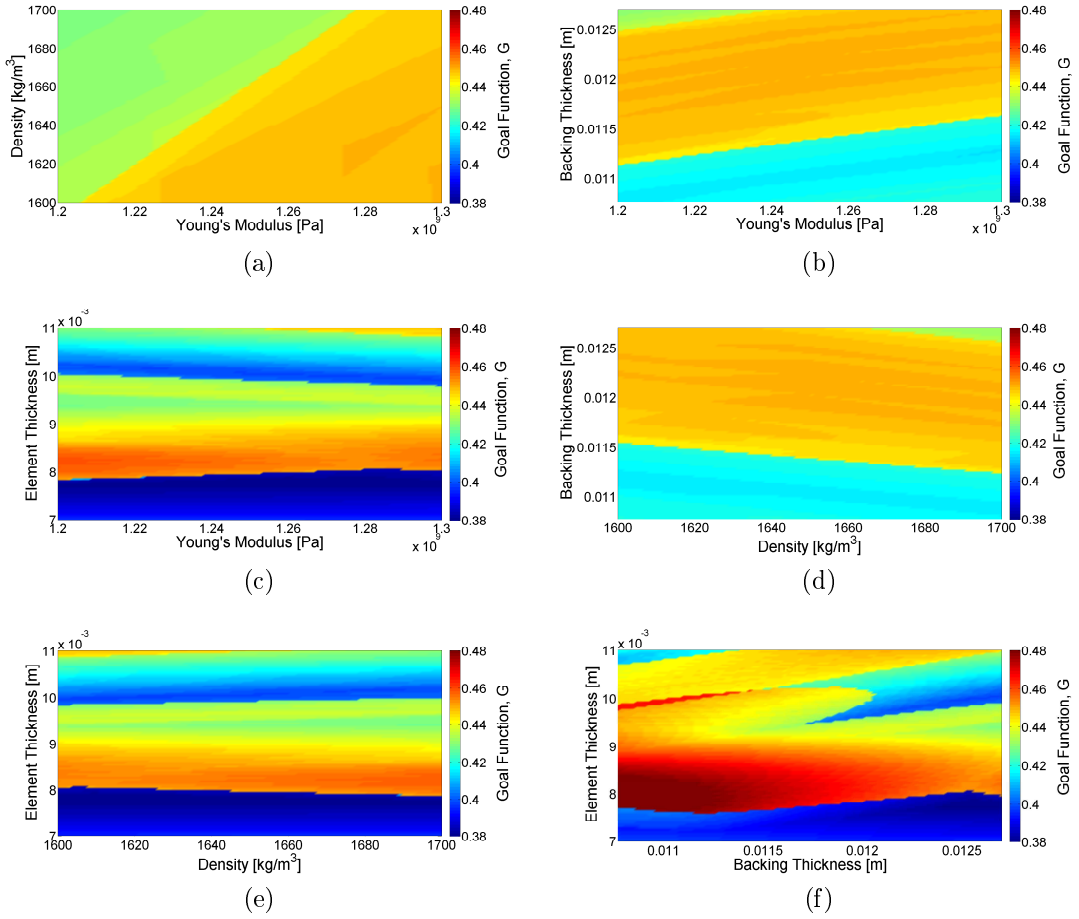

Figure 7.6: Final refined total goal function as a result of the first customer's specifications (a) varying the Young's modulus and density, (b) varying the Young's modulus and backing thickness, (c) varying the Young's modulus and element thickness, (d) varying the density and backing thickness, (e) varying the element thickness and density, and (f) varying the backing thickness and element thickness.

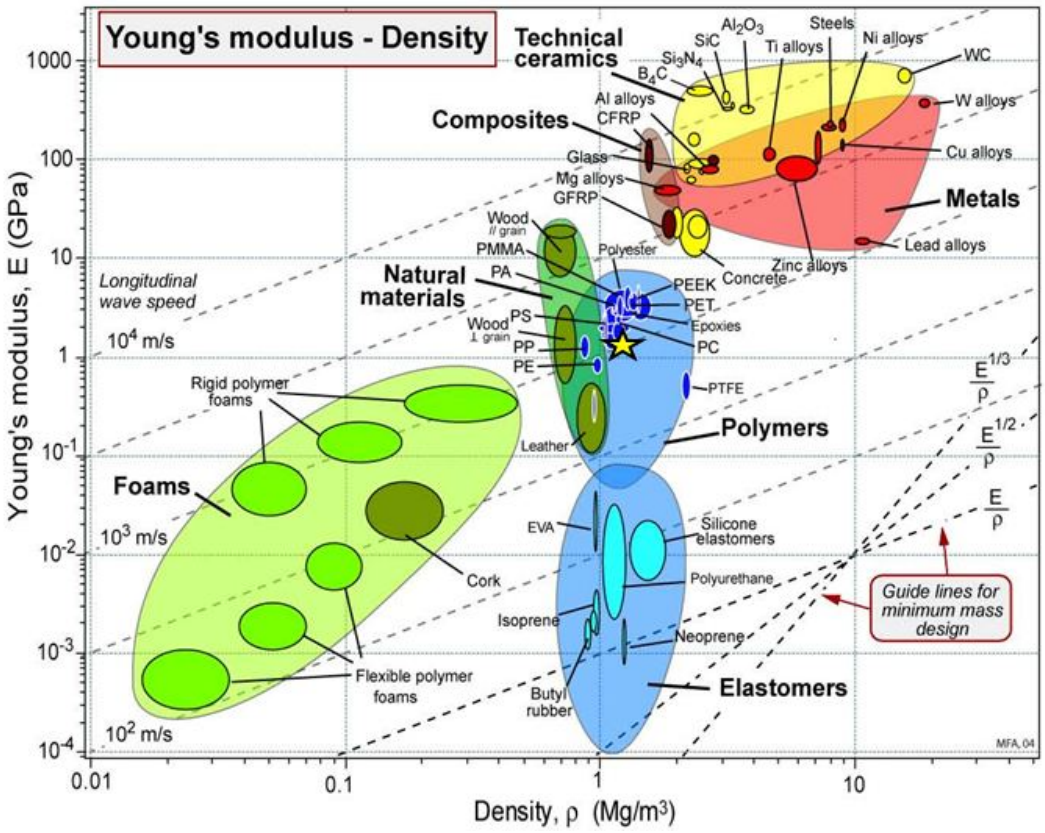

Figure 7.7: The optimal Young's Modulus and density based on the first customer's specifications is indicated by the yellow star.

Table 7.6: Results from three iterations of the optimization algorithm using the second customer's specifications.

Young's Modulus, E [Pa]	Density, ρ $\left[\frac{\text{kg}}{\text{m}^3}\right]$	Element Thickness, d_e [m]	Backing Thickness, d_b [m]
2.5×10^8	1000	0.007137	0.01103

included in Table 7.5 is a comparison of the G_f value with the real materials, the ideal material and the control case with SADM. The SADM in this case is of the ideal thickness and paired with an ideal element thickness. Any of these materials fit the first customer's specifications well. The fluoropolymer resin, HT-2183, from Dupont yields the smallest G_f and is also a material that may be injection molded greatly reducing the associated machining costs.

7.2.2 Customer 2

Applying the weighted goals of Customer 2 to the optimization algorithm generated Figure 7.8. These results were then narrowed down following the same steps outlined above. This process was iterated twice more to yield the results for the second customer in Table 7.6. As seen in Figure 7.9 these results lie in the Polymer and Natural materials families as before except now the ideal material is both less dense and stiff. This places the material on the denser side of leather. Leather's properties while ideal in this case are not known to remain constant over long periods of time. For this application a material that does not degrade over tens of years is preferable.

Table 7.7 contains several potential materials which are also compared to the ideal and control case. The SADM again in this table is of the new ideal backing thickness with an element of the ideal thickness as well. DuPont's Zytel FN714 [30]

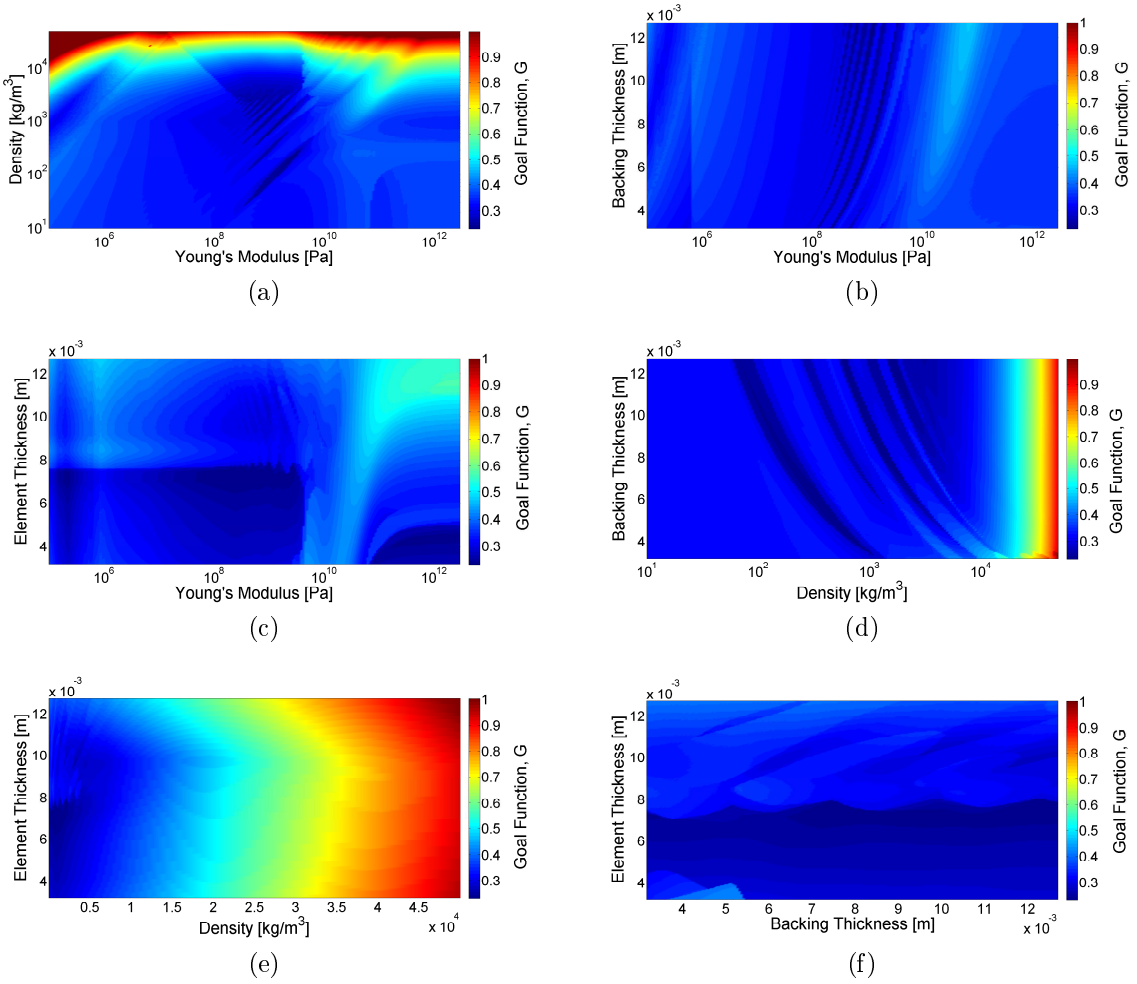

Figure 7.8: Total goal function results given the second customer's specifications (a) varying the Young's modulus and density, (b) varying the Young's modulus and backing thickness, (c) varying the Young's modulus and element thickness, (d) varying the density and backing thickness, (e) varying the element thickness and density, and (f) varying the backing thickness and element thickness.

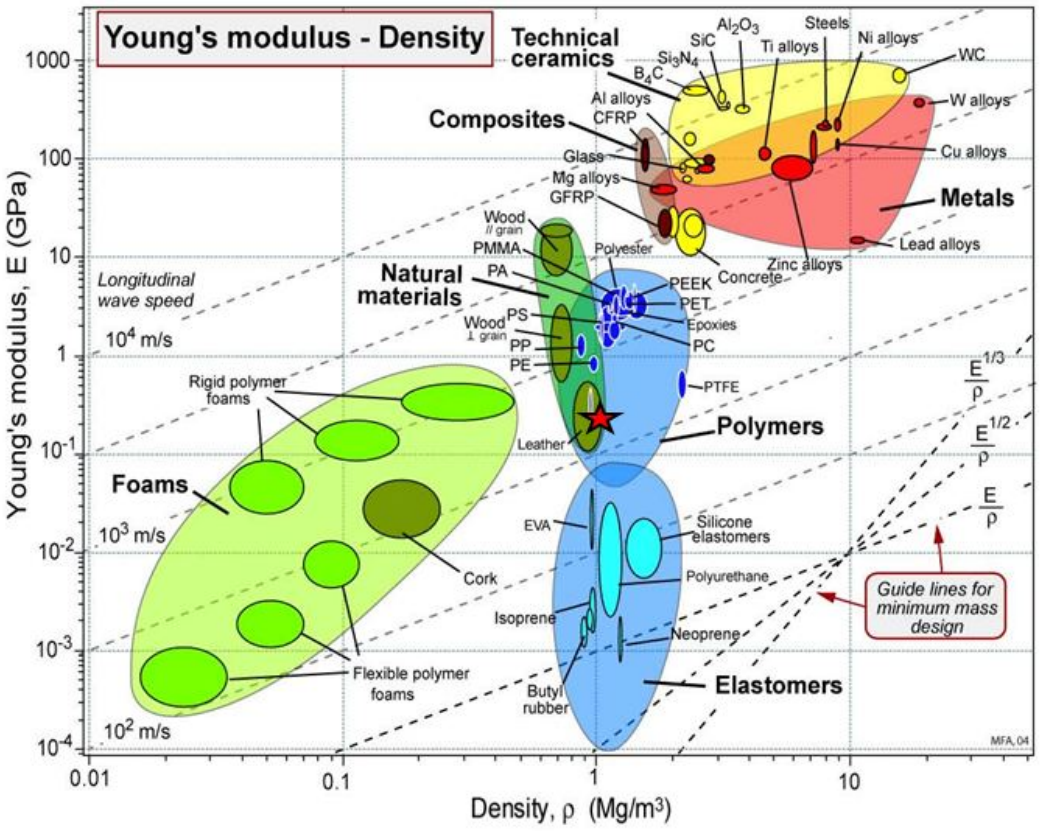

Figure 7.9: The optimal Young's modulus and density based on the second customer's specifications is indicated by the red star.

Table 7.7: List of potential materials that correspond with the second customer's specifications.

Material	Supplier	Part #	E[Pa]	$\rho \left[\frac{\text{kg}}{\text{m}^3}\right]$	G_f
Ideal Material			2.5×10^8	1000	0.218
Nylon Resin	DuPont	Zytel FN714	2.4×10^8	1020	0.219
Polyether Block Amide	Pebax	6333 SP 01	2.8×10^8	1010	0.219
Polyamide 12	Evonik	L2128	2.3×10^8	1050	0.220
SADM (Reference)	Syntech	SADM-0.5	4×10^8	2200	0.237

Table 7.8: Results from three iterations of the optimization algorithm using the second customer's specifications.

Case	Young's Modulus [Pa]	Density $\left[\frac{\text{kg}}{\text{m}^3}\right]$	Element Thickness [m]	Backing Thickness [m]
Original	4×10^8	2200	0.0127	0.0127
Customer 1	1×10^9	1800	0.00777	0.01095
Customer 2	2.5×10^8	1000	0.007137	0.01103

and Pebax's 6333 SP 01 [31] both match the second customer's requirements very well. Given that two materials provide near-optimal behavior; inspection of other factors may help decide which material is better such as price, chemical resistance, impact behavior, fracture toughness, etc. In this case, Pebax's 6333 SP 01 performs very well in the notched impact test which would be beneficial in applications where shock or impact loading may occur. Further, 6333 SP 01 has a lower melting temperature which would decrease the molding expense and improve mold-ability.

7.2.3 Comparing Customers

Customers 1 and 2 both have valid reasons for weighting the parameter values differently. The first customer believed a higher sensitivity was the most important criteria, while the second customer favored a smoother response over the entire frequency range. The parameters inspected and modified for these two cases are compared with the original case in Table 7.8. Figure 7.10 plots the expected receive sensitivity curves over the frequency range of interest for the two cases inspected along with the results from the original system. As can be seen, both redesigned systems have a significantly flatter response than the original system and the first customer's response has an improved gain while sacrificing smoothness and bandwidth around resonance.

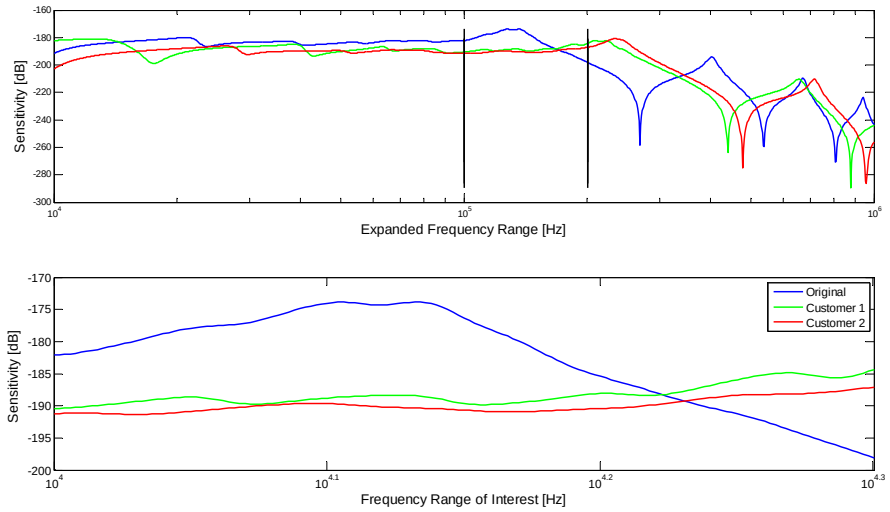

Figure 7.10: Response of the system with optimized variables derived from customer's weighted responses.

Since the system proposed by this work is fairly quick to run and iterate, the results may quickly be shown to the prospective customers and changes made based upon the resulting discussion. For example, a customer may want to explore options for decreasing the system weight while maintaining a relatively high sensitivity. The customer may then judge multiple runs with different criteria and have a much better understanding of the system before making a final decision.

7.3 Conclusions

As can be seen by comparing Tables 7.5 and 7.7, the material solutions for both system are significantly different. Both of these solutions may be developed very quickly decreasing the time spent analyzing materials and increasing the chances of a material working well when prototyped.

7.3.1 Recommending Baffles

Certain components of the methodology presented here individually contribute to the the design of sonar systems at ARL:UT. For example, the generic algorithm allows sonar systems to be tested quickly and easily whether it is a new system or a system being considered for use at different frequencies. While not as accurate as finite element simulations, this method is orders of magnitudes quicker in providing information important to baffle design. The optimization algorithm is a fast program that can be used to iterate through many possible configurations in order to determine an optimal solution given the constraints and objectives of the system. The images presented in the figures above utilized a very fine resolution in order to generate high quality images for publication, yet the program still computed every combination in three to four hours. In practice, a resolution of 20 data points per parameter has been found to perform adequately with a total computational time under 4 minutes. To compare, a system that takes ten minutes to solve using the optimization program would require hours using a finite element program. Finally, the material selection method offers a unique approach for narrowing available materials and making informed decisions. Combined, these algorithms offer a quick and unique method for finding optimal material and layer properties of a given system not seen currently in the literature.

7.3.2 Future Work

The above method, while currently useful, would benefit from work in a few key areas. The generic algorithm should be streamlined to reduce unnecessary calculations. This will minimally reduce the time required to run a single simulation but should significantly improve the total computation time of the optimization algorithms. The generic algorithm also currently only analyzes the system in one di-

mension. This is acceptable in many cases where the wavelength of interest is much smaller than any other dimension. However, at low frequencies, the generic algorithm would be more useful if it took into account length and width of the layers in order to improve the prediction of response and modes at lower frequencies.

The generic and optimization algorithms currently require extensive data entry and transcription between each other before different systems may be computed. In this case, the development of a graphical user interface GUI that keeps track of the properties and dimensions of each layer and applies them seamlessly across the algorithms would render the entire methodology more robust. The current generic algorithm is also very simple with the materials and properties input by hand. This is easy for simple systems but becomes tiresome as the number of layers increases. An intelligent GUI would address this problem by depicting the system as the inputs are entered and providing a more user-friendly interface eliminating confusion and transcription errors. The GUI should also include a materials database that is easy to access and modify. Currently, the materials are stored on a separate database which needs to be called multiple times with every response solution.

The current optimization process is quick where the computational time is mainly a function of the resolution and the number of parameters requested. Currently, the algorithm compares every possible material six times in order to compare four properties, once for each possible pair. For a high resolution or comparison of many variables, the algorithm slows down considerably. The current method relies on a brute force method of calculating every possible scenario in order to avoid missing a local minima at a convenient location. It may be possible however, to utilize more sophisticated optimization techniques to capture more minima while ignoring areas with poor results in order to save computation time. The optimization method also currently revolves around the comparison of two parameters at a time. Again,

this method works well for a few parameters, but may get complex quickly when the parameter space is expanded. At the moment, four parameters seem to be the limit at which it is still easy to follow trends and develop optimal material values.

The material selection method is unique in its use of a color-coded graphical representation of an optimal parameter range combined with potential material families in the same parameter ranges. Currently, the goal function and material map are independent and only considered side by side. An optimization map that was overlaid on top of the material map would reduce the time currently spent transcribing the optimal areas. The optimization algorithm also currently does not consider available materials. This was done in order to not limit the material selection process. However if the user has access to a large database of material properties, optimization of available materials would be a beneficial addition.

Finally, it would be valuable to know the response of materials as a function of temperature, frequency and pressure. While the developed algorithms in this work would accept complex values for every parameter, the current database only considers a single value. The development or compilation of such a material database would expand the validity of solutions over a wide frequency range. Finally, as mentioned above, integrated materials and optimization algorithms would add significant value in the ease of selecting materials both off the shelf and composite.

Appendix A

Finite Element Modeling

A.1 Introduction

Modeling a transducer using FE software is useful when verifying complex analytical models or, conversely, when modeling transducer geometries that are difficult or impossible to determine analytically. Agreement between the two methods or understanding of any differences yields a level of assurance in both models. This Appendix employs the FE software package Comsol Multiphysics for finite element analysis (FEA), but the results should be the same regardless of software package chosen. Every case described in this Appendix uses the Comsol 2D Acoustics Piezo Plane Strain and Pressure Acoustics modules and the terms and steps described here are specific to the Comsol 2D Acoustics software module.

A.2 Submerged Transducer

For a submerged transducer, the piezoelectric layer should be sandwiched between two layers of the same external fluid. One fluid layer will have a forcing time-harmonic pressure applied at the top and the other will have a Perfectly Matched Layer (PML) opposite the pressure source. The PML is impedance matched to the adjoining domain and absorbs any incoming pressure to simulate a radiation condition. This is necessary to simulate an infinite fluid surrounding the transducer.

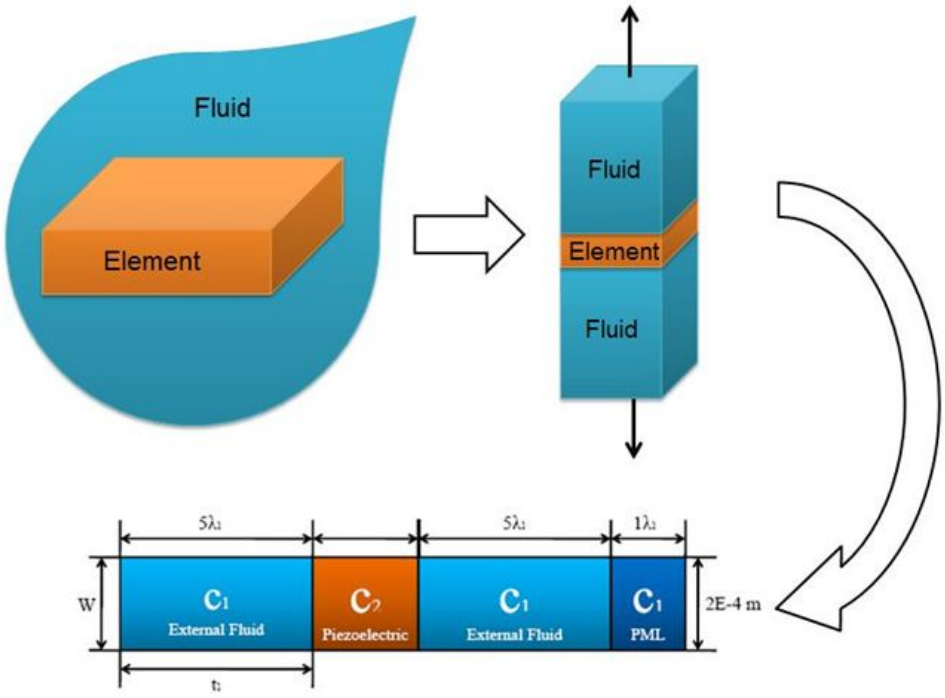

Figure A.1: Illustration of the conversion of a real system into a model suitable for finite element analysis.

A.2.1 Domains

This model's drawing will consist of multiple layers as illustrated in Figure A.2. These layers should be drawn as separate domains with care taken to prevent any overlapping. For a submerged transducer, the thickness of these layers will depend on the sound velocity, c, in each material and the minimum frequency, f_{min}, of interest. At the lowest frequency the thickness should be at least five wavelengths long or

$$t = 5\lambda = 5\frac{c}{f_{min}}.$$

For example, if the first layer is composed of water and the lowest frequency of interest is 500 kHz the thickness should be $5 \times 1500/5 \times 10^5$or 0.0150 m. Since the run time of even the largest models were not excessive, the PML was given a large thickness

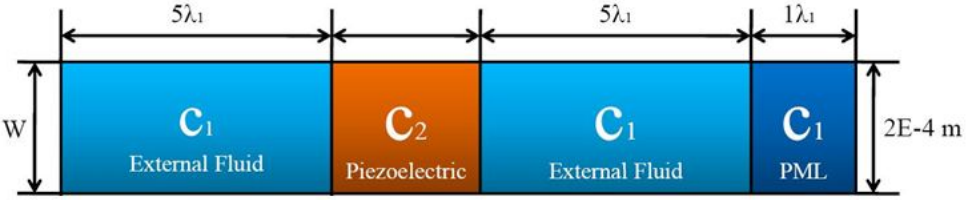

Figure A.2: Schematic representation of the domains for the implemented FEM.

to guarantee total absorption. Setting the PML thickness to one wavelength worked well in every case explored in this work.

Since only propagation in the x_3 direction is of interest, the width, W, of the domain should be minimized to eliminate variation in the plane of the transducer. Since there will only be one element in the width direction, one option is to make the width the same size as a mesh element. A width of 2×10^4 m wide was selected to facilitate the selection of boundaries.

These guidelines for thickness and width worked well when applied to every case described by this work. Figure A.2 of a submerged transducer is provided for reference.

A.2.2 Physics

Under physics, the sub-domains should be set first. For fluid domains, such as the water domain where the pressure originates, only the Pressure Acoustics module should be activated. For all solids, such as the piezoelectric element, only the Piezo Plane Strain module should be active. The PML sub-domain should be the same as the preceding layer, or in this case a fluid with only the Pressure Acoustics module active. In the fluids and piezoelectric layer damping has been neglected. As described later, only solids excluding the transducer will account for damping. After inputting

the correct values for the sub-domain fields, the boundary conditions are examined next.

Layers active in the Piezo Plane Strain sub-domain all have a Zero charge/Symmetry electric boundary condition except for the side opposite of the incoming pressure of the piezoelectric layer. This layer has the Ground electric boundary condition. The width faces all have the Symmetry plane constraint, illustrated in Figure A.3, simulating an infinite material along the width axis. Finally, every surface has no load except for the sides parallel to the incoming pressure of the piezoelectric layer. These boundaries have a value of $-p$ along the thickness axis representing the total pressure in the adjoining fluid domain at a given point.

Layers active in the Pressure Acoustics sub-domain will generally have a Sound hard boundary condition. The exceptions are the incident pressure at the fluid domain and interfaces between sub-domains. To simulate the incoming pressure a radiation condition is applied with a plane wave of one pascal amplitude, p_i, in the thickness direction only. In this case, 'radiation condition' is a term used by Comsol and should not be confused with Sommerfeld radiation. The amplitude value is arbitrary as it will be divided out when the sensitivity is calculated. Boundaries separating fluid and solid domains need to be properly coupled to capture the correct acoustic-structure interaction. The pressure in the fluid drives the elastic material with the total pressure, but simultaneously the acceleration of the solid influences the pressure field in the fluid at their interface. To apply the pressure between the two solids, the interior boundaries will need to be activated. This is accomplished by setting the Normal Acceleration boundary condition with the acceleration in the thickness direction value. In these cases the inward acceleration a_n is expressed as v_tt_smppn.

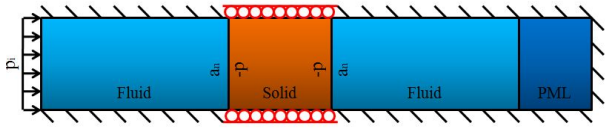

Figure A.3: Schematic representation of the submerged transducer boundary conditions for the implemented FEM.

A.2.3 Meshing

Meshing is simplified using the mapped mesh utility which creates a rectangular element grid within each domain. The mesh is simply specified with a fixed number of elements n defined per boundary. In these cases, the width will only have one element while the elements per layer thickness will be determined by the maximum frequency of interest f_{max}, the sound velocity in the layer and the layer thickness. The goal is to have at least seven elements per wavelength at f_{max}

$$n = \frac{7t}{\lambda} = \frac{7tf_{max}}{c}.$$

For example, in the first fluid layer 0.015 m thick with sound velocity of 1500 m/s at a maximum frequency of 5×10^6 Hz there should be 350 elements along the length of the domain.

A.2.4 Solver

For these cases the Parametric Direct Linear system solver (UMFPACK) was used. This solver found a solution over the frequency range of interest quicker than any other included solver. The solution was sought over the frequency range of 0.1 to 5 MHz. which represents the range over which there were interesting features in the sensitivity.

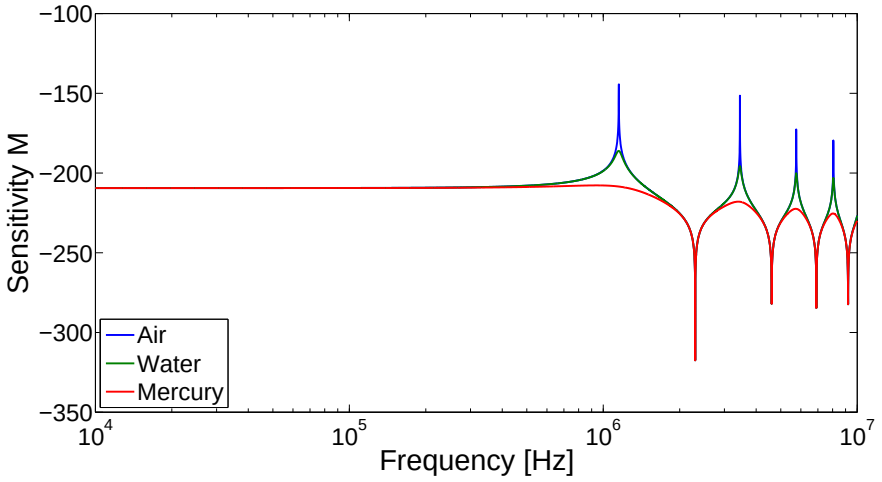

Figure A.4: FE model predictions of the submerged transducer response for three external impedances detailed in Table A.1

Table A.1: Values used to simulate and external fluid impedance.

Material	Density $\left[\frac{\text{kg}}{\text{m}^3}\right]$	Sound Speed $\left[\frac{\text{m}}{\text{s}}\right]$	Impedance $\left[\frac{\text{kg}}{\text{m}^2\text{s}}\right]$
Air	1.21	343	415
Water	1000	1500	1.5×10^6
Mercury	13600	1450	19.7×10^6

A.2.5 Results

After solving, the solution was plotted using the Domain Plot Parameters utility. Under the Point tab, the sensitivity M was expressed as

$$M = 20 \log_{10} \left(\frac{V/p_i}{M_{ref}} \right),$$

where M_{ref} is $1\,\text{V}/\mu\text{Pa}$ and p_i [Pa] is the input pressure. Figure A.4 plots this value at a point on the side closest to the incoming pressure of the piezoelectric layer with the fluid properties detailed in Table A.1.

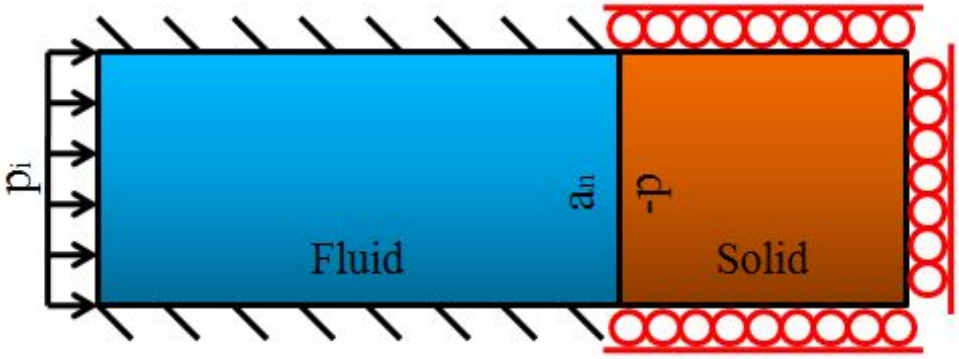

Figure A.5: Schematic representation of a rigidly terminated transducer domains and boundary conditions for the implemented FEM.

A.3 Rigid Termination

Another simple canonical case of interest is that of a transducer submerged in a fluid whose back face experiences no motion, i.e. it is rigidly terminated. The rigid termination condition can be understood to represent a special case of the submerged condition, discussed in Section 3.1, where the impedance at the back face of the piezoelectric domain approaches infinity. This rigid termination is achieved mathematically by setting a zero velocity condition at the surface and results in complete internal reflection in phase with the incident acoustic wave. In this case, the drawing and physics are similar to the submerged transducer case except the second fluid domain and PML have been removed. As illustrated in Figure A.5, the boundary furthest from the incoming pressure now has no Load and a Roller constraint while maintaining the Ground electric boundary condition.

Following the same parameters as above for the mesher and solver, Figure A.6 illustrates the sensitivity as a function of varying the external fluid properties described in Table A.1.

Combining Figures A.4 and A.6 into Figure A.7 illustrates the classic 6 dB gain [25] and doubling in number of resonances resulting from a rigid termination.

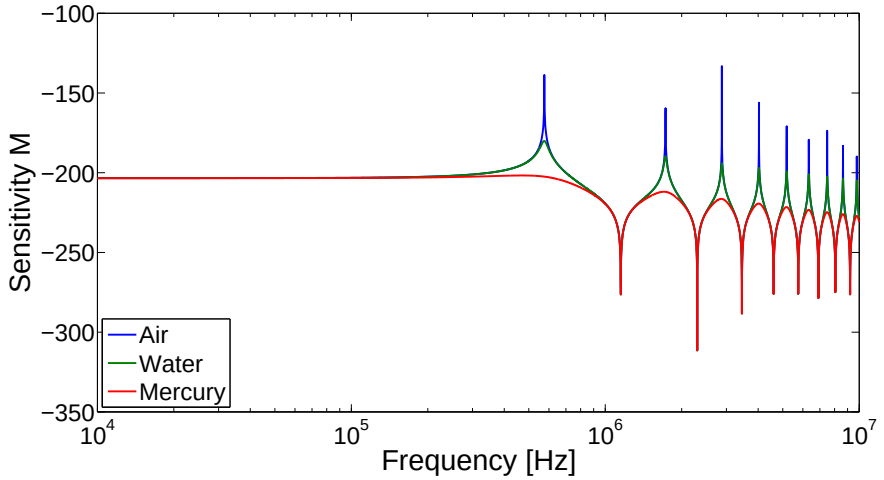

Figure A.6: FE model predictions of the response of a rigidly backed transducer for the three external impedances detailed in Table A.1

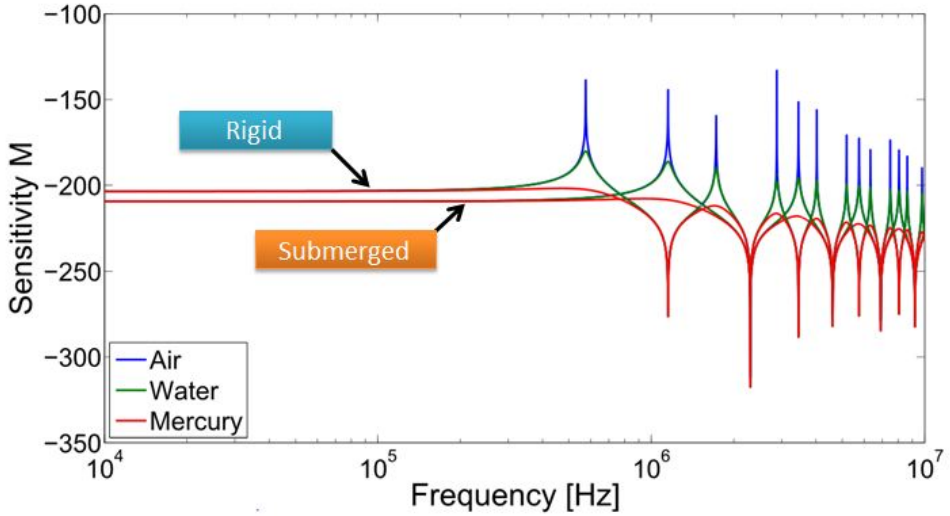

Figure A.7: Figures A.4 and A.6 superimposed to illustrate the different location and number of resonances resulting from the different end conditions as well as differing low frequency sensitivity.

A.4 Impedance Backing

The rigidly-terminated impedance backings investigated in this section. Impedance backings are more useful than the rigid backing of Section 3.2 as it accurately represents the effects of a mounting material. A transducer operating near a backing's resonance has a highly frequency dependent response. If left unchecked, this may lead to an unexpected sensitivity variation. Therefore, it is important to know how the hydrophone is terminated. The following cases could be modeled with either the submerged backing or the rigid termination. This work examines only the rigidly terminated case for the sake of space. Impedance backings are common as it generally better represents a mounting material than a rigid termination. Therefore, it is important to know how the material being used to mount the transducer will effect its receiving capabilities. If unchecked, a transducer operating near the resonance of the backing layer(s) may have a reduced sensitivity or frequency dependent response.

For a impedance backed piezoelectric layer, the physics will be similar to the submerged case unless the material is a solid. If this is the case, the material mode should be set to Decoupled, isotropic. The 'Decoupled' mode represents the fact that the material is simply elastic, not piezoelectric, the program will therefore not analyze the layer as another piezoelectric material. If the material is a fluid, the same boundary conditions will apply as described in the submerged case except a Sound Hard boundary condition will be applied to the side of the backing material furthest from the incoming pressure instead of a PML. If the material is a solid, the $-p$ and a_n interface condition is not necessary and it can be left as a Free constraint because Comsol already correctly couples elastic domains be establishing the proper continuity conditions. A Roller constraint condition will also be applied to every side of the backing layer not touching the piezoelectric layer as illustrated in Figure A.8.

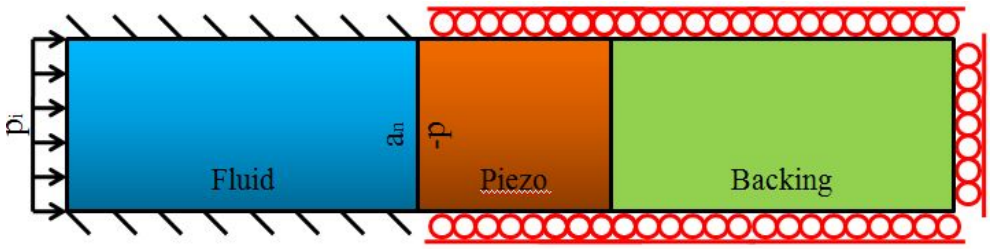

Figure A.8: Schematic representation of the impedance backed thickness vibrator domains and boundary conditions for the implemented FEM.

Table A.2: Backing Material Parameters

Material	Young's Modulus [GPa]	Poisson's Ratio	Density $\left[\frac{kg}{m^3}\right]$
Cork	0.032	0	240
Nylon	2	0.3	1150
Steel	195	0.28	7700
Oak	12.4	0.3	630
FR-4	22	0.28	1900

Using the parameters in Table A.2, Figure A.9 depicts the sensitivity of a thickness vibrator transducer mounted on various materials and submerged in water. Note the transition to a rigid termination in the lower frequencies as the wavelength becomes much larger than the backing thickness. Also note the transition to the rigid resonance as the backing material impedance increases.

A.5 Front Layers

Matching layers may be used to protect the transducers from debris, to damp flow noise or smooth out the sensitivity. Whatever the purpose, a material in front of a transducer will significantly effect its performance.

Following the same procedures detailed above, one can produce a impedance backed transducer with a front layer in between the incoming pressure and the piezoelectric layer as illustrated in Figure A.10. Again, using the same material from Ta-

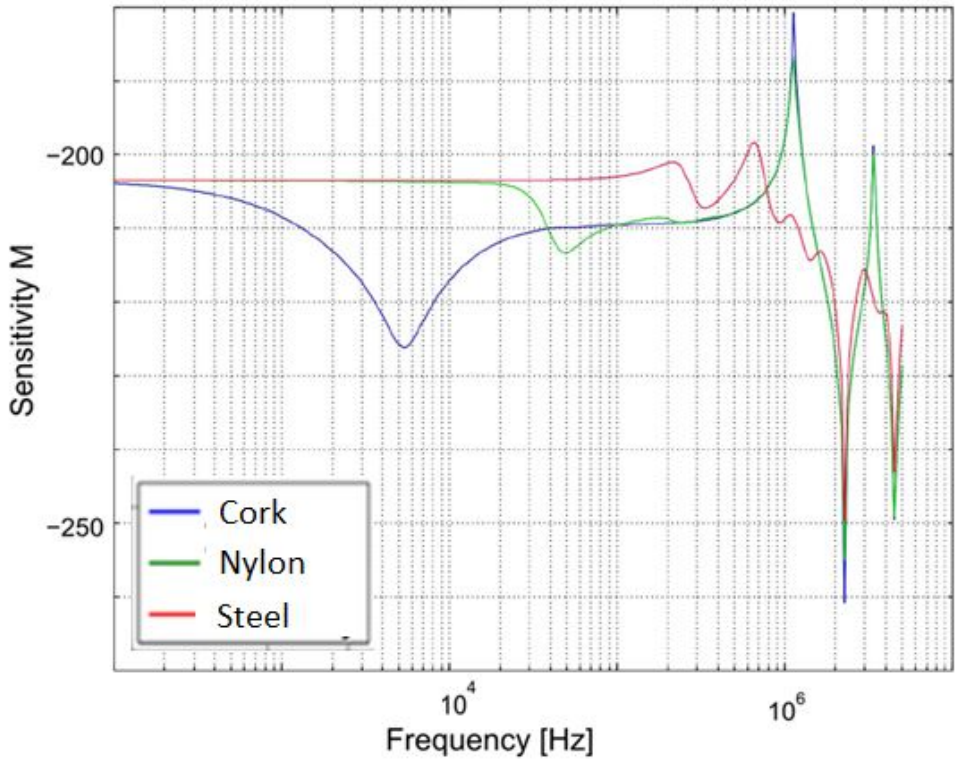

Figure A.9: Thickness vibrator transducer mounted on a varying backing layer, submerged in water

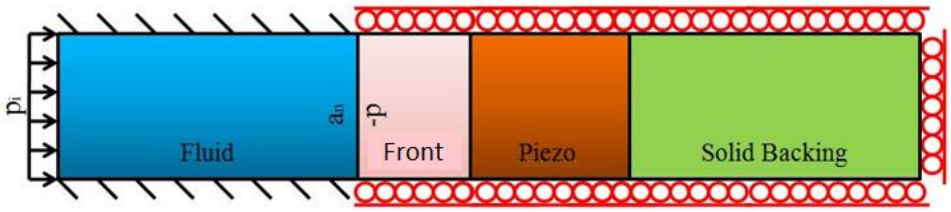

Figure A.10: Schematic of the domains and boundary conditions of a front layer and thickness vibrator for an implemented FEM.

ble A.2, Figure A.11 displays the sensitivity as a function of frequency. The matching layer thickness is much smaller than the backing layer thickness because of the large effect on the signal. In Figure A.11, nylon was used as the backing layer. Notice that cork reflects most of the signal before it has a chance to reach the transducer.

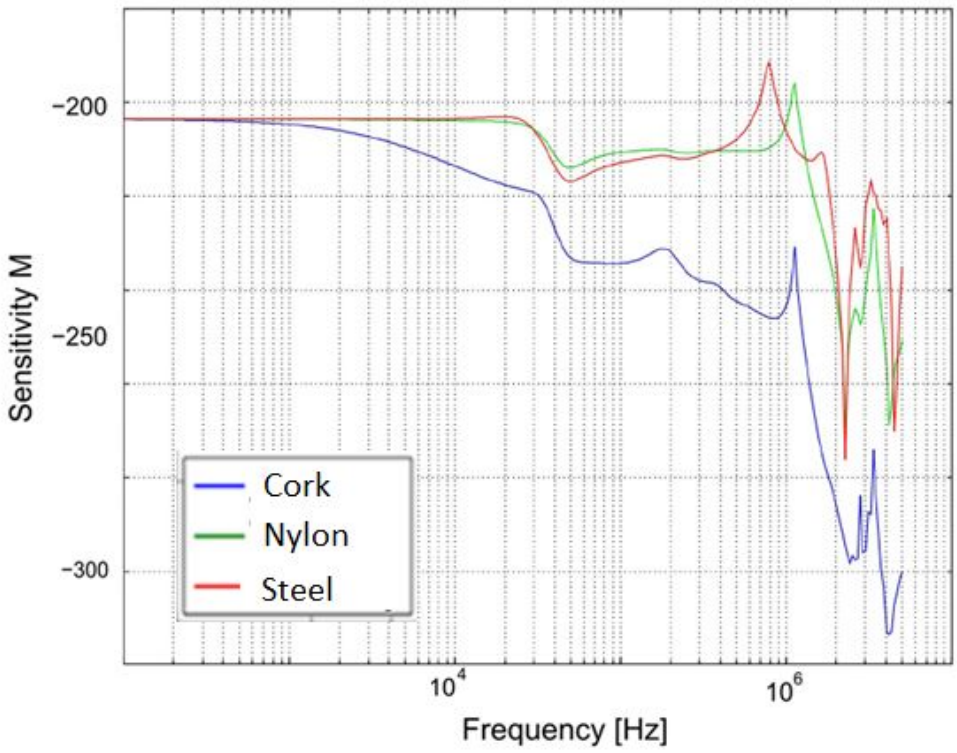

Figure A.11: Thickness vibrator transducer with matching layer of various materials, submerged in water

Bibliography

[1] M. F. Ashby, *Materials Selection in Mechanical Design.* Burlington, MA: Elsevier, 2005.

[2] D. G. Tucker and B. K. Gazey, *Applied Underwater Acoustics.* Pergamin, 1966.

[3] M. F. Ashby, R. W. Messler, R. Asthana, E. P. Furlani, R. E. Smallman, A. H. W. Ngan, R. J. Crawford, and N. Mills, *Engineering Materials & Processes Desk Reference.* Burlington, MA: Elsevier, 2009.

[4] R. J. Urick, *Principles of Underwater Sound for Engineers.* McGraw-Hill, 1975.

[5] X. Lurton, *An Introduction to Underwater Acoustics.* Heidelberg, NY: Springer, 2004.

[6] M. J. Crocker, *Handbook of Acoustics.* Hoboken, NJ: John Wiley & Sons, 1998.

[7] O. B. Wilson, *An Introduction to the Theory and Design of Sonar Transducers.* Los Altos, CA: Peninsula Publishing, 1985.

[8] B. V. Smith and B. K. Gazey, "High-frequency sonar transducers: A review of current practice," *IEEE Proceedings*, vol. 131, pp. 285–297, 1984.

[9] W. P. Mason, "Physical acoustics and the properties of solids," *The Journal of the Acoustical Society of America*, vol. 28, pp. 1197–1206, 1956.

[10] H. Koymen, B. V. Smith, and B. K. Gazey, "Equivalent circuits for high-frequency sonar transducers," *Electronic Letters*, vol. 15, pp. 600–601, 1979.

[11] A. Schroder, J. Rautnberg, and B. Henning, "Evauluation of cost functions for fea based transducer optimization," *Physics Procedia*, vol. 3, pp. 1003–1009, 2010.

[12] D. W. Hawkins and P. T. Gough, "Multiresonance design of a tonpilz transducer using the finite element method," *IEEE Transactions on Ultrasonics, Ferroelectrics and Frequency Control*, vol. 43, pp. 782–790, 1996.

[13] Y. Roh and X. Lu, "Design of an underwater tonpilz transducer with 2-2 mode piezocomposite materials," *The Journal of the Acoustical Society of America*, vol. 119, pp. 3734–3740, 2006.

[14] B. Henning, "Trends in ultrasonic transducer design," in *The Ninth International Conference on Electronic Measurement & Instruments*, 2009.

[15] E. Heikkola, K. Miettinen, and P. Nieminen, "Multiobjective optimization of an ultrasonic transducer using nimbus," *Ultrasonics*, vol. 44, pp. 368–380, 2006.

[16] R. N. Capps and C. M. Thompson, *Handbook of Sonar Transducer Passive Materials.* Washington, DC: National Research Laboratory, 1981.

[17] L. P. Lebedev, M. J. Cloud, and V. A. Eremeyev, *Tensor Analysis with Applications in Mechanics.* Hackensack, NJ: World Scientific Publishing, 2010.

[18] T. M. Atanackovic and A. Guran, *Theory of Elasticity for Scientists and Engineers.* New York, NY: Springer, 2000.

[19] P. S. Wilson, "Transducers lecture," in *Piezoelectric Transducers.* University of Texas at Austin, November 2008.

[20] R. N. Capps, "Dynamic young's moduli of some comemrcially available polyurethanes," *The Journal of the Acoustical Society of America*, vol. 73, pp. 2000–2005, 1983.

[21] A. D. Pierce, *Acoustics: an introduction to its physical principles and applications.* Melville, NY: Acoustical Society of America, 1989.

[22] D. Ensminger, *Ultrasonics: fundamentals, technology, applications.* Boca Raton, FL: CRC Press, 1988.

[23] A. Sommerfeld, *Partial Differential Equations in Physics.* Academic Press, 1949, translated by R. Radok.

[24] COMSOL, *Comsol Multiphysics Advanced Features Training Course Version 3.4.* COMSOL AB, 2008.

[25] D. T. Blackstock, *Fundamentals of Physical Acoustics.* New York, NY: Wiley-Interscience, 2000.

[26] M. Long, *Architectural Acoustics.* Burlington, MA: Elsevier Academic Press, 2006.

[27] M. F. Ashby, H. Shercliff, and D. Cebon, *Materials - North American Edition: engineering, science, processing and design.* Elsevier, 2009.

[28] R. M. German and S. J. Park, *Mathematical relations in particulate materials processing: ceramics, powder metals, cermets, carbides, hard metals and minerals.* Hoboken, NJ: John Wiley & Sons, 2008.

[29] R. M. Christensen, *Mechanics of Composite Materials.* Mineola, NY: Dover Publications, 2005.

[30] DuPont, "Dupont zytel nylon resin, zytel fn714 nc010," DuPont, Tech. Rep., 2005.

[31] Arkema, "Pebax 6333 sp 01," Pebax, Tech. Rep., 2009.

Vita

Steve Thomas Embleton was born in Austin, Texas on 2 December 1983, the son of Thomas H. Embleton and Lisa L. Embleton. He received his Bachelor of Science degree in Engineering from the University of Texas at Austin in 2006, while working part-time as an Student Engineer at Applied Research Laboratories. After graduation, he worked as a design engineer for Applied Research Laboratories briefly before applying and starting graduate studies at the University of Texas at Austin in 2007.

Permanent address: 3301 Denver Ave.
Austin, Texas 78723

This thesis was typeset with LaTeXby the author.